© 2022. Published by The Company of Biologists Ltd | Development (2022) 149, dev199676. doi:10.1242/dev.199676

TECHNIQUES AND RESOURCES

RESEARCH ARTICLE

Anatomy and development of the pectoral fin vascular network in the zebrafish

Scott M. Paulissen[1], Daniel M. Castranova[1], Shlomo M. Krispin[1,*], Margaret C. Burns[1,‡], Javier Menéndez[2], Jesús Torres-Vázquez[2] and Brant M. Weinstein[1,§]

ABSTRACT

The pectoral fins of teleost fish are analogous structures to human forelimbs, and the developmental mechanisms directing their initial growth and patterning are conserved between fish and tetrapods. The forelimb vasculature is crucial for limb function, and it appears to play important roles during development by promoting development of other limb structures, but the steps leading to its formation are poorly understood. In this study, we use high-resolution imaging to document the stepwise assembly of the zebrafish pectoral fin vasculature. We show that fin vascular network formation is a stereotyped, choreographed process that begins with the growth of an initial vascular loop around the pectoral fin. This loop connects to the dorsal aorta to initiate pectoral vascular circulation. Pectoral fin vascular development continues with concurrent formation of three elaborate vascular plexuses, one in the distal fin that develops into the fin-ray vasculature and two near the base of the fin in association with the developing fin musculature. Our findings detail a complex, yet highly choreographed, series of steps involved in the development of a complete, functional, organ-specific vascular network.

KEY WORDS: Pectoral fin, Endothelial, Artery, Vein, Forelimb development, Zebrafish

INTRODUCTION

The human forelimb is an essential part of the success of the human species. Unfortunately, major defects in forelimb development affect 2.3 out of 10,000 live births (Goldfarb et al., 2017). The biological causes of these defects are not all understood, underscoring the importance of studying the multitude of developmental processes that lead to formation of the mature appendage (Goldfarb et al., 2017; Rodríguez-Niedenführ et al., 2001). Fortunately, there are excellent animal models for studying the development of the human arm. Studies on forelimb development in chick (Bates et al., 2002), mouse (Martin, 1990), frog (Abu-Daya et al., 2011), zebrafish (Grandel and Brand, 2011; Isogai et al., 2001; Mercader, 2007) and other vertebrates have shown that the genetic and molecular pathways used to pattern different forelimbs are well conserved (Chiang et al., 2001; Crossley et al., 1996; Mateus et al., 2020; Niswander and Martin, 1992; Nomura et al., 2006; Riddle et al., 1993), including important transcription factors such as HoxA13, HoxD13 and Meis1 involved in regional patterning of the limb (Mercader et al., 2000; Tulenko et al., 2017). When compared, appendages as divergent as fish pectoral fins and human arms are well conserved at the molecular level (Tulenko et al., 2017).

Development of the tetrapod forelimbs begins prior to that of the rear limbs and starts as a small tissue protrusion, called the limb bud, on the side of the lateral plate mesoderm (Gros and Tabin, 2014). From this bump, an appendage builds outwards beneath the apical ectodermal ridge (AER) (Saunders, 1948). The AER is a thin ridge of tissue on the distal tip of the forelimb that promotes the growth of the limb bud mesenchyme that becomes the endoskeletal disk (Grandel and Schulte-Merker, 1998; Martin, 1990). In tetrapod forelimbs, the AER reduces and condenses into digits, whereas in fish pectoral fins the AER greatly expands and generates fin rays (Zhang et al., 2010). An additional difference is that, in fish, the fin bud rotates 90° as it transitions to a blade morphology (Grandel and Schulte-Merker, 1998), causing its anterior edge to point dorsally and the fin blade to extend towards the posterior.

Although the terminal morphology of the forelimb vasculature is well documented in several species, much less is known about the developmental processes that generate the terminal state. Over the past century, studies in model organisms, including quail, mouse and pig, have described stages of forelimb vascular development using methods such as histology, India ink perfusion or immunostaining of vascular structures, although though none of these studies used live imaging (Bates et al., 2002; Crossley et al., 1996; Marston et al., 2014; Rodríguez-Niedenführ et al., 2001; Shoham et al., 2012; Woollard, 1922). These studies highlighted that, although the number of digits and overall shape of the final limb differ between organisms, the overall process involves an early capillary plexus within the limb bud that sprouts from the dorsal aorta and cardinal vein and then eventually remodels into a more mature hierarchical and arborized vascular network with a contiguous circumferential vasculature and distal invasion of the AER, followed by further remodeling to surround the forming digits (Bates et al., 2002; Woollard, 1922).

Various aspects of fin development have been studied in zebrafish, including bone formation (Akiva et al., 2019; Dodo et al., 2020), muscle development (Thorsen and Hale, 2005), neuronal patterning (Dodo et al., 2020; Thorsen and Hale, 2007), regeneration (Marques et al., 2020; McMillan et al., 2013, 2018; Xu et al., 2014), endothelial cell behavior (Xu et al., 2014) and evolution of the fin-to-limb transition, among others (Lalonde and Akimenko, 2018; Petersen and Ramsay, 2020; Yano et al., 2012; Zhang et al., 2010). Development of the zebrafish vasculature has

[1]Division of Developmental Biology, Eunice Kennedy Shriver National Institute of Child Health and Human Development, NIH, Bethesda, MD 20892, USA. [2]Department of Cell Biology, Skirball Institute of Biomolecular Medicine, New York University Langone Medical Center, NY 10016, USA.
*Present address: Israeli Biotechnology Research Ltd., Yavneh, 8121001, Israel.
‡Present address: Department of Cellular and Molecular Medicine, University of California – San Diego, La Jolla, CA 92093-0021, USA.

§Author for correspondence (flyingfish2@nih.gov)

S.M.P., 0000-0002-9258-2380; S.M.K., 0000-0003-0747-1174; M.C.B., 0000-0001-5380-4676; B.M.W., 0000-0003-4136-4962

Handling Editor: Steve Wilson
Received 1 April 2021; Accepted 24 January 2022

Development (2022) 149, dev199676. doi:10.1242/dev.199676

been studied extensively (Aydogan et al., 2015; Betz et al., 2016; Cha et al., 2012; Fujita et al., 2011; Gore et al., 2012; Hasan et al., 2017; Isogai et al., 2001; Jung et al., 2017; Lawson and Weinstein, 2002; Okuda et al., 2012; Reischauer et al., 2016; Torres-Vázquez et al., 2004; Weinstein, 1999; Xu et al., 2014). Study of the fin vasculature has mainly been done in the caudal fin. Blood vessels associated with the caudal fin-ray bones form stereotypic structures with a single artery flowing through paired hemi-cylindrical bones and two veins draining blood back to the base of the fin ray on either side of the bone (Akiva et al., 2019; Huang et al., 2003; Tu and Johnson, 2011; Xu et al., 2014). Sparse capillary vessels form in the membranous region between the bony fin rays (Huang et al., 2003). Embryonic pectoral fin circulation begins at ∼3 days post-fertilization (dpf) with blood flow from the dorsal aorta that loops from ventral to dorsal around the edge of the pectoral fin before emptying into the common cardinal vein (CCV) (Grandel and Schulte-Merker, 1998; Isogai et al., 2001; McMillan et al., 2013; Yano et al., 2012). The developmental process that creates this initial embryonic pectoral fin vessel and its subsequent elaboration to form the extraordinarily complex adult pectoral fin vasculature has not been reported.

The importance of a well-developed, functional forelimb vasculature for proper growth and development of the limb/fin has been highlighted by research on the teratogenic drug thalidomide. Exposure to thalidomide during a critical window of limb development causes severe perturbation of limb formation (Kajii et al., 1973; Vargesson, 2013), and a major part of these teratogenic effects appear to be through anti-angiogenic effects of the drug (Therapontos et al., 2009), which has led to exploration of the use of thalidomide and thalidomide analogs as potential anti-angiogenic anticancer agents (Rehman et al., 2011). Zebrafish research has shown a correlation between the teratogenicity of thalidomide analogs and their anti-angiogenic capacity (Mahony et al., 2013), further reinforcing this idea.

In this study, we document the development of the zebrafish pectoral fin vasculature from its first sprouts from the CCV in the zebrafish embryo to an adult-like pectoral fin vascular network in ∼1-month-old juvenile fish. Formation of the pectoral fin vasculature involves a highly stereotyped and reproducible stepwise series of events. These include formation of an initial vascular loop around the pectoral fin, connection of this loop to arterial blood flow to initiate pectoral vascular circulation, development of an elaborate distal vascular plexus in conjunction with condensation and growth of the bony fin rays, and assembly of two parallel proximal vascular networks near the base of the fin in association with the endoskeletal disk. The successive remodeling and complex elaboration of the pectoral fin vasculature involves a number of interesting events, including shunting and re-routing of blood flow at different steps, and plexus formation followed by plexus pruning and remodeling, among other fascinating processes. Together, our findings detail a complex and highly choreographed series of steps involved in the development of a complete, functional, organ- and tissue-specific vascular network.

RESULTS

Vascular anatomy of the adult zebrafish pectoral fin

The pectoral fin of the adult zebrafish (Fig. 1A,B) is a structure supplied with oxygen and nutrients by a complex vascular network (Fig. 1C-I). In gross anatomy, the pectoral fin can be divided into two major regions: a membranous distal region supported by 11-13 fin rays (lepidotrichia), and a muscular base near the body wall of the zebrafish where the membranous distal region emerges (Fig. 1A,B). The proximal portion of the pectoral fin is composed primarily of muscle and bones that articulate and anchor the pectoral fin to the pectoral girdle; its depth and opacity make it difficult to image in the adult. In contrast, the thinner fin ray-containing distal region and its elaborate vascular network are readily visualized using high-resolution optical imaging. Viewed in profile, each fin ray comprises two closely apposed hemicylindrical bones that form a hollow tube between them (Fig. 1C; Huang et al., 2003). Transmitted light imaging of blood circulation in intact adult fins, and tiled confocal imaging of vessels dissected adult fins visualized using the pan-endothelial *Tg(fli1a:egfp)*^{y1} reporter line (Lawson and Weinstein, 2002), reveal blood vessels running in the channel between and along either side of the fin-ray bones, as well as sparse inter-ray vessels running through the membranous tissues between the rays (Fig. 1D-I; Movie 1). The pectoral fins of male and female zebrafish are similar, but a few sex-specific differences were noted. Fin rays and associated vessels undergo proximal-to-distal branching, and whereas the terminal distal fin-ray bifurcations occur at approximately the same distance from the distal end of the pectoral fin in males and females, the penultimate branches of the fin rays and fin-ray vessels occur at a more proximal position in male pectoral fins (Fig. S1, white arrowheads). Male pectoral fins (Fig. 1D-F; Fig. S1, cyan arrowheads) also had a higher density of inter-ray vessels than female pectoral fins (Fig. 1G-I; Fig. S1, magenta arrowheads). As has been previously reported (McMillan et al., 2013), male pectoral fins also have a dense network of vessels associated with the breeding tubercles, specialized toothlike keratinized epidermal protrusive structures on the dorsal surfaces of male pectoral fin rays that are thought to be involved in helping maintain contact during spawning (Fig. S1) (McMillan et al., 2015).

The vessels inside the fin rays generally flow in a proximal-to-distal direction, whereas the paired vessels along either side of the fin rays generally flow in a distal-to-proximal direction, suggesting that these represent arterial and venous vessels, respectively (Fig. 2A; Movie 1). The arterial identity of the vessel running down the center of each fin ray is supported by confocal imaging of the fin vasculature using the arterial *Tg(kdrl:mcherry)*^{y206} transgenic line. In medial areas of the fin, *Tg(kdrl:mcherry)*^{y206}-positive arterial vessels could be seen running down the center of each weakly blue autofluorescent fin ray (Fig. 2B-E), whereas the parallel venous vessels on either side of the fin rays and the inter-ray vessels were only weakly *Tg(kdrl:mcherry)*^{y206} positive or *Tg(kdrl:mcherry)*^{y206} negative. In more distal areas of the fin, the fin-ray arteries were only weakly *Tg(kdrl:mcherry)*^{y206} positive, although, interestingly, small lateral segments projecting from these distal arteries remained more strongly *Tg(kdrl:mcherry)*^{y206} positive (Fig. 2B,F-I). To confirm the identity of fin-ray arteries and other arterial vessels, we also imaged pectoral fin vessels in artery-specific *Tg(flt1:nlsmcherry)*^{skt7} transgenic fish (Carretero-Ortega et al., 2019), and showed that the same vessels were positive for this transgene (Fig. S2); we found similar results using *Tg(flt1:egfp-sv40)*^{skt8} transgenic fish (J.M. and J.T.-V., unpublished).

The fin-ray central arteries and paired lateral veins are connected to arterial feed and venous drainage at the base of each fin ray (Fig. 2A). The arterial feed for the fin vasculature is supplied by a vascular branch emerging from the dorsal aorta, whereas venous drainage is accomplished primarily via the CCV (described further below). In addition to the more distal fin-ray vasculature, the adult fin also contains an elaborate plexus of vessels in the proximal area of the fin below the base of the fin rays (Fig. 1D,G). As also described below, this proximal vascular plexus provides at least a portion of the arterial feed for the distal fin-ray arteries

Development (2022) 149, dev199676. doi:10.1242/dev.199676

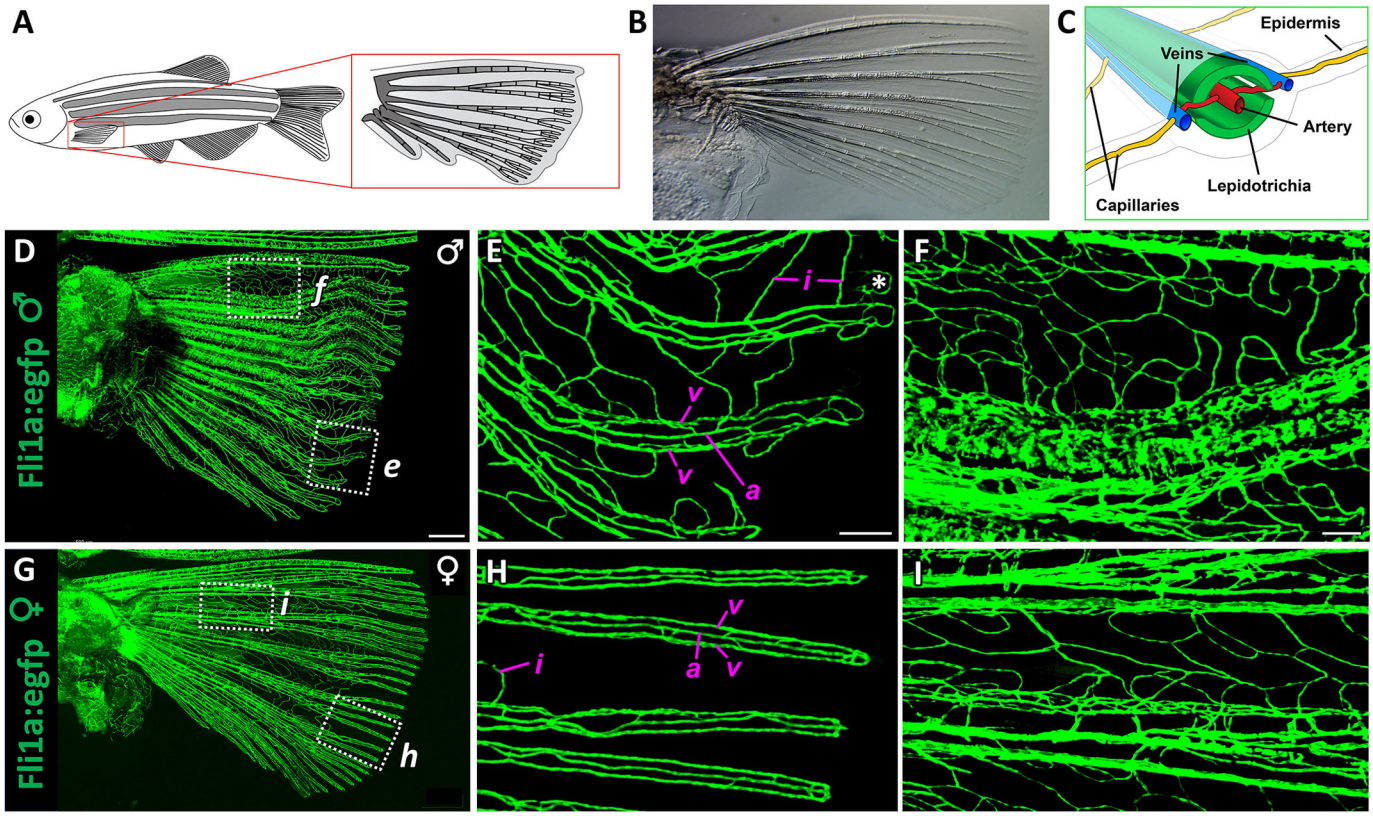

Fig. 1. Vascular anatomy of the adult zebrafish pectoral fin. (A) Drawing of an adult zebrafish with a magnified view of the pectoral fin and its lepidotrichia (fin-ray bones). (B) Transmitted light image of a dissected pectoral fin. (C) Schematic showing a cross-section of a zebrafish fin ray. (D-I) Tiled confocal images of pectoral fins dissected from adult male (D-F) or adult female (G-I) *Tg(fli1a:egfp)*^{y1} transgenic zebrafish. E and F show higher-magnification views of the boxed regions in D. H and I show higher-magnification views of the boxed regions in G. a, fin-ray artery; i, fin-ray interlinking vessels; v, paired fin-ray veins. The asterisk in E denotes an artifact of image stitching. Images shown are representative of data collected from three separate male and three separate female adult fins, with consistent observation of the overall patterning of major vessels. Scale bars: 500 µm (B,D,G); 150 µm (E,H); 100 µm (F,I).

(Fig. S1, yellow arrowheads). The vasculature of the pectoral fin becomes more complex in the proximal plexus near the base of the fin rays. As noted above, imaging of the proximal regions of the adult pectoral fin is extremely challenging owing to the thickness and opacity of this bony and muscular tissue. In the sections below, we describe the stepwise development of the distal and proximal vascular networks of the pectoral fin, from the first vascular sprouts into the fin bud in ∼1.5-day-old embryos, to a complex vascular network with most of the major features of the adult pectoral fin vascular network in the 4-week-old juvenile zebrafish.

Pectoral fin vascular development: formation and perfusion of the primitive pectoral artery

Initial assembly of the vascular network of the pectoral fin is highly stereotypic (Fig. 3; Movie 2). Pectoral fin vascular development begins at ∼30-34 h post-fertilization (hpf) with the emergence of a pair of dorsal and ventral vascular sprouts from the caudal edge of the CCV (Fig. 3A,D; Movie 2). These sprouts invade and then elongate along the rim of the endoskeletal disk (Fig. 3B,E; Movie 2), eventually joining together at the posterior end of the fin to form a complete primitive pectoral artery by ∼38-40 hpf (Fig. 3C,F; Fig. S2; Movie 2). The primitive vascular arc that becomes the pectoral artery initially possesses only venous connections to the CCV at either end, and does not immediately carry blood flow.

Shortly after, or concomitant with, completion of the primitive pectoral fin artery, a new vascular sprout emerges from the pectoral artery close to its ventral connection point with the CCV (Fig. 4A,D; Movie 2). This sprout grows medially, dorsally and caudally along a reproducible path (Fig. 4B,E; Movie 2), traveling ∼200 µm in total and migrating underneath and between the somites before eventually connecting to the dorsal aorta at the base of the second intersegmental vessel (ISV), or to the second (arterial) ISV itself (Fig. 4C,F). Although several nerve axons are found in the same general area as this new vessel segment, entering the pectoral fin near where the initial pec fin vascular sprouts emerge (Bremer et al., 2017; Okamoto and Kuwada, 1991a), careful imaging of *Tg(kdrl:egfp)*^{s843}, *Tg(elavl3:mCherry)*^{nia02tg} double-transgenic embryos showed that these nerves do not align closely with this vessel, suggesting they do not play a role in guiding its growth (Fig. S3; Movie 3). Once the new vessel connects to the dorsal aorta, flow begins (Fig. 4G-U; Movies 2, 4). In most cases, a direct shunt to the CCV forms, as a connection directly to the CCV is still present when flow initiates, leaving the majority of the primary arc unperfused (Fig. 4H,N-Q; Movies 4-6). However, this ventral connection is generally severed within a few hours and flow is redirected through the pectoral artery primary arc, emptying into the CCV via the dorsal connection only (Fig. 4I,R-U; Movies 4-6). A CCV shunt was present in at least 63.6% of fish observed (n=11), persisting 110±95 min before being severed (Fig. S4). The remainder of the time, either the entire primary arc perfused immediately without a shunt to the CCV, or the shunt disconnected too rapidly to be observed in our imaging. The average onset of flow through the complete pectoral artery arc was 57.4±1.8 hpf, with pruning of the

Development (2022) 149, dev199676. doi:10.1242/dev.199676

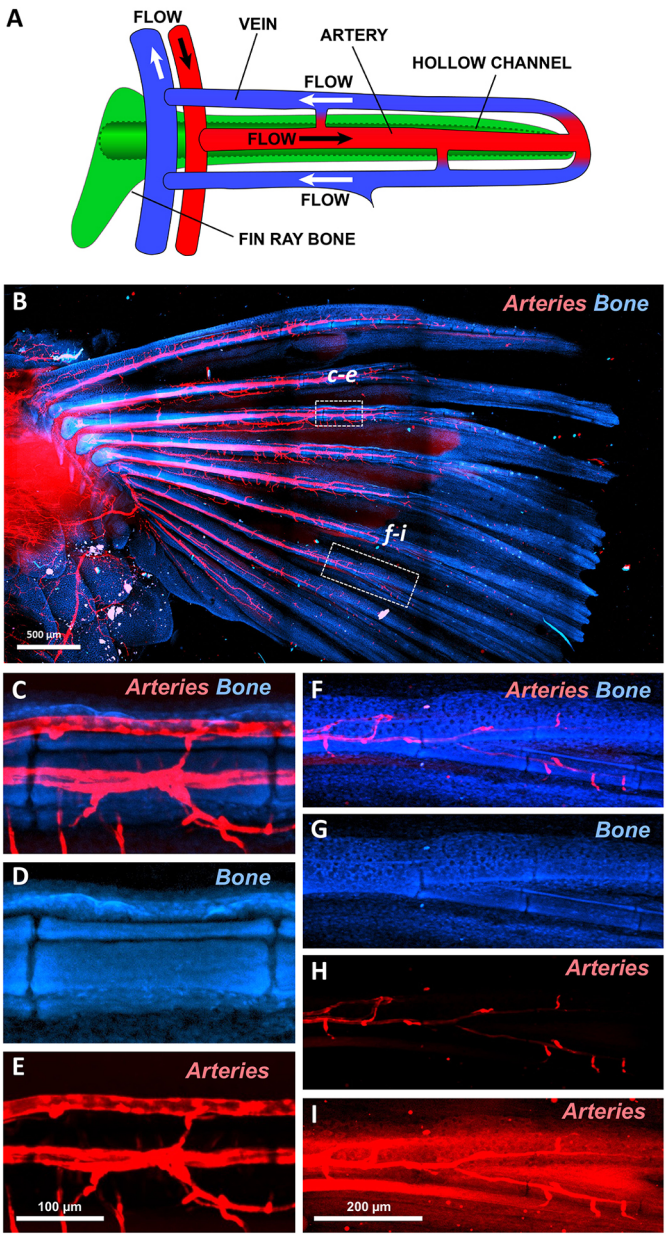

Fig. 2. Fin ray-associated vasculature of the adult zebrafish pectoral fin. (A) Schematic illustrating circulatory flow through an individual adult zebrafish fin ray. Arteries are in red, veins in blue, and fin-ray bone in green. (B-I) Confocal images of an adult pectoral fin dissected from a *Tg(kdrl:mcherry)*^{y206} zebrafish, showing *Tg(kdrl:mcherry)*^{y20}-positive arterial blood vessels (red) and autofluorescent bone (blue). (B) Low-magnification tiled confocal image of a dissected adult pectoral fin. (C-E) Higher-magnification confocal images of the boxed region (c-e) in B, showing *Tg(kdrl:mcherry)*^{y206}-positive arteries (C,E) running through the center of autofluorescent bones (C,D) in the proximal region of a fin ray. (F-I) Higher-magnification confocal images of the boxed region (f-i) in B, showing weakly *Tg(kdrl:mcherry)*^{y206}-positive arteries (F,H,I) running through the center of autofluorescent bones (F,G) in the distal region of a fin ray. I shows an 'overexposed' image of the fluorescence in H. Images shown are representative of three separate adult fins, with consistent observation of the overall patterning of major vessels. Scale bars: 500 µm (B); 100 µm (C-E); 200 µm (F-I).

endothelial cell bridge to the CCV preventing further resumption of shunting (Fig. S4B; Movies 4, 6).

To examine the cellular dynamics of shunt disconnection, we carried out time-lapse imaging and tracing of individual endothelial cells in *Tg(kdrl:nlsmCherry)*^{skt7}, *Tg(kdrl:egfp)*^{s843} double-transgenic fish through the onset of blood flow to the fin. Analysis of 67 nuclei across 16 embryos revealed that endothelial cells that began in or entered the junctional region eventually settled in roughly equal numbers in the pectoral fin vasculature, the CCV, or in a persistent, unlumenized vestigial sprout linked to the CCV (33.3%, 31.9% and 34.8%, respectively) (Fig. S4C-E; Movies 7, 8). Although a number of endothelial cells divided over the course of these time-lapse sequences, no nuclei were observed to fragment, suggesting that shunt pruning occurs via cell rearrangement without any loss of endothelial cells.

As Notch signaling has been shown to be important for a number of endothelial cell behaviors, including tip cell selection and arterial specification (Geudens et al., 2019; Suchting et al., 2007; Weijts et al., 2018; reviewed briefly in Weinstein and Lawson, 2002), we wondered whether it might play a role in the pectoral fin. We treated embryos at 30 hpf (prior to initial limb bud invasion by endothelial cell sprouts) with either DAPT or LY411575, two different inhibitors of Notch signaling (γ-secretase inhibitors), examining phenotypes after 24 h of treatment (Fig. S5). Although overall fin morphology and formation of the initial pectoral fin vascular loop appeared normal in inhibitor-treated animals, there were major defects in formation of the ventral arterial sprout connecting to the dorsal aorta (Fig. S5). Growth of the ventral sprout was stalled or blocked entirely in animals treated with either inhibitor, and approximately one-quarter of the ventral sprouts that did emerge made aberrant connections to the CCV instead of to the dorsal aorta (Fig. S5), suggesting that Notch signaling plays an important role in proper growth and targeting of the pectoral artery.

Pectoral fin vascular development: formation of the distal fin-ray vascular network

Once established, the initial pectoral artery circulatory loop changes little over the next several days, although to a variable degree a small plexus forms at the distal tip of the growing fin (Fig. 5A-F; Movie 9; Fig. S6). Branching and complexity of the distal vascular plexus began to increase dramatically at 13.7±1.0 dpf, or 5.3±0.3 mm in total animal length (Fig. 5G-K; Movie 10; Figs S6, S7). Note that at later stages fin vessel development correlated less well with chronological age than with animal size, which can vary substantially for same-age animals (Fig. S7). From ∼7.0 mm (17 dpf) to ∼9.0 mm (22 dpf), a progressive dorsal-to-ventral remodeling of the distal plexus takes place that leads to the formation of an adult-like fin-ray vascular network with well-defined arterial and venous vessels (Fig. 5L-Q; Movies 10, 11). As visualized in *Tg(kdrl:mcherry)*^{y206}, *Tg(mrc1a:egfp)*^{y251} double-transgenic animals, this remodeling begins with localized hypersprouting in the dorsal-most region of the distal plexus, spreading to more ventral areas of the plexus at size 7.6±0.3 mm or age 21.1±2.0 dpf (Fig. 5N-Q; Movies 10, 11; Figs S6, S7). At size 7.8 mm±0.4 mm or age 21.6±2.0 dpf, a small part of this dorsal plexus begins to develop into an arterial network with persistently *Tg(kdrl:mcherry)*^{y206}-positive and progressively *Tg(mrc1a:egfp)*^{y251}-negative arterial vessels (Figs S2, S6) that extend into the developing fin rays. As this occurs, most of the remaining *Tg(mrc1a:egfp)*^{y251}-positive plexus realigns just dorsal to each fin ray and a single, *Tg(mrc1a:egfp)*^{y251}-positive, *Tg(kdrl:mcherry)*^{y206}-negative (presumptive venous) vessel coalesces along the ventral side of each fin ray (Fig. 5N-R; Movies 10, 11). These arterial and venous vessels appear at size 8.41 mm±0.3 mm or age 23.4±2.2 dpf, and continue to extend with the fin ray as it grows in length (Fig. 5L,N-Q; Figs S2, S6; Movies 10, 11). Starting

Development (2022) 149, dev199676. doi:10.1242/dev.199676

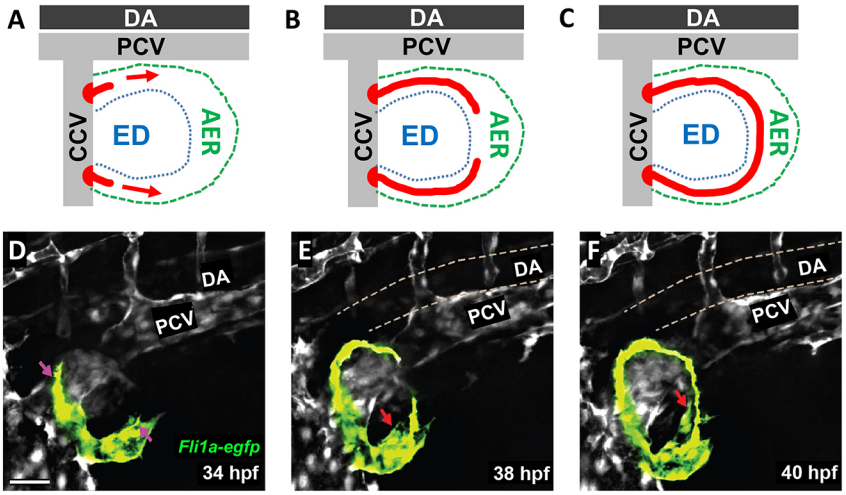

Fig. 3. Formation of the primitive pectoral artery. (A-C) Schematics illustrating the stages of primitive pectoral artery formation, including initial dorsal and ventral sprouts from the CCV (A), elongation of these sprouts along the rim of the growing fin (B), and linkage of the two segments to form a complete primitive pectoral artery vascular arc (C). DA, dorsal aorta; ED, endoskeletal disk; PCV, posterior cardinal vein. (D-F) Still images taken from a time-lapse confocal time series of primitive pectoral artery formation in a *Tg(fli1a:egfp)*^{y1} transgenic zebrafish at 34 hpf (D), 38 hpf (E) and 40 hpf (F). Pink arrows indicate the emerging sprouts migrating into the pectoral fin, and red arrows indicate the emerging ventral arterial sprout. See Movie 2 for the complete time-lapse series. Images shown are representative of data collected from 12 separate embryos. Scale bar: 40 µm (D-F).

at ∼9.0 mm, new venous sprouts emerge dorsally from near the end of each developing fin ray and then grow proximally and distally along the dorsal side of the fin rays to give rise to the paired dorsal fin-ray veins (Fig. 5N-Q; Fig. S6; Movies 10, 11). Completion of this process results in formation of a very adult-like independent fin-ray vasculature with a single arterial feed running down each fin ray and paired venous drains on either side (Fig. 5P,Q; Figs S2, S6; see Figs 1 and 2 for comparison to the adult).

Distal plexus remodeling and formation of the fin-ray arteries are temporally and spatially correlated with fin-ray bone formation, as visualized in six *Tg(kdrl:egfp)*^{s843}, *Tg(Ola.Sp7:mCherryEco.NfsB)*^{pd46} double-transgenic embryos with EGFP and mCherry expression in vessels and bone, respectively (Fig. 6). Initial *Tg(Ola.Sp7:mCherryEco.NfsB)*^{pd46}-positive bone condensations are closely associated with local formation of a hypersprouting, densely branched plexus of smaller vessel segments (Fig. 5O,P; Fig. 6A,B; Movies 9, 10). As the second fin-ray bone begins to coalesce, a new bidirectional angiogenic sprout begins to migrate out from the distal plexus near the base of the future second fin-ray bone (Fig. 6A-C). The proximal/dorsal tip of this sprout grows into the pectoral fin, eventually connecting with a separate, proximal plexus of vessels developing in the center of the fin in association with the endoskeletal disk (Fig. 6C-F, yellow arrows; formation of the proximal plexus is discussed below). The ventral tip of the sprout grows ventrally, parallel and in close proximity to the original primary pectoral artery, to which it connects near the ventral side of the fin (Fig. 6C-F, blue arrows). Branches of this newly developing arterial network grow into each of the fin-ray bones in dorsal-to-ventral sequence as the bones develop and extend (Fig. 6E,F, asterisks). The developing arterial network (Fig. S2) maintains strong *Tg(kdrl:egfp)*^{s843} expression as the remainder of the distal fin vascular network either regresses (see Fig. 5P,Q) or progressively loses (Fig. 6E,F; Fig. S5J-R) *Tg(kdrl:egfp)*^{s843} expression and remodels into veins (Fig. 5P,Q). Once the newly developing arterial network connects to the proximal plexus dorsally and the primitive pectoral artery arc ventrally (yellow and blue arrows in Fig. 6F), it begins to receive arterial blood flow from both ends, acting as a 'manifold' to supply blood to the fin-ray arteries that drain into the fin-ray veins. The fin-ray veins then flow back to a separate venous manifold developing at the base of the fin rays that drains dorsally into the CCV. This new venous manifold emerges at least in part from the original dorsal part of the primitive primary pectoral artery arc, extending further ventrally by angiogenic sprouting and growth alongside the arterial network (Fig. 6F).

Pectoral fin vascular development: formation of the proximal plexus

As development of the fin-ray vascular network is taking place in the distal fin, a separate but equally elaborate vascular network is beginning to develop in the proximal fin in association with the endoskeletal disk (Fig. 7). At 4.8±0.3 mm (n=7), sprouts emerge from the pectoral fin artery, from the body wall vicinity of the common cardinal vein, and from an unidentified venous source rostral to the pectoral fin; these sprouts invade the limb on the lateral and medial sides of the endoskeletal disk (Fig. 7A-D; Fig. S8; Movies 12, 13). Over the next several days, these sprouts rapidly elaborate into two new stratified vascular plexuses (Fig. 7A,B,E-G; Movie 13). The two plexuses form within the abductor and adductor muscles on the lateral and medial sides of the endoskeletal disk. Although the detailed vascular pattern of each of these new plexuses is highly variable, they have some consistent features. The arterial feed for both the medial and lateral plexuses originates from a single sprout from the pectoral fin artery, which later splits into the individual feeds for the two separate plexuses (Fig. S8; Movie 12). In contrast to their common arterial feeds, the medial and lateral plexuses appear to have distinct venous drainage pathways, although owing to their depth the precise drainage points have not been determined. The medial plexus drains to a deep location at or close to the CCV (Fig. 7B,G,I; Movie 12), whereas the lateral proximal plexus drains to different, very deep, high-caliber vessel at a more rostral location (Fig. 7H,I). By 20 dpf (∼8 mm) the proximal plexus exists as two elaborate vascular plexuses arranged in parallel to the plane of the fin endoskeletal disk, with a limited number of connections between them (Fig. 5Q; Movie 13).

Although the vasculature of both the proximal vascular plexus and the fin rays increases in complexity and the vessels form additional interconnections between the first 3 weeks of development and the adult pectoral fin, the basic arrangement of circulatory flow patterns in the fin is largely maintained into adulthood, although it becomes highly elaborated to accommodate the increased size of the adult. However, we take note below of the formation of links between the proximal and distal pectoral fin vasculature in older embryos.

Formation of links between the proximal and distal pectoral fin vasculature

Observation of older larval/early juvenile fish revealed later-stage addition of links between the newly developed medial proximal plexus and fin-ray arterial networks described above (Fig. 8A-G).

Development (2022) 149, dev199676. doi:10.1242/dev.199676

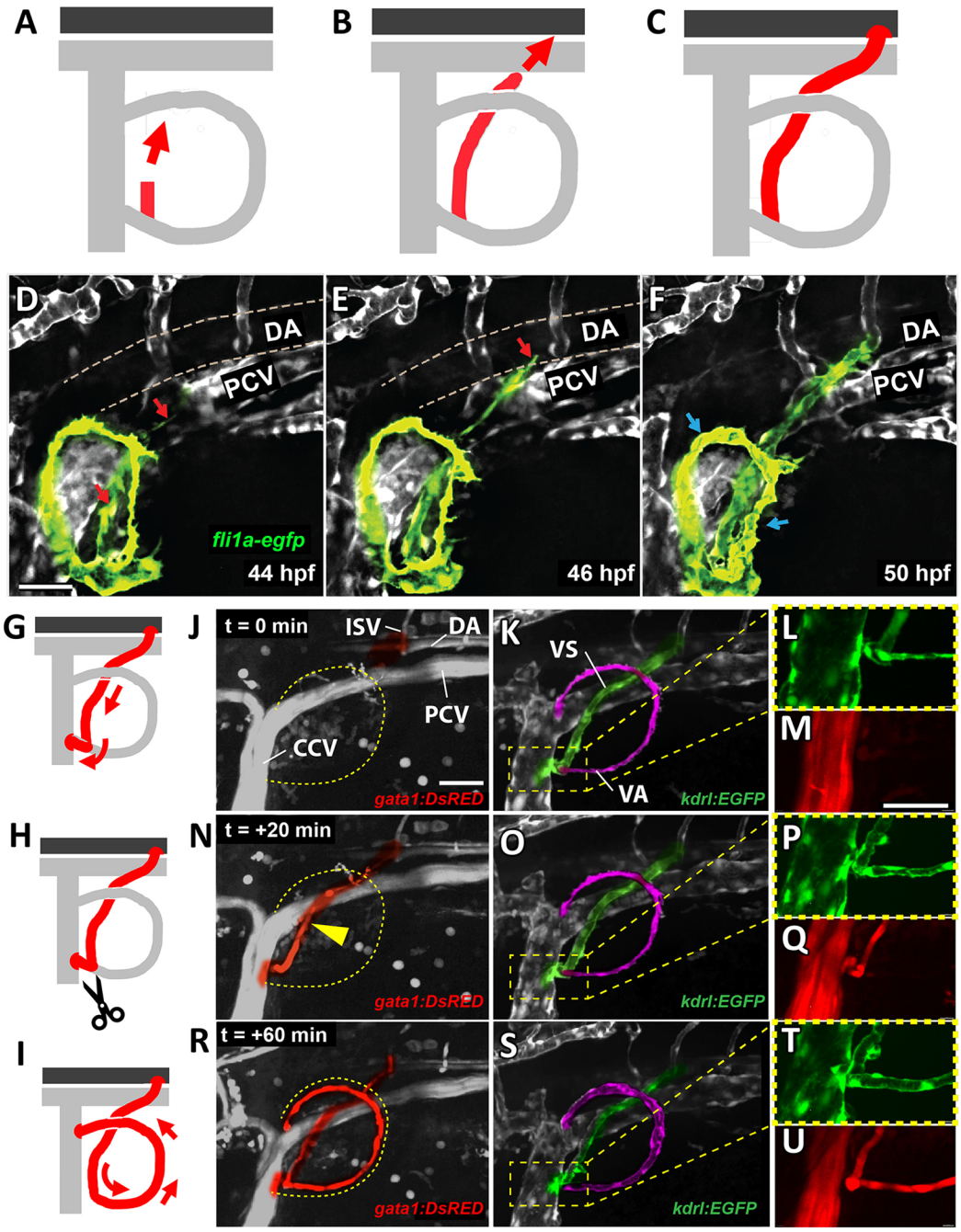

Fig. 4. Perfusion of the primitive pectoral artery. (A-C) Schematics illustrating stages in the formation of a connecting link between the primitive pectoral artery and the dorsal aorta, including formation of a new sprout from the base of the primitive pectoral artery where it connects ventrally to the CCV (A), medial and dorsal-caudal elongation of the new vessel segment (B), and linkage to the dorsal aorta at or near the base of the second ISV (C). (D-F) Confocal still images from a time-lapse series showing formation of a connecting link between the primitive pectoral artery and the dorsal aorta in a *Tg(fli1a:egfp)*^{y1} transgenic zebrafish at 44 hpf (D), 46 hpf (E) and 50 hpf (F). Red arrows indicate the migratory direction of the arterial sprout, and blue arrows indicate perfusion of the primary arc. See Movie 2 for the complete time-lapse series. (G-I) Schematics illustrating initial shunting of flow from the dorsal aorta through the base of the pectoral fin directly to the CCV (G), followed by disconnection of this shunt (H) and re-routing of flow through the primitive pectoral artery primary arc (I). (J-U) Confocal images from a time-lapse series of the pectoral fin and adjacent structures in a 2-day-old *Tg(gata1:dsred)*^{sd2Tg}*, Tg(kdrl:egfp)*^{s843} double-transgenic zebrafish, showing *Tg(gata1:dsred)*^{sd2Tg}-positive blood cells (J,M,N,Q,R,U) and *Tg(kdrl:egfp)*^{s843}-positive blood vessels (K,L,O,P,S,T). L, P and T show higher-magnification images of the boxed areas in K, O and S, respectively; likewise, M, Q and U are higher-magnification images of the corresponding areas in J, N and R, respectively. (J-M) t=0 min. The vascular link to the dorsal aorta has assembled (highlighted green in K) but has not yet lumenized, and no blood flow is present. (N-Q) t=+20 min. The connection to the dorsal aorta (highlighted green in O) has been completed and blood is now flowing through this connecting vessel (highlighted red in N and Q), but the blood is being shunted directly to the CCV without perfusing the primitive pectoral artery arc (highlighted magenta in K,O,S). (R-U) t=+60 min. The shunt to the CCV has disconnected and all blood flow has been rerouted into the primitive pectoral artery arc (highlighted red in R and U). Blood is only emptying into the CCV through the dorsal connection. See Movie 4 for the complete time-lapse series. See Movies 5 and 6 for higher-magnification images and 3D reconstructions of the ventral junction to the CCV and its shunting and then disconnection. Images shown are representative of data collected from 11 separate embryos. Yellow arrowhead in N indicates red blood cells flowing through the arterial sprout, and dashed yellow line encircles primary arc in J,N,R. DA, dorsal aorta; PCV, posterior cardinal vein; VA, ventral arm of the primary arc; VS, ventral arterial sprout. Scale bars: 30 µm (D-F); 40 µm (J-U).

Development (2022) 149, dev199676. doi:10.1242/dev.199676

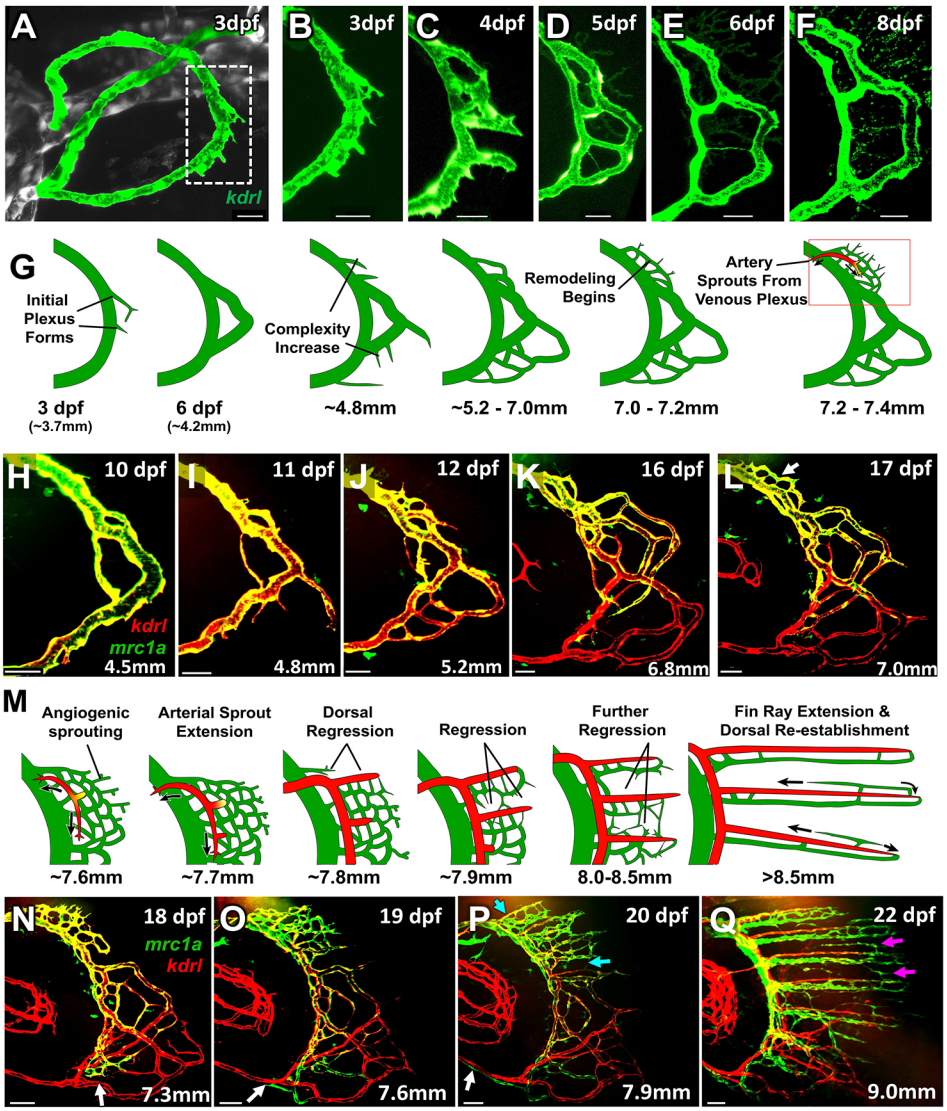

Fig. 5. Formation of the distal fin-ray vasculature. (A) Confocal image of the pectoral fin vessels (green) of a 3 dpf *Tg(kdrl:egfp)*^{s843} transgenic zebrafish (other surrounding vessels in gray). Dashed box indicates the approximate area imaged in B-F. (B-F) Confocal image time series of the pectoral fin distal vascular plexus of the same *Tg(kdrl:egfp)*^{s843} transgenic zebrafish as in A, imaged at 3 (B), 4 (C), 5 (D), 6 (E) and 8 (F) dpf. (G) Schematic illustrating the series of events occurring in the distal fin from ∼3 dpf to 18 dpf (up to ∼7.4 mm), encompassing the stages shown in A-L. (H-L) Confocal image time series of the pectoral fin distal vascular plexus of the same *Tg(kdrl:mcherry)*^{y206}, *Tg(mrc1a:egfp)*^{y251} double-transgenic larva imaged at 10 (H), 11 (I), 12 (J), 16 (K) and 17 (L) dpf (4.5, 4.8, 5.2, 6.8 and 7.0 mm in length, respectively). See Movie 9 for 3D reconstructions of the image in L. (M) Schematic illustrating the series of events occurring in the distal fin from ∼18 dpf to 22 dpf (7.3 to 9.0 mm), encompassing the stages shown in N-Q. (N-Q) Confocal image time series of the pectoral fin distal vascular plexus of the same *Tg(kdrl:mcherry)*^{y206}, *Tg(mrc1a:egfp)*^{y251} double-transgenic larva imaged at 18 (N), 19 (O), 20 (P) and 22 (Q) dpf (7.3, 7.6, 7.9 and 9.0 mm in length, respectively). See Movie 10 for 3D reconstructions of the images in N-Q. White arrows denote the ventral extent of the *Tg(mrc1a:egfp)*^{y251} blood vessel; cyan arrows denote rarified areas of the distal plexus; magenta arrows denote the new venous sprouts that will form the dorsal fin-ray vein. A 'time series' of the images in H-Q is shown in Movie 11. Images shown are representative of data collected from 12 separate larvae. Scale bars: 50 µm.

Using a *Tg(flt1:nmcherry)*^{skt7} transgenic line, these links were shown to have arterial identity (Fig. S2), and they begin to form when the larva is ∼9.0 mm long, extending from the medial proximal plexus to the artery at the base of each fin ray. The links also robustly express the *Tg(kdrl:mcherry)*^{y206} transgene but express little or no *Tg(mrc1a:egfp)*^{y251}, and begin to appear first on the dorsal-most portion of the pectoral fin. They form from sprouts that emerge from both the medial proximal plexus and from the artery at the base of the fin rays. Once the inter-plexus links have formed, they become new arterial feeds for the fin-ray 'arterial manifold'. No connections form with the 'venous manifold' at the base of the fin rays, consistent with an arterial identity for the new inter-plexus links.

Replacement of the venous dorsal arm of the primary arc vasculature

Observation of later stages in our pectoral fin imaging series also revealed that the dorsal arm of the primary vascular arc of the pectoral fin becomes replaced by a new vascular segment emerging from the CCV (Fig. 8H-L). At 7.00±0.17 mm, a *Tg(flt1:nmcherry)*^{skt7}-negative (Fig. S2), *Tg(mrc1a:egfp)*^{y251}-positive sprout emerges from the CCV ventral to the base of the original dorsal arm (Fig. 8I,J). This sprout enters the developing fin then moves distally at a greater depth than the dorsal arm (Fig. 8J), continuing until it reaches just below the dorsal-most fin ray, where it connects to the venous manifold for the distal fin-ray vasculature (Fig. 8K) to create a second venous drainage route to the CCV. By ∼9 mm the original primitive drainage route regresses (Fig. 8L), leaving only the new, deeper venous drain.

Pectoral fin vascular development is both similar to and distinct from that of the caudal fin

To explore whether our observations in the pectoral fin are generalizable to other fins, we used a *Tg(kdrl:mcherry)*^{y206}, *Tg(mrc1a:egfp)*^{y251} double-transgenic line to document the development of the vasculature of the caudal fin in five larvae, across multiple time points. The caudal fin and its vasculature develop over a much shorter time window than the pectoral fin, beginning at about 5.0 mm and forming an adult-like network by 7.2 mm (Fig. S9A). Caudal fin vascular development begins at the distal end of the dorsal aorta and posterior cardinal vein at ∼5.0 mm of larval length, with extension of a *Tg(kdrl:mcherry)*^{y206}, *Tg(mrc1a:egfp)*^{y251}-positive sprout ventrally into the fin fold (Fig. S9A, arrows). This sprout quickly begins to arborize into a *Tg(mrc1a:egfp)*^{y251}-positive plexus by 5.3 mm and is joined by a separate *Tg(kdrl:mcherry)*^{y206}-positive sprout that enters the fin

Development (2022) 149, dev199676. doi:10.1242/dev.199676

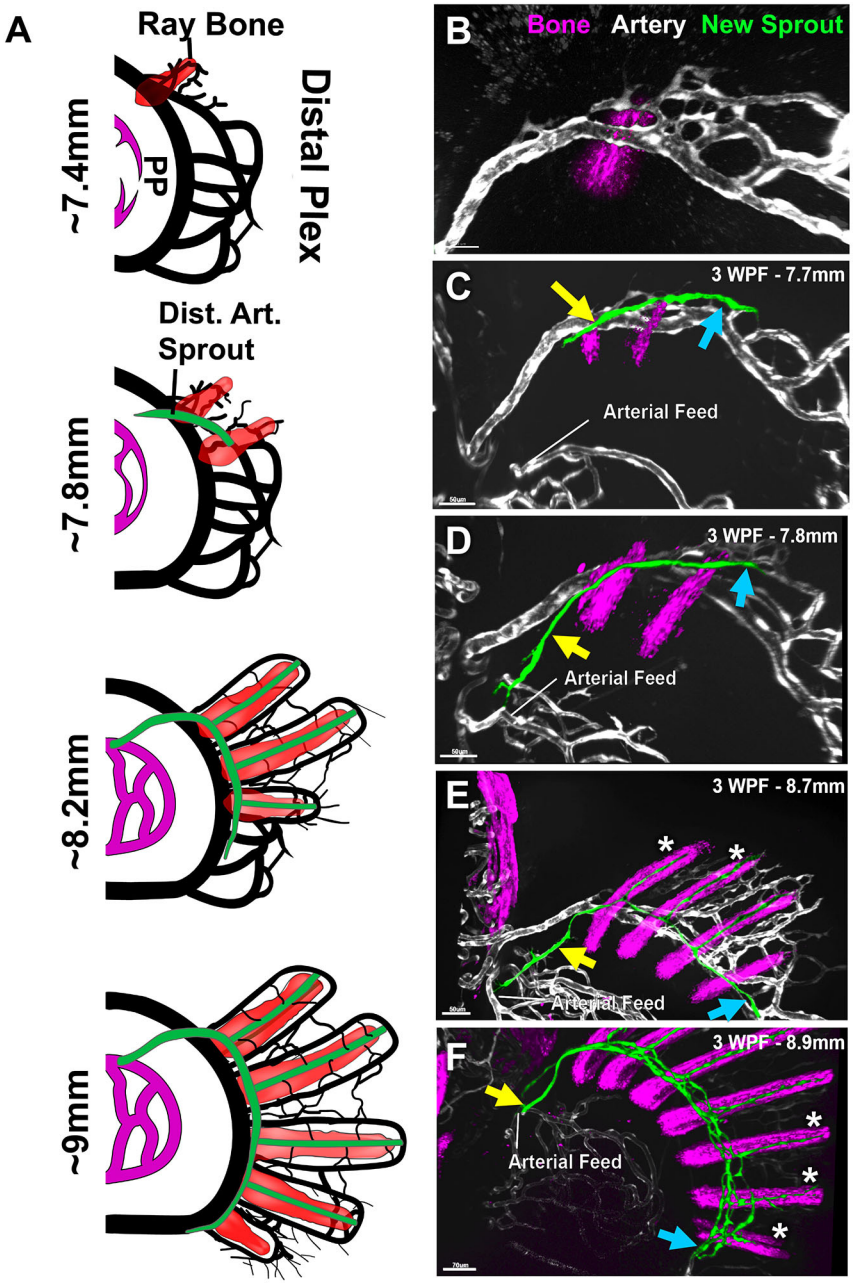

Fig. 6. The formation of the distal fin-ray arterial network begins as a sprout from the distal venous plexus. (A) Schematic of the relationship between the developing fin-ray bones (red) and developing fin-ray arterial network (green) that emerges from the pectoral fin distal vascular plexus (black) in ∼7.4-9.0 mm fish. (B-F) Confocal images of the pectoral fin distal vascular plexuses of separate 3-week-old *Tg(Ola.Sp7:mCherryEco.NfsB)*^{pd46}*, Tg(kdrl:egfp)*^{s843} double-transgenic zebrafish of different sizes, with *Tg(Ola.Sp7:mCherryEco.NfsB)*^{pd46}-positive condensing bone in magenta and *Tg(kdrl:egfp)*^{s843}-positive vessels in gray, except for the emerging fin-ray arterial network which is false-colored in green. Larvae shown are 7.4 mm, (B), 7.7 mm (C), 7.8 mm (D), 8.7 mm (E) and 8.9 mm (F) in length. Yellow and blue arrows indicate the proximal/dorsal and distal/ventral ends, respectively, of the developing fin-ray arterial vascular network. White asterisks indicate developing fin-ray arteries. Images shown are representative of data collected from six separate larvae. Dist. Art., distal arterial sprout; Distal Plex, distal plexus; PP, proximal plexus; WPF, weeks post-fertilization. Scale bars: 50 µm (B-E); 70 µm (F).

alongside the developing *Tg(mrc1a:egfp)*^{y251}-positive network. The separated arterial and venous networks continue to develop more complex arbors, and by 5.7 mm begin to align with the forming fin rays. At the same time that the ventrally directed arbors are developing, separate dorsal branches of the original arterial and venous sprouts (Fig. S9A, arrowheads) are extending caudally to form a temporary loop between the dorsal edge of the developing plexus and the tip of the posterior cardinal vein. This loop regresses by 6.5 mm, leaving a single artery feeding an arterial manifold and a single vein draining a venous manifold at the original entry point of the vasculature into the fin fold. Until about 6.5 mm, the vasculature and fin rays remain pointed at an angle roughly 45° ventral to that of the axial blood vessels, but starting at around 6.5 mm they begin to turn dorsally, such that they eventually point directly to the posterior by ∼7.2 mm (Fig. S9A). As in the pectoral fins, the caudal fin vascular network is divided into rostral/proximal muscular plexuses followed by an avascular zone, and then by separated arterial and venous manifolds (Fig. S9B, magenta and white arrowheads, respectively) supplying distal fin-ray arteries and veins (Fig. S9B,C).

DISCUSSION

Although growth of smaller vessels in adult animals and later in development is largely driven by the metabolic needs of local tissues, these vessels develop without reproducible patterns. The formation of major vessels during early development occurs stereotypically and is strongly guided by intrinsic genetic programs (Weinstein, 1999). Previous studies have shown that major vascular networks assembling during early development, such as the trunk intersegmental vessels (Childs et al., 2002; Gebala et al., 2016; Geudens et al., 2019; Isogai et al., 2001; Torres-Vázquez et al., 2004; Weijts et al., 2018), the hindbrain central arteries (Bussmann et al., 2011; Fujita et al., 2011; Ulrich et al., 2011; Zhang et al., 2018) and trunk lymphatic vessels (Cha et al.,

Development (2022) 149, dev199676. doi:10.1242/dev.199676

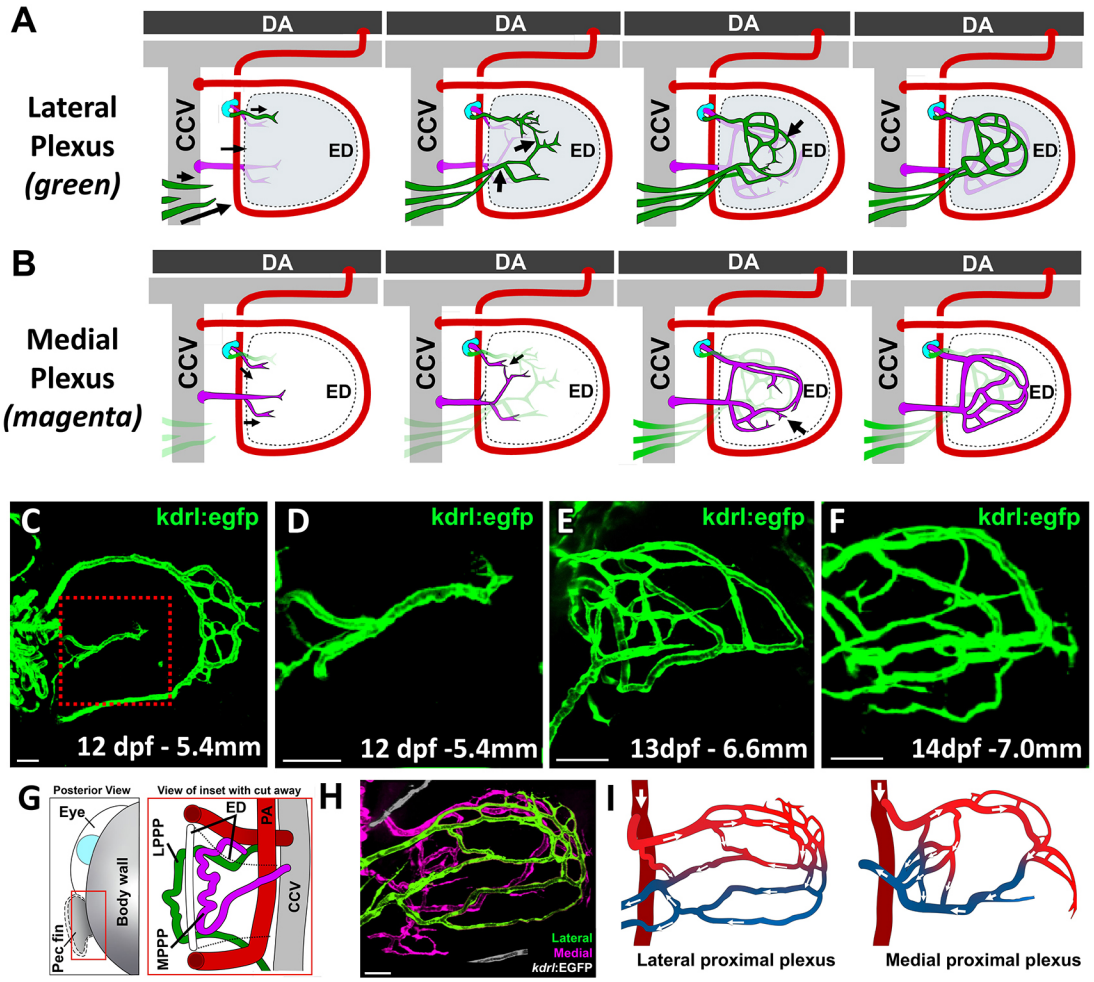

Fig. 7. Formation of the proximal vascular plexus. (A,B) Schematics illustrating the growth and development of the lateral (A; in green) and medial (B; in magenta) proximal plexuses in association with the pectoral fin endoskeletal disk, occurring approximately between 6 mm and 8 mm larval length. (C-F) Confocal images of the pectoral fin vasculature of three separate *Tg(kdrl:egfp)*^{s843} larvae at 12 dpf (C,D), 13 dpf, (E) and 14 dpf (F). The red box in C indicates the approximate location of the higher-magnification images in D-F, which show the proximal plexus in progressively older animals. (G) Schematic illustrating the positioning of the lateral and medial pectoral proximal plexuses, (LPPP and MPPP, respectively) on either side of the endoskeletal disk within the larval pectoral fin. (H) Confocal image of an 18 dpf *Tg(kdrl:egfp)*^{s843} fish with the medial and lateral proximal plexuses false-colored in magenta and green, respectively. Note the vessels in the lateral plexus that disappear rostrally from the image. See Movie 13 for D image reconstructions of the same confocal stack shown in H. (I) Schematics illustrating the morphology and circulatory flow patterns of the lateral (left) and medial (right) proximal vascular plexuses shown in the confocal image in H. Red and blue labeling facilitates visualization of vessels supplying or draining the plexuses. Images shown are representative of data collected from ten separate larvae. DA, dorsal aorta; ED, endoskeletal disk; PA, pectoral artery; Pec fin, pectoral fin. Scale bars: 50 µm.

2012; Jung et al., 2017; Okuda et al., 2012), all form in a highly stereotyped, choreographed manner, and that the patterning of these vascular networks is guided by genetically programmed guidance cues (Astin et al., 2014; Cha et al., 2012; Fujita et al., 2011; Goi and Childs, 2015; Lim et al., 2011; Torres-Vázquez et al., 2004; Ulrich et al., 2011). This study uses careful imaging of at least five separate animals for each step of early fin vascular development to document assembly of the major vessels of the pectoral fin vascular network and reveals a similarly stereotyped process (Fig. 9), suggesting that assembly of these vessels is also likely guided by as-yet-unidentified genetically programmed cues (see below).

Pectoral vessel formation begins with the emergence of dorsal and ventral sprouts from the CCV. The timing and positioning of these two sprouts and their growth along the fin margin is reproducible, suggesting directed guidance by defined cues. It has been previously noted that the primitive pectoral artery (aka 'circumferential blood vessel of the fin bud') grows precisely along the border between the proximal endoskeletal disk and the distal apical fold (AF) (Yano et al., 2012). Attractive cues from the AF coupled with repulsive cues from the endoskeletal disk could be sufficient to direct formation of two dorsally and ventrally positioned sprouts near the fin margin (see Fig. 3A-C). Many different potential guidance cues are found in the fin, including localized matrix proteins (Mateus et al., 2020) and angiogenic factors such as VEGFA, FGF and BMP; VEGF signaling has already been shown to be required for formation of the primitive pectoral artery (Habeck et al., 2002; Mateus et al., 2020; Nomura et al., 2006). However, further studies will be needed to define which cues are relevant and how they cooperate to direct primitive pectoral artery sprouting and pathfinding.

Once the circumferential loop of the primitive pectoral artery forms, it becomes connected to the dorsal aorta by long-distance angiogenic growth of a new vessel that follows a reproducible >200 µm long path along the side of the fish from the ventral base of the developing fin to the bottom of the second and third somites

Development (2022) 149, dev199676. doi:10.1242/dev.199676

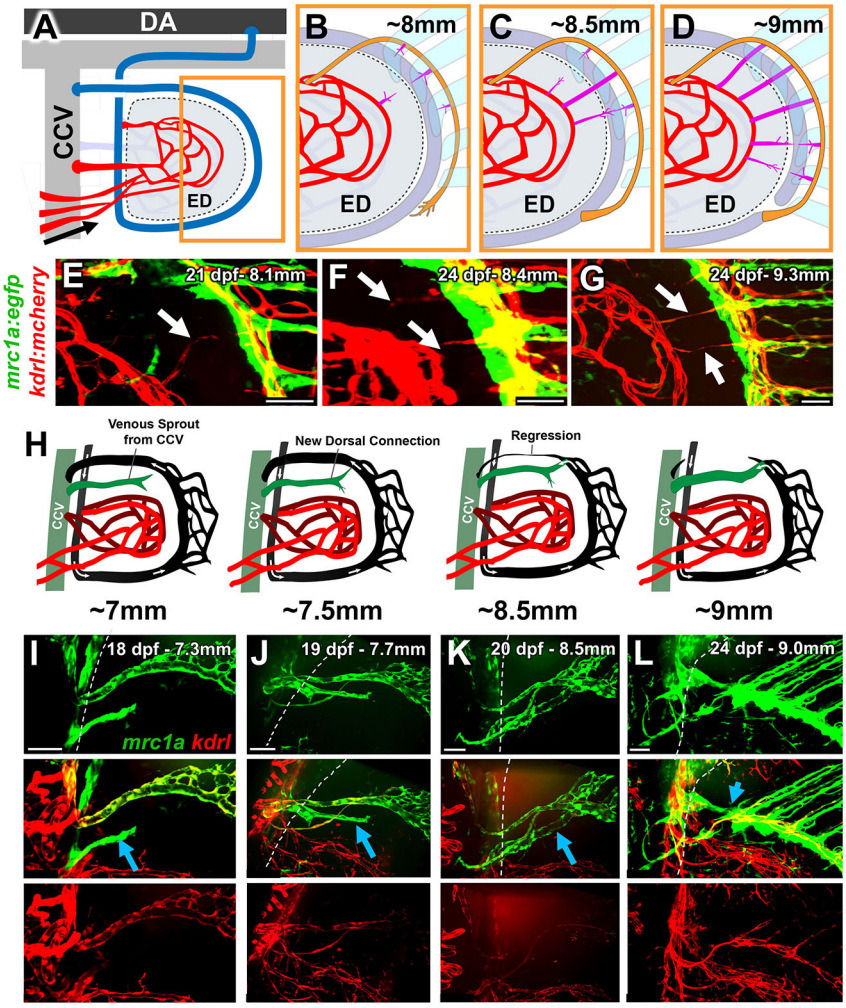

Fig. 8. Late-stage remodeling leading to the formation of the interplexus bridges and regression of the dorsal arm of the primary arc. (A-D) Schematics illustrating the formation of links between proximal and distal vascular plexuses. DA, dorsal aorta; ED, endoskeletal disk. (A) Simplified overview diagram of the pectoral fin vasculature at ∼3.5 weeks, showing the proximal plexus (red) and arterial feed for the distal fin-ray vascular network (orange). Orange box in A shows the approximate magnified area depicted in B-D. (B-D) Stages in the formation of inter-plexus links. (E-G) Confocal images of the inter-plexus region of the pectoral fin of three separate 3.5-week-old *Tg(kdrl:mcherry)*^{y206}, *Tg(mrc1a:egfp)*^{y251} double-transgenic zebrafish, showing the formation of arterial [*Tg(kdrl:mcherry)*^{y206} positive, *Tg(mrc1a:egfp)*^{y251} negative] links (white arrows) between the medial proximal plexus (left) and the arterial fin-ray vascular plexus (right). (H) Schematics of the replacement of the dorsal arm of the primary arc. (I-L) Confocal images of the dorsal arm of the pectoral fin primary arc showing the early *Tg(mrc1a:egfp)*^{y251}-positive, *Tg(kdrl:mcherry)*^{y206}-negative sprout (I), the elongation of the sprout toward the distal plexus (J), two lumenized connections leading to the CCV (K), and the regression of the original dorsal arm of the primary arc, leaving only the new, deeper connection (L). Cyan arrows emphasize the new venous sprout in each panel. Dashed lines indicate the common cardinal vein. Images shown in E-G and I-L are representative of data collected from 12 separate larvae. Scale bars: 50 µm.

(Fig. 4A-C). This vessel connects to the dorsal aorta at the base of the second intersegmental artery (Fig. 4A-C). Our preliminary findings suggest that Notch signaling is required for correct formation of this new ventral arterial segment, because treatment with either of two different Notch inhibitors just prior to the emergence of the ventral arterial sprout leads to incomplete or stalled formation of this segment and/or its inappropriate connection to the CCV rather than to the dorsal aorta (Fig. S5). Notch signaling already has well-documented roles in arterio-venous fate determination and ‘tip cell’ selection in the vasculature, but further work will be needed to clarify its specific role in this context. It seems likely that additional local cues also help direct the growth of this vessel along its path. Several nerves innervate the pectoral fin (Banerjee et al., 2015; Okamoto and Kuwada, 1991b), but careful imaging of *Tg(kdrl:egfp)*^{s843}, *Tg(elavl3:mCherry)*^{nia02tg} double-transgenic fish shows that their paths are dissimilar from that of the pectoral fin artery and they are unlikely to be guiding each other or being directed by the same cues (Fig. S3; Movie 3). Although the nearby axons do not seem instructive, other anatomical landmarks in this area, such as the anterior pronephros, may play a role in this vessel’s guidance.

Once the ventral segment has connected to the dorsal aorta, blood flow to the pectoral fin begins, although it often bypasses the circumferential loop of the primitive pectoral artery and drains directly into the CCV via a ventral shunt (Fig. 4G). However, this shunt usually disconnects within an hour and blood flow becomes re-routed properly around the circumferential loop (Fig. 4H,I). A number of studies have shown that flow is a crucial signal for vascular remodeling (Isogai et al., 2001; Kochhan et al., 2013; Lucitti et al., 2007), with high flow rates resulting in vessel enlargement/retention and low flow leading to vessel size decrease and/or regression (Baeyens and Schwartz, 2016; Kamiya and Togawa, 1980; Langille, 1996; Langille and O’Donnell, 1986; Tuttle et al., 2001). However, unchecked vessel growth resulting from increased flow would lead to non-functioning vascular networks (Pries et al., 2010), and recent studies have reported TGFβ and Notch pathways as mechanisms limiting vessel growth and/or directing/restricting vessel connections (Ito et al., 2009; Phng et al., 2009; Suchting et al., 2007). In the developing pectoral fin, the ventral shunt to the CCV has robust flow, but is nevertheless pruned in order to send blood through a circumferential vessel that has no flow and initially may not even be fully lumenized, instead following a longer, likely higher-resistance, flow path. This suggests that ventral fin shunt disconnection and re-routing of blood flow through the circumferential pectoral vasculature is hardwired by specific programmed disconnection cues, not flow dynamics. Additionally, our time-lapse imaging experiments show that CCV shunt pruning occurs via endothelial cell rearrangements rather than by death of endothelial cells in the shunt region (Fig. S4C,D; Movies 7, 8). Further studies will be needed to elucidate fully the mechanisms involved in this unusual pruning event.

Development (2022) 149, dev199676. doi:10.1242/dev.199676

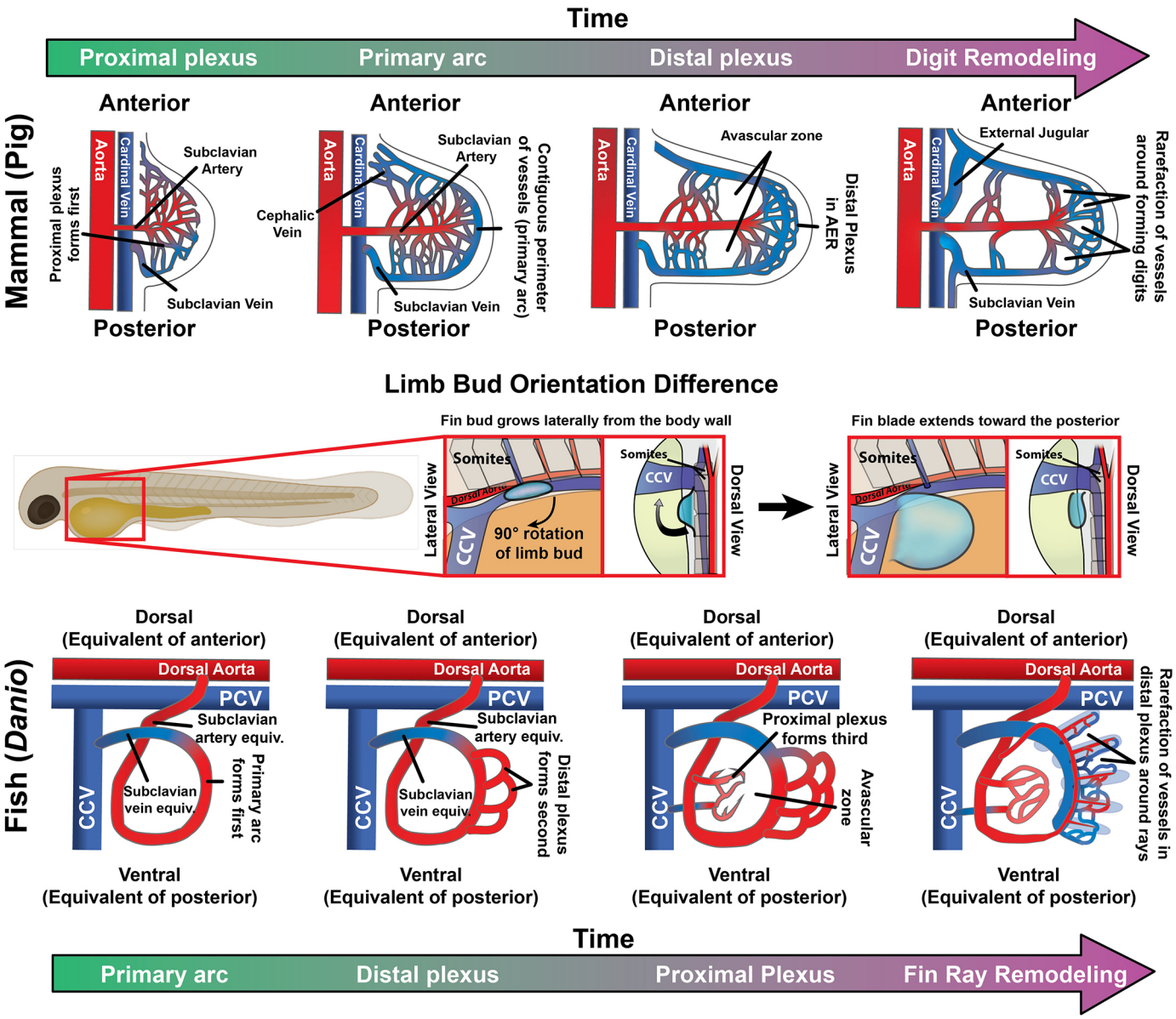

Fig. 9. Schematic of pectoral fin vascular development. Schematics comparing broad stages of forelimb vasculature development in zebrafish and mammals. (A) In mammalian forelimbs, vascular development begins with initial growth of a limb bud-associated capillary plexus and formation of a single predominant arterial feed, the subclavian artery, followed by assembly of a complete circumferential vessel draining to the subclavian vein (and eventually into the cardinal vein). This primitive network expands as the limb grows out, elaborating mid-limb and distal (AER-associated) vascular plexuses separated by an avascular zone. Finally, the distal-most portion of the limb vasculature remodels around the forming digits. (B) In comparison to mammals, the fish limb bud is rotated 90° so that the anterior portion of the fin bud is pointed dorsally instead (the *z*-axis, from a lateral view of the embryo as in B). A, anterior; P, posterior. (C) In the zebrafish pectoral fin, a circumferential vessel forms first, drawing arterial blood from the dorsal aorta as in mammals but draining into the CCV rather than the (posterior) cardinal vein as in mammals. This circumferential vessel (the primary arc) is analogous to the subclavian artery and vein of mammals. Next, a distal AER-associated plexus forms followed closely by formation of a proximal plexus, leaving a mid-limb avascular zone as in mammals. Lastly, the distal plexus remodels to generate the fin-ray vasculature. PCV, posterior cardinal vein.

Formation of an elaborate distal plexus in the fin begins at ∼12 dpf (Fig. 5). As fin-ray bones begin to condense, this distal plexus undergoes remodeling in a dorsal-to-ventral progression in coordination with dorsal-to-ventral development of successive fin rays. This series of events resembles chondrogenesis-associated remodeling of a distal vascular plexus in the developing human forelimb (Bates et al., 2002; Rodríguez-Niedenführ et al., 2001). In the fish, there is minimal flow through much of this plexus during early remodeling stages, suggesting that flow is not a significant driver of this process. Again, it seems likely that signals associated with developing bone or bone-associated cells provide cues for fin-ray vascular development. During regeneration of zebrafish fins, chemokine signals associated with newly forming bone appear to be important for directing vascular cell migration and organization into new fin ray-associated vessels (Sivaraj and Adams, 2016; Thorimbert et al., 2015; Xu et al., 2014). However, it is unclear whether chemokine signaling plays a similar role in directing vessel remodeling during normal fin development. It is also unclear whether distal plexus and fin-ray vessels play a role in directing development of fin-ray bones (Akiva et al., 2019). The influence each of these tissues has on the development of the other could be tested by disruption of fin-associated bone or vessels; the

Development (2022) 149, dev199676. doi:10.1242/dev.199676

fin-specific manipulations needed to avoid the confounding effects of systemic tissue disruption are, at present, difficult or impossible to carry out in the fish.

Remodeling of the distal vascular plexus in the fin to form the complex adult fin-ray vasculature also involves formation of separate, parallel arterial and venous fin-ray vascular networks (Fig. 6). The initial sprout for the nascent arterial network emerges reliably in the vicinity of the most dorsal pectoral fin-ray bone. It grows ventrally through the fin, sending new branches distally as it reaches each successive fin ray. This suggests that the developing fin rays provide cues not just for vessel growth but also for vessel 'arterialization' in the central channel between the paired fin-ray bones where fin-ray arteries form. Fibroblasts and actinotrichia in the center channel of the fin ray could provide cues (Akiva et al., 2019; Huang et al., 2009), such as chemokines or VEGF, which promotes both vessel growth and, at higher levels, arterial differentiation (Weinstein and Lawson, 2002).

Although they are similar in many ways, there are some interesting differences between pectoral fin and caudal fin vascular development. Like the pectoral fins, the caudal fin has a proximal plexus within the muscular base of the fin, followed by a largely avascular zone and then a caudal fin-ray vascular network (Fig. S9C; Huang et al., 2003; Xu et al., 2014). As in the pectoral fin, there are also large parallel arterial and venous manifolds running along the base of the fin rays (Fig. S9B). However, the caudal fin-ray arterial manifold grows into the fin as an artery-derived network instead of emerging from a vein as the pectoral fin vasculature does. The caudal fin-ray vasculature also develops concurrently with condensation of the fin-ray bones, without having a persistent, lumenized plexus that subsequently undergoes remodeling with the developing fin rays (Fig. S9A).

There are also strong parallels between the vascular architecture of the fish pectoral fin and the developing mammalian forelimb. Major steps required for assembly of both vascular networks are shared, although their temporal order differs (Fig. 9). In the pectoral fin, formation of a primary vascular arc is followed by a distal plexus and emergence of a proximal plexus, and later by fin-ray vascular network assembly. In the developing forelimb, a proximal plexus forms initially, remodeling at its outer edge to form a primary arc, followed by emergence of an avascular zone and a distal plexus that undergoes subsequent distal remodeling to form vessels associated with the developing digits.

Together, our findings provide a detailed description of pectoral fin vascular network assembly (Fig. S10). It is worth noting that although major patterns of vascular development are highly stereotyped and highly conserved, there can be substantial variability in the precise positioning of individual vessels, vessel branches or vessel sprouts. In our descriptions and diagrams, we have sought to capture the major patterns. In the future, understanding the molecular cues and mechanisms directing formation of these vascular networks will require additional in-depth studies employing cutting-edge tools and methods not yet available in the fish, such as tissue-specific optogenetic activation to specifically manipulate expression in the fin or in fin bone, endothelium, or other fin cell or tissue types. Although extremely challenging, successful completion of these future studies will not only provide important insights into mechanisms directing the assembly of vascular networks during development, but also could potentially provide new therapeutic targets for cardiovascular disease, vascular malformations, and cancer.

MATERIALS AND METHODS

Fish husbandry and fish strains

Fish were housed in a large zebrafish-dedicated recirculating aquaculture facility (four separate 22,000 l systems) in 6 l and 1.8 l tanks. Fry were fed rotifers and adults were fed Gemma Micro 300 (Skretting) once per day. Water quality parameters were routinely measured, and appropriate measures were taken to maintain water quality stability (water quality data available upon request). The following transgenic fish lines were used for this study: *Tg(fli1a:egfp)*^{y1} (Lawson and Weinstein, 2002), *Tg(mrc1a:egfp)*^{y251} (Jung et al., 2017), *Tg(kdrl:mcherry)*^{y206} (Gore et al., 2011), *Tg(kdrl:egfp)*^{s843} (Jin et al., 2005), *Tg(elavl3:mCherry)*^{nia02tg} (Won et al., 2011), *Tg(kdrl:nlsmcherry)*^{y173} (Fujita et al., 2011), *Tg(gata1:dsred)*^{sd2Tg} (Traver et al., 2003), *Tg(flt1:nmcherry)*^{skt7} (Carretero-Ortega et al., 2019), Tg(*flt1:egfp-sv40)*^{skt8} (this study), *Tg(Ola.Sp7:mCherryEco.NfsB)*^{pd46} [also known as *Tg(sp7:mcherry-ntr)*, previously known as *Tg(osterix:mCherry-NTRo)*^{pd46}; Singh et al., 2012]. Some of the lines imaged were maintained and imaged in a *casper* (*roy, nacre* double mutant) (White et al., 2008) genetic background in order to increase clarity for visualization of the pectoral fin; this reduces the problem of melanocytes that develop on the fin itself as well as around the embryonic kidney. This study was performed in an AAALAC-accredited facility under an active research project overseen by the NICHD ACUC, Animal Study Proposal #18-015.

Image acquisition

Confocal images were acquired primarily with a Nikon Ti2 inverted microscope with Yokogawa CSU-W1 spinning disk confocal (Hamamatsu Orca Flash 4 v3 camera with the following Nikon objectives: 4× Air 0.2 N.A., 10× Air 0.45 N.A., 20× water immersion 0.95 N.A., 25× silicone immersion 1.05 N.A., 40× water immersion 1.15 N.A., 60× water immersion 1.20 N.A.). A minority of images were taken using a Zeiss 880 with Fast Airyscan using a 40× Water Immersion or 10× Air lens. Stereo microscope images were acquired using a Leica M205 microscope using MultiFocus focus stacking, or on a Leica M165 microscope with Leica DFC 7000T camera. For bone autofluorescence, fish were illuminated with 405 nm laser excitation and imaged for 461 nm fluorescence emission (Castranova et al., 2021a). Time-lapse imaging for nuclear tracking and caudal plexus still images were captured on Nikon CSU-A1 scanning confocal using the resonance scanner and Nikon image.ai denoising, and a 20× water immersion 0.95 N.A. or 40× water immersion 1.15 N.A. objective.

Nuclear tracking

3D reconstructions of the time-lapse imaging acquired as mentioned above was oriented as in Fig. S4D and made into a 2D movie by maximum intensity projection. This movie was analyzed manually, tracking each nucleus until the end of the movie or until they exited the field of view or descended into the CCV. Any ambiguity in position of a nucleus because of the 2D perspective of the movie was resolved by returning to the relevant time point in the 3D source data and disambiguating the nuclear position. The selection of nuclei analyzed was based on their presence in, or entering, the three-way junction through the time course. Two representative videos were imported into Adobe Premiere/After effects and nuclei were false-colored to illustrate their movements.

Image processing

Images were processed using Nikon Elements and Photoshop. Unless otherwise specified, maximum intensity projections of confocal stacks are shown. Focus stacking of confocal images with DIC was performed using Nikon Elements EDF (Extended Depth of Focus). 3D rotation movies and time-lapse movies were made using Nikon Elements and exported to Adobe Premiere Pro CC 2019. Adobe Premiere Pro CC 2019 and Adobe Photoshop CC 2019 were used to add labels and arrows to movies and to add coloring or pseudocoloring. Schematics were made using Adobe Photoshop CC 2019 and Adobe Illustrator CC 2019.

Embryonic Notch inhibitor treatments

Double-transgenic *Tg(mrc1a:egfp)*^{y251}, *Tg(kdrl:mcherry)*^{y206} embryos at ∼30 hpf were carefully staged by CCV and central artery progression prior

Development (2022) 149, dev199676. doi:10.1242/dev.199676

to the first appearance of the pectoral fin primary arc sprouts. These embryos were separated into six-well Costar plates at a density of 20 larvae per well and bathed in equal volumes of E3 supplemented with 400 µl DMSO only, or DAPT or LY411575 to a final concentration of 50 µM, or 30/50 µM, respectively [similar to the methods of Dirian et al. (2014)]. After 24 h of inhibitor treatment, embryos were embedded in 1.5% E3-agarose and imaging was performed with a Nikon CSU-A1 scanning confocal using the resonance scanner and Nikon image.ai denoising, as above. Resulting 3D reconstructions were then analyzed for completion and length of the ventral arterial sprout. Two biological replicates, on different days, were conducted on embryos from single clutches of eggs and split into roughly equal portions of approximately 9-12 embryos and treated with inhibitors as above. All embryos were mounted and assessed for vascular morphology and statistics. Student's *t*-test was used for Fig. S4G.

Fluorescence quantification

Images quantified for relative fluorescence were generated using Imaris 9.1 by taking a flattened image of a max intensity 3D reconstruction of a *z*-stack. The flattened images were then quantified in Adobe Photoshop CC2019 by selecting relevant vascular beds in the indicated regions and measuring the average pixel intensity. To remove the influence of varying vascular density and region size, non-vascular pixels were excluded by threshold-including pixels with intensity numbers above background noise.

Time-lapse imaging and shunt quantification

Fish from 2 dpf to 4 dpf were imaged live by anesthetizing them in 168 mg/l tricaine in system water and mounting them in the common lateral position in 0.8% low melting point agarose in a 35 mm glass-bottomed Petri dish (MatTek, P35-1.5-14-C). These fish were imaged at the indicated time intervals over a 36 h period on the Nikon W1 confocal, as described above. Shunting was quantified from live time-lapse imaging every 20 min of 12 *Tg(kdrl:egfp)*^{s843}*, Tg(gata1:dsred)*^{sd2Tg} double-transgenic animals imaged from ∼48 hpf (before flow onset) until 66 hpf. *Tg(gata1:dsred)*^{sd2T}-positive red blood cells were monitored to determine whether they were shunting to the CCV or passing through the full primary arc of the primitive pectoral artery. Nuclear tracking was quantified from live time-lapse imaging every 20 min of 12 *Tg(kdrl:egfp)*^{s843}*, Tg(kdrl:nlsmcherry)*^{y173} double-transgenic animals imaged from ∼42 hpf (before flow onset) until ∼60 hpf.

Mounting and imaging of later larval and adult fish

To image larval zebrafish at stages from ∼5 dpf to 1 month of age, fish were anesthetized in 168 mg/l tricaine in E3 media and mounted laterally in 0.8% low melting point agarose in a 35 mm glass-bottomed Petri dish (MatTek, P35-1.5-14-C) for pectoral fin imaging. In some experiments, animals were pre-anesthetized in 79 mg/l tricaine in system water; the fish were kept responsive to touch to await mounting, then transferred to 126 mg/l tricaine in system water for mounting and imaging as described above. Animals repeatedly imaged at multiple time points were gently recovered from the agarose and returned to fresh E3 where they were gently continuously swirled until conscious and actively swimming and then returned to their tank on the system.

Fish older than 1 month were mounted for imaging by anesthetizing them in 126-168 mg/l tricaine in system water and then placed into a slit in a sponge (Jaece Identi-Plugs L800-D) moistened with tricaine water, cut into a rectangle to fit inside a single-chamber imaging dish (Lab-TekII, 155360). The sponge containing the fish was placed 'belly-down' into the imaging chamber and the chamber was filled with tricaine water. Fish lengths are reported as standard length from the tip of the snout to most proximal part of the fork between caudal fin lobes. For visualization of blood flow in Movie 1, fish were intubated as described by Castranova et al. (2022), and mounted as above for time-lapse imaging.

Animals repeatedly imaged at multiple time points were recovered from the agarose after collecting images at each time point and returned to fresh E3.

Acknowledgements

We thank Andrew Davis, Van Pham, Jordyn Greenbaum and Biniam Sileshi, as well as the rest of the current and former Weinstein Lab members who have given their invaluable time to help prepare this manuscript for publication.

Competing interests

The authors declare no competing or financial interests.

Author contributions

Conceptualization: S.M.P., S.M.K., B.M.W.; Methodology: S.M.P., D.M.C., B.M.W.; Validation: S.M.P.; Formal analysis: S.M.P.; Investigation: S.M.P., D.M.C., S.M.K., M.C.B., B.M.W.; Resources: J.M., J.T.-V., B.M.W.; Data curation: S.M.P., B.M.W.; Writing - original draft: S.M.P., B.M.W.; Writing - review & editing: S.M.P., B.M.W.; Visualization: S.M.P., D.M.C., B.M.W.; Supervision: S.M.P., B.M.W.; Project administration: B.M.W.; Funding acquisition: B.M.W.

Funding

This work was supported by the intramural program of the Eunice Kennedy Shriver National Institute of Child Health and Human Development (ZIA-HD001011 and ZIA-HD008915, to B.M.W.). Open Access funding provided by the National Institutes of Health. Deposited in PMC for immediate release.

References

Abu-Daya, A., Nishimoto, S., Fairclough, L., Mohun, T. J., Logan, M. P. O. and Zimmerman, L. B. (2011). The secreted integrin ligand nephronectin is necessary for forelimb formation in Xenopus tropicalis. *Dev. Biol.* **349**, 204-212. doi:10.1016/j.ydbio.2010.10.015

Akiva, A., Nelkenbaum, O., Schertel, A., Yaniv, K., Weiner, S. and Addadi, L. (2019). Intercellular pathways from the vasculature to the forming bone in the zebrafish larval caudal fin: Possible role in bone formation. *J. Struct. Biol.* **206**, 139-148. doi:10.1016/j.jsb.2019.02.011

Astin, J. W., Haggerty, M. J. L., Okuda, K. S., Le Guen, L., Misa, J. P., Tromp, A., Hogan, B. M., Crosier, K. E. and Crosier, P. S. (2014). Vegfd can compensate for loss of Vegfc in zebrafish facial lymphatic sprouting. *Development* **141**, 2680-2690. doi:10.1242/dev.106591

Aydogan, V., Lenard, A., Denes, A. S., Sauteur, L., Belting, H.-G. and Affolter, M. (2015). Endothelial cell division in angiogenic sprouts of differing cellular architecture. *Biol. Open* **4**, 1259-1269. doi:10.1242/bio.012740

Baeyens, N. and Schwartz, M. A. (2016). Biomechanics of vascular mechanosensation and remodeling. *Mol. Biol. Cell* **27**, 7-11. doi:10.1091/mbc.E14-11-1522

Banerjee, S., Hayer, K., Hogenesch, J. B. and Granato, M. (2015). Zebrafish foxc1a drives appendage-specific neural circuit development. *Dev.* **142**, 753-762. doi:10.1242/dev.115816

Bates, D., Taylor, G. I. and Newgreen, D. F. (2002). The pattern of neurovascular development in the forelimb of the quail embryo. *Dev. Biol.* **249**, 300-320. doi:10.1006/dbio.2002.0771

Betz, C., Lenard, A., Belting, H.-G. and Affolter, M. (2016). Cell behaviors and dynamics during angiogenesis. *Development* **143**, 2249-2260. doi:10.1242/dev.135616

Bremer, J., Skinner, J. and Granato, M. (2017). A small molecule screen identifies in vivo modulators of peripheral nerve regeneration in zebrafish. *PLoS ONE* **12**, e0178854. doi:10.1371/journal.pone.0178854

Bussmann, J., Wolfe, S. A. and Siekmann, A. F. (2011). Arterial-venous network formation during brain vascularization involves hemodynamic regulation of chemokine signaling. *Development* **138**, 1717-1726. doi:10.1242/dev.059881

Carretero-Ortega, J., Chhangawala, Z., Hunt, S., Narvaez, C., Menéndez-González, J., Gay, C. M., Zygmunt, T., Li, X. and Torres-Vázquez, J. (2019). GIPC proteins negatively modulate Plexind1 signaling during vascular development. *eLife* **8**, e30454. doi:10.7554/eLife.30454

Castranova, D., Samasa, B., Venero Galanternik, M., Jung, H. M., Pham, V. N. and Weinstein, B. M. (2021a). Live imaging of intracranial lymphatics in the zebrafish. *Circ. Res.* **128**, 42-58. doi:10.1161/CIRCRESAHA.120.317372

Castranova, D., Samasa, B., Galanternik, M. V., Gore, A. V, Goldstein, A. E., Park, J. S. and Weinstein, B. M. (2022). Long-term imaging of living adult zebrafish. *Development* **149**, dev.199667. doi:10.1242/dev.1999667

Cha, Y. R., Fujita, M., Butler, M., Isogai, S., Kochhan, E., Siekmann, A. F. and Weinstein, B. M. (2012). Chemokine signaling directs trunk lymphatic network formation along the preexisting blood vasculature. *Dev. Cell* **22**, 824-836. doi:10.1016/j.devcel.2012.01.011

Chiang, C., Litingtung, Y., Harris, M. P., Simandl, B. K., Li, Y., Beachy, P. A. and Fallon, J. F. (2001). Manifestation of the limb prepattern: Limb development in the absence of sonic hedgehog function. *Dev. Biol.* **236**, 421-435. doi:10.1006/dbio.2001.0346

Childs, S., Chen, J.-N., Garrity, D. M. and Fishman, M. C. (2002). Patterning of angiogenesis in the zebrafish embryo. *Development* **129**, 973-982. doi:10.1242/dev.129.4.973

Crossley, P. H., Minowada, G., MacArthur, C. A. and Martin, G. R. (1996). Roles for FGF8 in the induction, initiation, and maintenance of chick limb development. *Cell* **84**, 127-136. doi:10.1016/S0092-8674(00)80999-X

Dirian, L., Galant, S., Coolen, M., Chen, W., Bedu, S., Houart, C., Bally-Cuif, L. and Foucher, I. (2014). Spatial regionalization and heterochrony in the formation

of adult pallial neural stem cells. *Dev. Cell* **30**, 123-136. doi:10.1016/j.devcel.2014.05.012

Dodo, Y., Chatani, M., Azetsu, Y., Hosonuma, M., Karakawa, A., Sakai, N., Negishi-Koga, T., Tsuji, M., Inagaki, K., Kiuchi, Y. et al. (2020). Myelination during fracture healing in vivo in myelin protein zero (p0) transgenic medaka line. *Bone* **133**, 115225. doi:10.1016/j.bone.2020.115225

Fujita, M., Cha, Y. R., Pham, V. N., Sakurai, A., Roman, B. L., Silvio Gutkind, J. and Weinstein, B. M. (2011). Assembly and patterning of the vascular network of the vertebrate hindbrain. *Development* **138**, 1705-1715. doi:10.1242/dev.058776

Gebala, V., Collins, R., Geudens, I., Phng, L.-K. and Gerhardt, H. (2016). Blood flow drives lumen formation by inverse membrane blebbing during angiogenesis in vivo. *Nat. Cell Biol.* **18**, 443-450. doi:10.1038/ncb3320

Geudens, I., Coxam, B., Alt, S., Gebala, V., Vion, A.-C., Meier, K., Rosa, A. and Gerhardt, H. (2019). Artery-vein specification in the zebrafish trunk is pre-patterned by heterogeneous Notch activity and balanced by flow-mediated fine-tuning. *Dev.* **146**, 1-13. doi:10.1242/dev.181024

Goi, M. and Childs, S. J. (2015). Patterning mechanisms of the sub-intestinal venous plexus in zebrafish. *Dev. Biol.* 409, 114-128. doi:10.1016/j.ydbio.2015.10.017

Goldfarb, C. A., Shaw, N., Steffen, J. A. and Wall, L. B. (2017). The prevalence of congenital hand and upper extremity anomalies based upon the New York Congenital Malformations Registry. *J. Pediatr. Orthop.* **37**, 144-148. doi:10.1097/BPO.0000000000000748

Gore, A. V., Swift, M. R., Cha, Y. R., Lo, B., McKinney, M. C., Li, W., Castranova, D., Davis, A., Mukouyama, Y.-S. and Weinstein, B. M. (2011). Rspo1/wnt signaling promotes angiogenesis via vegfc/vegfr3. *Development* **138**, 4875-4886. doi:10.1242/dev.068460

Gore, A. V., Monzo, K., Cha, Y. R., Pan, W. and Weinstein, B. M. (2012). Vascular development in the zebrafish. *Cold Spring Harb. Perspect. Med.* **2**, a006684. doi:10.1101/cshperspect.a006684

Grandel, H. and Brand, M. (2011). Zebrafish limb development is triggered by a retinoic acid signal during gastrulation. *Dev. Dyn.* **240**, 1116-1126. doi:10.1002/dvdy.22461

Grandel, H. and Schulte-Merker, S. (1998). The development of the paired fins in the zebrafish (Danio rerio). *Mech. Dev.* **79**, 99-120. doi:10.1016/S0925-4773(98)00176-2

Gros, J. and Tabin, C. J. (2014). Vertebrate limb bud formation is initiated by localized epithelial-to-mesenchymal transition. *Science (80-.)* **343**, 1253-1256. doi:10.1126/science.1248228

Habeck, H., Odenthal, J., Walderich, B., Maischein, H.-M., Schulte-Merker, S. and **Tübingen 2000 Screen Consortium**. (2002). Analysis of a zebrafish VEGF receptor mutant reveals specific disruption of angiogenesis. *Curr. Biol.* **12**, 1405-1412. doi:10.1016/S0960-9822(02)01044-8

Hasan, S. S., Tsaryk, R., Lange, M., Wisniewski, L., Moore, J. C., Lawson, N. D., Wojciechowska, K., Schnittler, H. and Siekmann, A. F. (2017). Endothelial Notch signalling limits angiogenesis via control of artery formation. *Nat. Cell Biol.* **19**, 928-940. doi:10.1038/ncb3574

Huang, C.-C., Lawson, N. D., Weinstein, B. M. and Johnson, S. L. (2003). reg6 is required for branching morphogenesis during blood vessel regeneration in zebrafish caudal fins. *Dev. Biol.* **264**, 263-274. doi:10.1016/j.ydbio.2003.08.016

Huang, C.-C., Wang, T.-C., Lin, B.-H., Wang, Y.-W., Johnson, S. L. and Yu, J. (2009). Collagen IX is required for the integrity of collagen II fibrils and the regulation of vascular plexus formation in Zebrafish caudal fins. *Dev. Biol.* **332**, 360-370. doi:10.1016/j.ydbio.2009.06.003

Isogai, S., Horiguchi, M. and Weinstein, B. M. (2001). The vascular anatomy of the developing zebrafish: An atlas of embryonic and early larval development. *Dev. Biol.* **230**, 278-301. doi:10.1006/dbio.2000.9995

Ito, C., Akimoto, T., Ioka, T., Kobayashi, T. and Kusano, E. (2009). TGF-β inhibits vascular sprouting through TGF-β type I receptor in the mouse embryonic aorta. *Tohoku J. Exp. Med.* **218**, 63-71. doi:10.1620/tjem.218.63

Jin, S.-W., Beis, D., Mitchell, T., Chen, J.-N. and Stainier, D. Y. R. (2005). Cellular and molecular analyses of vascular tube and lumen formation in zebrafish. *Development* **132**, 5199-5209. doi:10.1242/dev.02087

Jung, H. M., Castranova, D., Swift, M. R., Pham, V. N., Venero Galanternik, M., Isogai, S., Butler, M. G., Mulligan, T. S. and Weinstein, B. M. (2017). Development of the larval lymphatic system in zebrafish. *Dev.* **144**, 2070-2081. doi:10.1242/dev.145755

Kajii, T., Kida, M. and Takahashi, K. (1973). The effect of thalidomide intake during 113 human pregnancies. *Teratology* **8**, 163-166. doi:10.1002/tera.1420080208

Kamiya, A. and Togawa, T. (1980). Adaptive regulation of wall shear stress to flow change in the canine carotid artery. *Am. J. Physiol. Hear. Circ. Physiol.* **8**, 14-21. doi:10.1152/ajpheart.1980.239.1.H14

Kochhan, E., Lenard, A., Ellertsdottir, E., Herwig, L., Affolter, M., Belting, H.-G. and Siekmann, A. F. (2013). Blood flow changes coincide with cellular rearrangements during blood vessel pruning in zebrafish embryos. *PLoS ONE* **8**, e75060. doi:10.1371/journal.pone.0075060

Lalonde, R. L. and Akimenko, M.-A. (2018). Contributions of 5'HoxA/D regulation to actinodin evolution and the fin-to-limb transition. *Int. J. Dev. Biol.* **62**, 705-716. doi:10.1387/ijdb.180248rl

Langille, B. L. (1996). Arterial remodeling: Relation to hemodynamics. *Can. J. Physiol. Pharmacol.* **74**, 834-841. doi:10.1139/y96-082

Langille, B. L. and O'Donnell, F. (1986). Reductions in arterial diameter produced by chronic decreases in blood flow are endothelium-dependent. *Science (80-.)* **231**, 405-407. doi:10.1126/science.3941904

Lawson, N. D. and Weinstein, B. M. (2002). In vivo imaging of embryonic vascular development using transgenic zebrafish. *Dev. Biol.* **248**, 307-318. doi:10.1006/dbio.2002.0711

Lim, A. H., Suli, A., Yaniv, K., Weinstein, B., Li, D. Y. and Chien, C.-B. (2011). Motoneurons are essential for vascular pathfinding. *Development* **138**, 3847-3857. doi:10.1242/dev.068403

Lucitti, J. L., Jones, E. A. V., Huang, C., Chen, J., Fraser, S. E. and Dickinson, M. E. (2007). Vascular remodeling of the mouse yolk sac requires hemodynamic force. *Development* **134**, 3317-3326. doi:10.1242/dev.02883

Mahony, C., Erskine, L., Niven, J., Greig, N. H., Figg, W. D. and Vargesson, N. (2013). Pomalidomide is nonteratogenic in chicken and zebrafish embryos and nonneurotoxic in vitro. *Proc. Natl. Acad. Sci. USA* **110**, 12703-12708. doi:10.1073/pnas.1307684110

Marques, F. G., Carvalho, L., Sousa, J. S., Rino, J., Diegues, I., Poli, E., Pina, F., Saúde, L. and Constantino Rosa Santos, S. (2020). Low doses of ionizing radiation enhance angiogenesis and consequently accelerate post-embryonic development but not regeneration in zebrafish. *Sci. Rep.* **10**, 3137. doi:10.1038/s41598-020-60129-9

Marston, A. L., Agarwal, R., Cohen-Fix, O., Akiyoshi, B., Nelson, C. R., Ranish, J. A., Biggins, S., Akiyoshi, B., Nelson, C. R., Ranish, J. A. et al. (2014). Chromosome segregation in budding yeast: sister chromatid cohesion and related mechanisms. *Genetics* **196**, 31-63. doi:10.1534/genetics.112.145144

Martin, P. (1990). Tissue patterning in the developing mouse limb. *Int. J. Dev. Biol.* **34**, 323-336.

Mateus, R., Holtzer, L., Seum, C., Hadjivasiliou, Z., Dubois, M., Jülicher, F. and Gonzalez-Gaitan, M. (2020). BMP signaling gradient scaling in the zebrafish pectoral fin. *Cell Rep.* **30**, 4292-4302.e7. doi:10.1016/j.celrep.2020.03.024

McMillan, S. C., Xu, Z. T., Zhang, J., Teh, C., Korzh, V., Trudeau, V. L. and Akimenko, M.-A. (2013). Regeneration of breeding tubercles on zebrafish pectoral fins requires androgens and two waves of revascularization. *Development* **140**, 4323-4334. doi:10.1242/dev.095992

McMillan, S. C., Géraudie, J. and Akimenko, M.-A. (2015). Pectoral fin breeding tubercle clusters: a method to determine zebrafish sex. *Zebrafish* **12**, 121-123. doi:10.1089/zeb.2014.1060

McMillan, S. C., Zhang, J., Phan, H.-E., Jeradi, S., Probst, L., Hammerschmidt, M. and Akimenko, M.-A. (2018). A regulatory pathway involving retinoic acid and calcineurin demarcates and maintains joint cells and osteoblasts in regenerating fin. *Development* **145**, dev161158. doi:10.1242/dev.161158

Mercader, N. (2007). Early steps of paired fin development in zebrafish compared with tetrapod limb development. *Dev. Growth Differ.* **49**, 421-437. doi:10.1111/j.1440-169X.2007.00942.x

Mercader, N., Leonardo, E., Piedra, M. E., Martinez-A, C., Ros, M. A. and Torres, M. (2000). Opposing RA and FGF signals control proximodistal vertebrate limb development through regulation of Meis genes. *Development* **127**, 3961-3970. doi:10.1242/dev.127.18.3961

Niswander, L. and Martin, G. R. (1992). Fgf-4 expression during gastrulation, myogenesis, limb and tooth development in the mouse. *Development* **114**, 755-768. doi:10.1242/dev.114.3.755

Nomura, R., Kamei, E., Hotta, Y., Konishi, M., Miyake, A. and Itoh, N. (2006). Fgf16 is essential for pectoral fin bud formation in zebrafish. *Biochem. Biophys. Res. Commun.* **347**, 340-346. doi:10.1016/j.bbrc.2006.06.108

Okamoto, H. and Kuwada, J. Y. (1991a). Outgrowth by fin motor axons in wildtype and a finless mutant of the Japanese medaka fish. *Dev. Biol.* **146**, 49-61. doi:10.1016/0012-1606(91)90445-9

Okamoto, H. and Kuwada, J. Y. (1991b). Alteration of pectoral fin nerves following ablation of fin buds and by ectopic fin buds in the Japanese medaka fish. *Dev. Biol.* **146**, 62-71. doi:10.1016/0012-1606(91)90446-A

Okuda, K. S., Astin, J. W., Misa, J. P., Flores, M. V., Crosier, K. E. and Crosier, P. S. (2012). Lyve1 expression reveals novel lymphatic vessels and new mechanisms for lymphatic vessel development in zebrafish. *Dev.* **139**, 2381-2391. doi:10.1242/dev.077701

Petersen, J. C. and Ramsay, J. B. (2020). Walking on chains: the morphology and mechanics behind the fin ray derived limbs of sea-robins. *J. Exp. Biol.* **223**, jeb227140. doi:10.1242/jeb.227140

Phng, L.-K., Potente, M., Leslie, J. D., Babbage, J., Nyqvist, D., Lobov, I., Ondr, J. K., Rao, S., Lang, R. A., Thurston, G. et al. (2009). Nrarp coordinates endothelial Notch and Wnt signaling to control vessel density in angiogenesis. *Dev. Cell* **16**, 70-82. doi:10.1016/j.devcel.2008.12.009

Pries, A. R., Höpfner, M., Le Noble, F., Dewhirst, M. W. and Secomb, T. W. (2010). The shunt problem: control of functional shunting in normal and tumour vasculature. *Nat. Rev. Cancer* **10**, 587-593. doi:10.1038/nrc2895

Rehman, W., Arfons, L. M. and Lazarus, H. M. (2011). The rise, fall and subsequent triumph of thalidomide: lessons learned in drug development. *Ther. Adv. Hematol.* **2**, 291-308. doi:10.1177/2040620711413165

Reischauer, S., Stone, O. A., Villasenor, A., Chi, N., Jin, S.-W., Martin, M., Lee, M. T., Fukuda, N., Marass, M., Witty, A. et al. (2016). Cloche is a bHLH-PAS transcription factor that drives haemato-vascular specification. *Nature* **535**, 294-298. doi:10.1038/nature18614

Riddle, R. D., Johnson, R. L., Laufer, E. and Tabin, C. (1993). Sonic hedgehog mediates the polarizing activity of the ZPA. *Cell* **75**, 1401-1416. doi:10.1016/0092-8674(93)90626-2

Rodríguez-Niedenführ, M., Burton, G. J., Deu, J. and Sañudo, J. R. (2001). Development of the arterial pattern in the upper limb of staged human embryos: Normal development and anatomic variations. *J. Anat.* **199**, 407-417. doi:10.1046/j.1469-7580.2001.19940407.x

Saunders, J. W.Jr. (1948). The proximo–distal sequence of origin of the parts of the chick wing and the role of the ectoderm. *J. Exp. Zool.* **108**, 363-403. doi:10.1002/jez.1401080304

Shoham, A. B., Malkinson, G., Krief, S., Shwartz, Y., Ely, Y., Ferrara, N., Yaniv, K. and Zelzer, E. (2012). S1P1 inhibits sprouting angiogenesis during vascular development. *Dev.* **139**, 3859-3869. doi:10.1242/dev.078550

Singh, S. P., Holdway, J. E. and Poss, K. D. (2012). Regeneration of amputated zebrafish fin rays from de novo osteoblasts. *Dev. Cell* **22**, 879-886. doi:10.1016/j.devcel.2012.03.006

Sivaraj, K. K. and Adams, R. H. (2016). Blood vessel formation and function in bone. *Development* **143**, 2706-2715. doi:10.1242/dev.136861

Suchting, S., Freitas, C., Le Noble, F., Benedito, R., Bréant, C., Duarte, A. and Eichmann, A. (2007). The Notch ligand Delta-like 4 negatively regulates endothelial tip cell formation and vessel branching. *Proc. Natl. Acad. Sci. USA* **104**, 3225-3230. doi:10.1073/pnas.0611177104

Therapontos, C., Erskine, L., Gardner, E. R., Figg, W. D. and Vargesson, N. (2009). Thalidomide induces limb defects by preventing angiogenic outgrowth during early limb formation. *Proc. Natl. Acad. Sci. USA* **106**, 8573-8578. doi:10.1073/pnas.0901505106

Thorimbert, V., König, D., Marro, J., Ruggiero, F. and Jaźwińska, A. (2015). Bone morphogenetic protein signaling promotes morphogenesis of blood vessels, wound epidermis, and actinotrichia during fin regeneration in zebrafish. *FASEB J.* **29**, 4299-4312. doi:10.1096/fj.15-272955

Thorsen, D. H. and Hale, M. E. (2005). Development of zebrafish (Danio rerio) pectoral fin musculature. *J. Morphol* **266**, 241-255. doi:10.1002/jmor.10374

Thorsen, D. H. and Hale, M. E. (2007). Neural development of the zebrafish (Danio rerio) pectoral fin. *J. Comp. Neurol.* **504**, 168-184. doi:10.1002/cne.21425

Torres-Vázquez, J., Gitler, A. D., Fraser, S. D., Berk, J. D., Pham, V. N., Fishman, M. C., Childs, S., Epstein, J. A. and Weinstein, B. M. (2004). Semaphorin-plexin signaling guides patterning of the developing vasculature. *Dev. Cell* **7**, 117-123. doi:10.1016/j.devcel.2004.06.008

Traver, D., Paw, B. H., Poss, K. D., Penberthy, W. T., Lin, S. and Zon, L. I. (2003). Transplantation and in vivo imaging of multilineage engraftment in zebrafish bloodless mutants. *Nat. Immunol.* **4**, 1238-1246. doi:10.1038/ni1007

Tu, S. and Johnson, S. L. (2011). Fate restriction in the growing and regenerating zebrafish fin. *Dev. Cell* **20**, 725-732. doi:10.1016/j.devcel.2011.04.013

Tulenko, F. J., Massey, J. L., Holmquist, E., Kigundu, G., Thomas, S., Smith, S. M. E., Mazan, S. and Davis, M. C. (2017). Fin-fold development in paddlefish and catshark and implications for the evolution of the autopod. *Proc. R. Soc. B Biol. Sci.* **284**, 20162780. doi:10.1098/rspb.2016.2780

Tuttle, J. L., Nachreiner, R. D., Bhuller, A. S., Condict, K. W., Connors, B. A., Herring, B. P., Dalsing, M. C. and Unthank, J. L. (2001). Shear level influences resistance artery remodeling: Wall dimensions, cell density, and eNOS expression. *Am. J. Physiol. Hear. Circ. Physiol.* **281**, H1380-H1389. doi:10.1152/ajpheart.2001.281.3.H1380

Ulrich, F., Ma, L.-H., Baker, R. G. and Torres-Vázquez, J. (2011). Neurovascular development in the embryonic zebrafish hindbrain. *Dev. Biol.* **357**, 134-151. doi:10.1016/j.ydbio.2011.06.037

Vargesson, N. (2013). Thalidomide embryopathy: an enigmatic challenge. *ISRN Dev. Biol.* **2013**, 1-18. doi:10.1155/2013/241016

Weijts, B., Gutierrez, E., Saikin, S. K., Ablooglu, A. J., Traver, D., Groisman, A. and Tkachenko, E. (2018). Blood flow-induced Notch activation and endothelial migration enable vascular remodeling in zebrafish embryos. *Nat. Commun.* **9**, 5314. doi:10.1038/s41467-018-07732-7

Weinstein, B. M. (1999). What guides early embryonic blood vessel formation? *Dev. Dyn.* **215**, 2-11. doi:10.1002/(SICI)1097-0177(199905)215:1<2::AID-DVDY2>3.0.CO;2-U

Weinstein, B. M. and Lawson, N. D. (2002). Arteries, veins, notch, and VEGF. *Cold Spring Harb. Symp. Quant. Biol.* **67**, 155-162. doi:10.1101/sqb.2002.67.155

White, R. M., Sessa, A., Burke, C., Bowman, T., LeBlanc, J., Ceol, C., Bourque, C., Dovey, M., Goessling, W., Burns, C. E. et al. (2008). Transparent adult zebrafish as a tool for in vivo transplantation analysis. *Cell Stem Cell* **2**, 183-189. doi:10.1016/j.stem.2007.11.002

Won, Y.-J., Ono, F. and Ikeda, S. R. (2011). Identification and modulation of voltage-gated Ca2+ currents in zebrafish Rohon-Beard neurons. *J. Neurophysiol.* **105**, 442-453. doi:10.1152/jn.00625.2010

Woollard, H. H. (1922). The development of the principal arterial stems in the forelimb of the pig. *Contrib. Embryol., Carnegie Inst. Wash. Publ.* **70**, 139-154.

Xu, C., Hasan, S. S., Schmidt, I., Rocha, S. F., Pitulescu, M. E., Bussmann, J., Meyen, D., Raz, E., Adams, R. H. and Siekmann, A. F. (2014). Arteries are formed by vein-derived endothelial tip cells. *Nat. Commun.* **5**, 5758. doi:10.1038/ncomms6758

Yano, T., Abe, G., Yokoyama, H., Kawakami, K. and Tamura, K. (2012). Mechanism of pectoral fin outgrowth in zebrafish development. *Development* **139**, 4291. doi:10.1242/dev.090324

Zhang, J., Wagh, P., Guay, D., Sanchez-Pulido, L., Padhi, B. K., Korzh, V., Andrade-Navarro, M. A. and Akimenko, M.-A. (2010). Loss of fish actinotrichia proteins and the fin-to-limb transition. *Nature* **466**, 234-237. doi:10.1038/nature09137

Zhang, Y., Xu, B., Chen, Q., Yan, Y., Du, J. and Du, X. (2018). Apoptosis of endothelial cells contributes to brain vessel pruning of zebrafish during development. *Front. Mol. Neurosci.* **11**, 1-6. doi:10.3389/fnmol.2018.00222

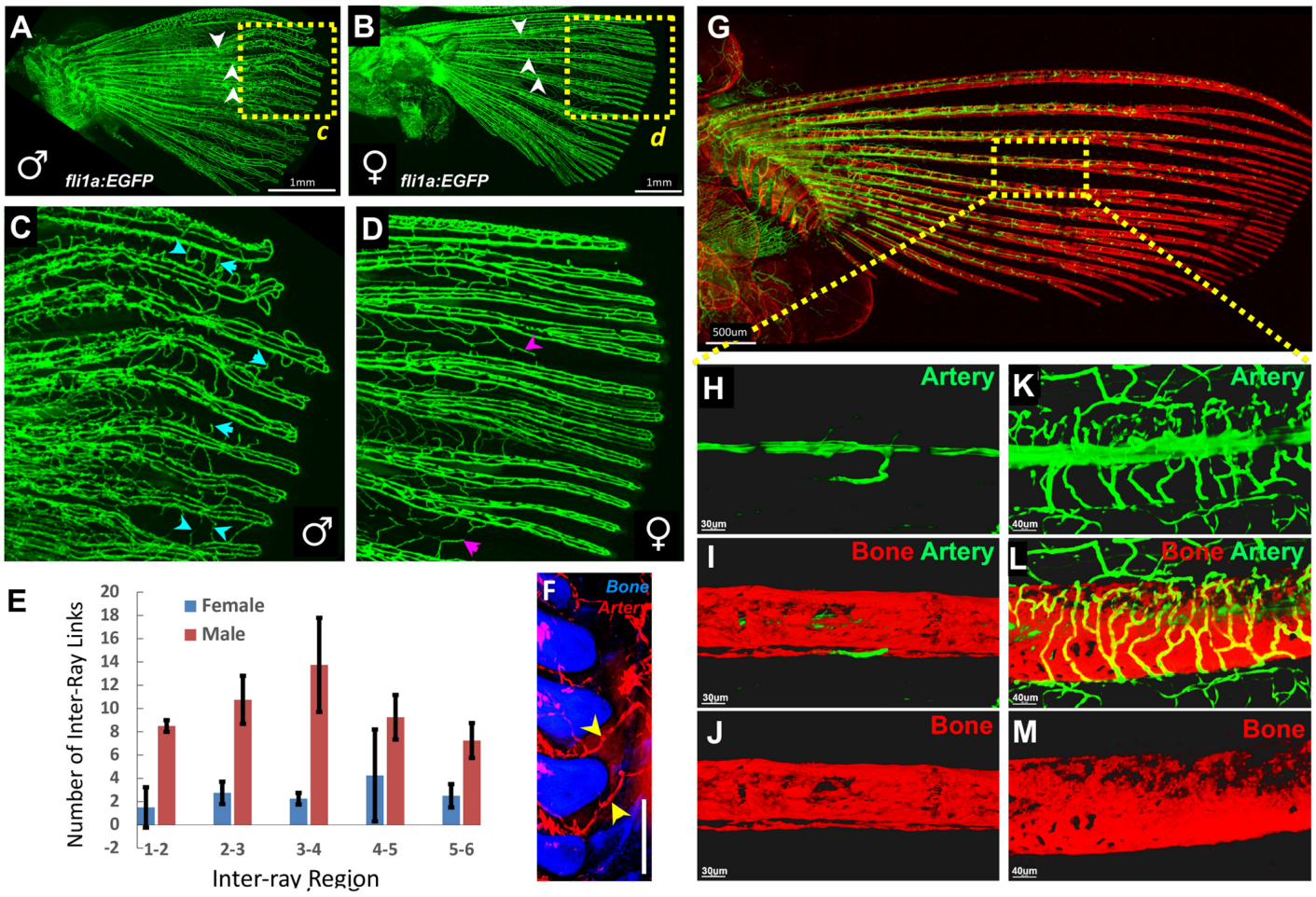

Fig. S1. Sex-specific vascular features of the adult zebrafish pectoral fin.
(A-D) Tiled confocal images of vessels in pectoral fins dissected from *Tg(fli1a:egfp)*^{y1} transgenic adult male (A,C) and female (B,D) zebrafish. Boxes in A and B indicate the approximate areas shown in the magnified images in panels C and D, respectively. Greater numbers of inter-ray vessels in are present in male pectoral fins. **(E)** Quantitation of the number of inter-ray vessels linking different sets of fin rays in adult male or female zebrafish. **(F)** Higher magnification confocal image of the same *Tg(kdrl:mcherry)*^{y206} adult zebrafish fin as in Fig. 2B, showing kdrl:mcherry-positive arterial blood vessels (red, arrowheads) running between autofluorescent bones (blue) to interconnect the proximal and fin ray vascular networks. **(G-M)** Tiled confocal images of vessels in pectoral fins dissected from *Tg(Ola.Sp7:mCherryEco.NfsB)*^{pd46}, *Tg(kdrl:egfp)*^{s843} double transgenic adult female (G-J) and male (K-M) zebrafish, with *Tg(O/a.Sp7:mCherryEco.Nfs8)*^{pd46}-positive bone in red and *Tg(kdrl:egfp)*^{s843}-positive vessels in green. The box on the image of an adult female fin in panel G indicates the approximate location of the magnified images shown in panels H-J. Panels K-M show magnified images from the comparable location in a separately imaged adult male fin, showing a complex network of vessels on the outside of the fin ray bone associated with the male breeding tubercles that are not present in the female fin. Representative images from one of three embryos observed of each sex. Scale bars = 1 mm, A; 200 μm, F-H; 500 μm, I; 30 μm, J-L; 40 μm, M-0.

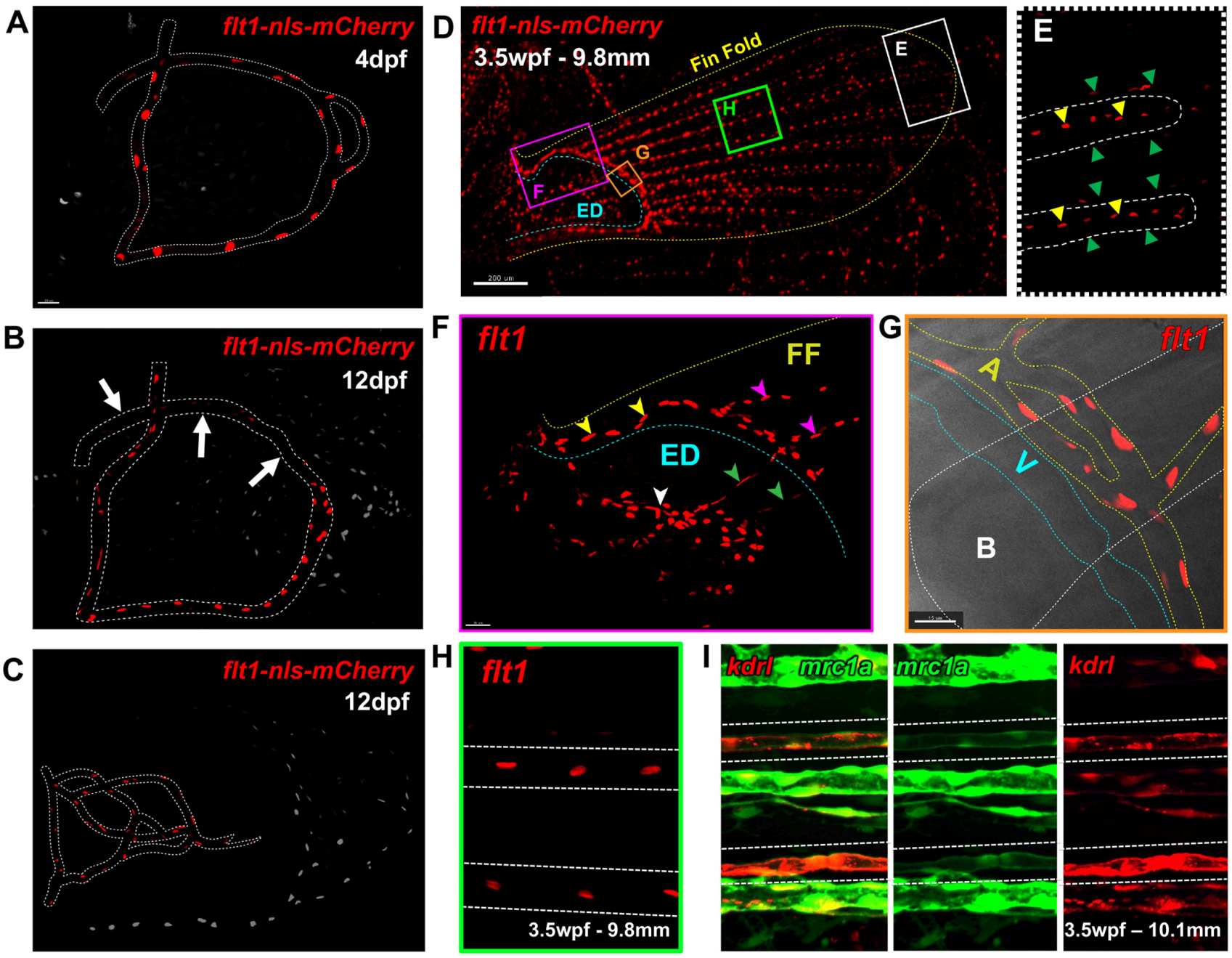

Fig. S2. Flt1:mcherry expression identifies arterial endothelial cells in the pectoral fin vasculature

(A-H) Lateral view confocal images of *Tg(flt1:nmcherry)*^{skt7}-positive arterial endothelial cell (EC) nuclei in 4 dpf (A), 12 dpf (B,C), and 3.5 week post-fertilization (wpf; D-1) *Tg(flt1:nmcherry)*^{skt7} transgenic zebrafish. (A,B) ECs of the primitive arc are all *Tg(ft1:nmcherry)*^{skt7}-positive at 4 dpf (A), but by 12 dpf the developing dorsal venous outflow (arrows) has become *Tg(flt1:nmcherry)*^{skt7}-negative (B). (C) ECs of the proximal plexus are *Tg(flt1:nmcherry)*^{skt7}-positive from the beginning. **(D-H)** Arterial ECs of the 3.5 wpf fin are all *Tg(flt1:nmcherry)*^{skt7}-positive. Panels E-H show higher magnification images of the boxed regions of the 3.5 wpf fin in panel D. (E) At the fin ray tips, artery ECs are *Tg(flt1:nmcherry)*^{skt7}-positive (yellow arrow) while lateral vein ECs are mostly *Tg(flt1:nmcherry)*^{skt7}-negative (green arrows). (F) The fin ray network arterial feed (yellow arrows), fin ray arteries (magenta arrows), interplexus connections (green arrows), and proximal plexus (white arrow) are all *Tg(flt1:nmcherry)*^{skt7}-pos itive. (G) Higher magnification image of adjacent *Tg(flt1:nmcherry)*^{skt7}-positive arterial (yellow dashed line) and *Tg(flt1:nmcherry)*^{skt7}-negative venous (teal dashed line) vessels at the base of the fin rays. (H) *Tg(flt1:nmcherry)*^{skt7}-positive fin ray arteries in the mid-fin (bone outlined in dashed white). **(I)** Lateral view confocal image of *Tg(kdrl:mcherry)*^{y206}-positive fin ray artery ECs in the mid-fin of a 3.5 wpf *Tg(kdrl:mcherry)*^{y206}, *Tg(mrc1a:egfp)*^{y251} double transgenic zebrafish (bone outlined in dashed white), for comparison to panel H). Representative imaqes from one of three embrvos observed.

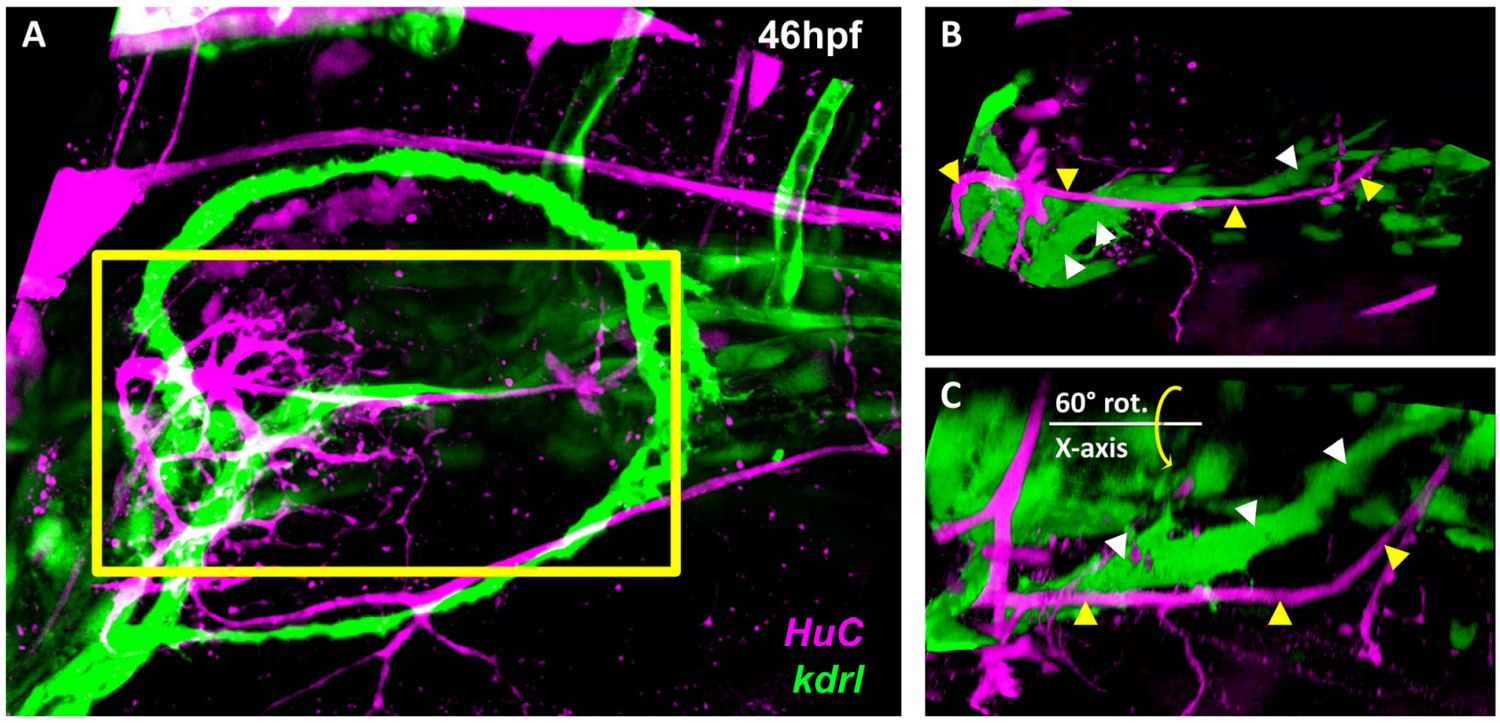

Fig. S3. The ventral arterial sprout and axons innervating the pectoral fin follow different paths

(A) Lateral view confocal image of a 48 hpf *Tg(kdrl:egfp)*^{s843}, *Tg(elav/3:mCherry)*^{niao2tg} double transgenic zebrafish with green endothelial cells and magenta nerves. Z-cropped versions of the yellow boxed region are shown in panels B and C. **(B)** Image of the boxed region in (A) with some of the upper and lower Z-planes removed before reconstruction to allow easier visualization of the ventral pectoral fin artery (white arrowheads) and 3rd nerve axon (yellow arrowheads). **(C)** Same image as in panel B but reconstructed at a 60°-rotation around the y-axis to more clearly show that the pectoral fin artery (white arrowheads) and 3rd nerve axon (yellow arrowheads) take different paths. Representative images from one of six embryos observed.

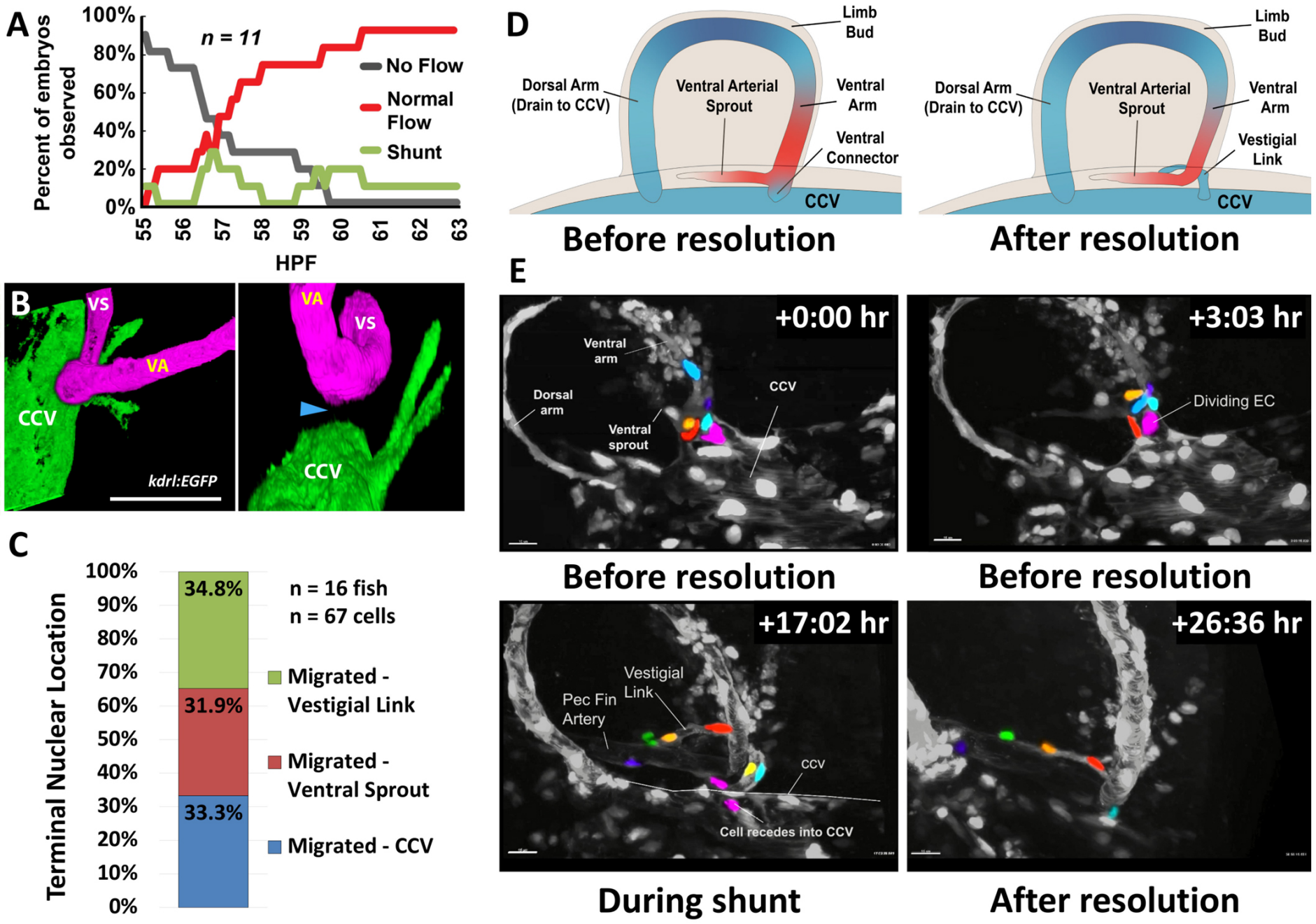

Fig. S4. Quantitation of shunt formation and persistence

(A) A graph showing the total percentage of embryos with no flow, shunting flow, and normal flow, at the indicated time post fertilization. *n*=11. **(B)** Two different reconstructed views of the same image data showing the ventral arm of the primary pectoral fin artery in a 4 dpf *Tg(kdrl:egfp)*^{s843} embryo with the ventral arterial segment (VS) and ventral primary arc arm (VA) false colored in magenta and the common cardinal vein (CCV) in green. Left, lateral view. Right, ventral view with a blue arrowhead noting the complete separation of the ventral arm from the CCV. **(C)** Quantitation of the eventual nuclear position of 67 shunt-associated endothelial cells from 16 different *Tg(kdrl:egfp)*^{s843}, *Tg(kdrl:nlsmcherry)*^{y173} double transgenic animals after flow onset through the primary arc and shunt disconnection. **(D)** Schematics illustrating the orientation and features imaged in panel E. **(E)** Selected time points from a representative time-lapse sequence used to collect data quantitated in panel C, with false-coloring of shunt-associated tracked endothelial cells and with other endothelial cells in greyscale. See **Movie 7** for the complete time lapse series shown in panel E, and **Movie 8** for a second separate representative time lapse series. Scale bars = 20 μm.

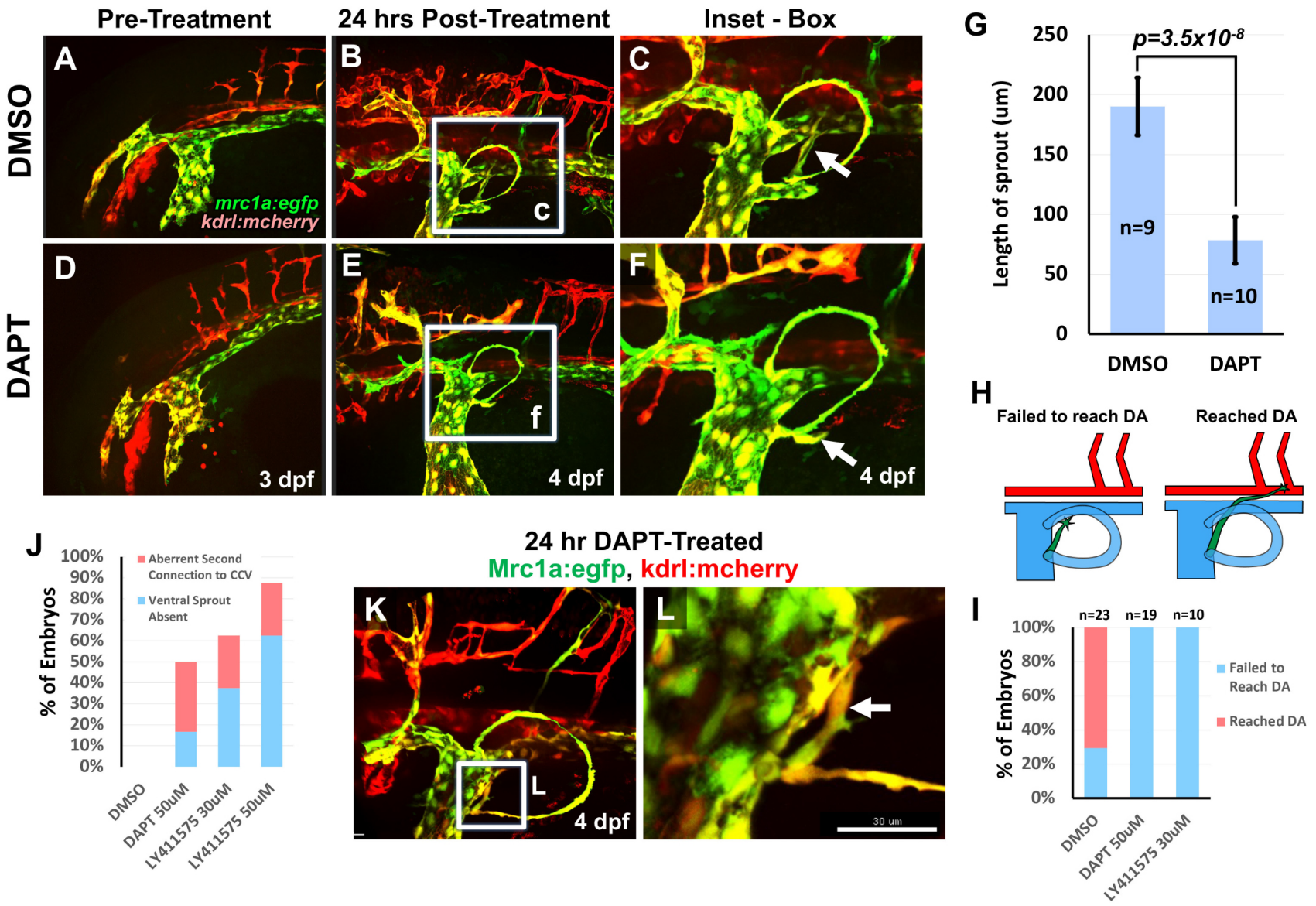

Fig. S5. Notch signaling is required for proper pectoral fin artery formation

(A-F) Confocal images of representative DMSO carrier (A-C) or DAPT (D-F) treated *Tg(kdrl:mcherry)*^{y206}, *Tg(mrc1a:egfp)*^{y251} double transgenic zebrafish. (A,D) Images collected just prior to the initiation of treatment at approximately 30 hpf. (B,E) Images collected after 24 hours of treatment at approximately 54 hpf. Boxes note regions shown magnified in panels C and F. (C,F) Magnified views of the boxed regions in panels B and E, respectively, showing normal ventral pectoral fin artery in the DMSO-treated animal (C, arrow) but only a vestigial misdirected ventral pectoral fin artery sprout in the DAPT-treated animal (F, arrow). (G) Quantitation of the length of the ventral pectoral fin artery sprout in 4 dpf DMSO or DAPT treated animals. (H) Schematic diagrams showing ventral sprouts that have failed to reach the DA (left) and that have reached the DA (right). (I) Quantitation of the number of ventral pectoral fin artery sprouts that have successfully reached the dorsal aorta at 54 hpf in animals treated with DMSO, DAPT, or LY411575 for 24 hours. (J) Quantitation of the number of ventral pectoral fin artery sprouts that are either entirely absent (blue) or aberrantly making ectopic connections to the CCV (red) at 54 dpf in animals treated with DMSO, DAPT, or LY411575 for 24 hours. (K) Representative confocal image of a ventral sprout aberrantly connecting to the CCV. Box notes region shown magnified in panels L. (L) Magnified view of the boxed region in panel K showing a ventral pectoral fin artery segment (arrow) ectopically connecting to the CCV.

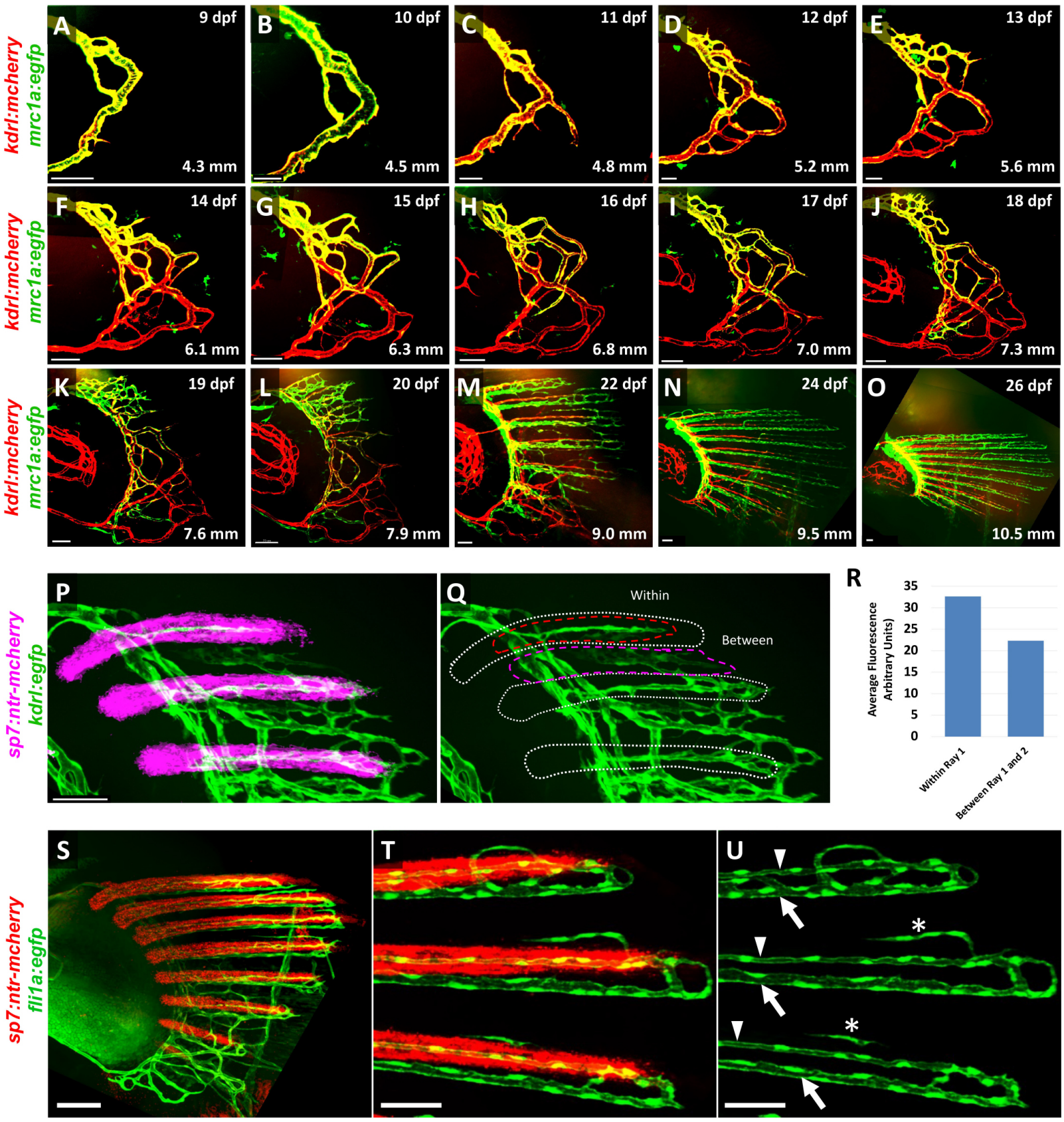

Fig. S6. Pectoral fin image series

(A-0) Confocal images of pectoral fin distal plexus vascular development from 9 dpf to 26 dpf (4.3 mm to 10.5 mm) in a single representative *Tg(kdrl:mcherry)*^{y206}, *Tg(mrc1a:egfp)*^{y251} double transgenic zebrafish larva (of 12 observed), with *Tg(kdrl:mcherry)*^{y206} in red and Tg(mrc1a:egfp)Y251 in green. **(P,Q)** Confocal images of the pectoral fin distal vascular plexus in a 21 dpf *Tg(Ola.Sp7:mCherryEco.NfsB)*^{pd46}) , *Tg(kdrl:egfp)*^{s843} double transgenic zebrafish, showing bone in magenta (P) and vessels in green (P,Q). White dashed lines in panel Q show the position of the bones, red and magenta dashed lines demarcate vascular areas in ray 1 and between rays 1 and 2, respectively. **(R)** Quantitation of *Tg(kdrl:egfp)*^{s843} fluorescence intensity of vessels in fin ray 1 and between fin rays 1 and 2. **(S-U)** Confocal images of the pectoral fin distal vascular plexus in 21 dpf *Tg(Ola.Sp7:mCherryEco.NfsB)*^{pd46}, *Tg(fli1a:egfp)*^{y1} double transgenic zebrafish , showing bone in red (S,T) and vessels in green (S-U). Panel S shows a lower- magnification overview of a distal vascular plexus, panels T and U show a higher magnification image of the tip of three fin rays from a separate fish. In panel U arrowheads indicate arteries, arrows indicate veins, and initial sprouts developing that will give rise to the dorsal paired fin ray veins are note with asterisks. All scale bars = 50 μm, except panel S, which is 100 μm.

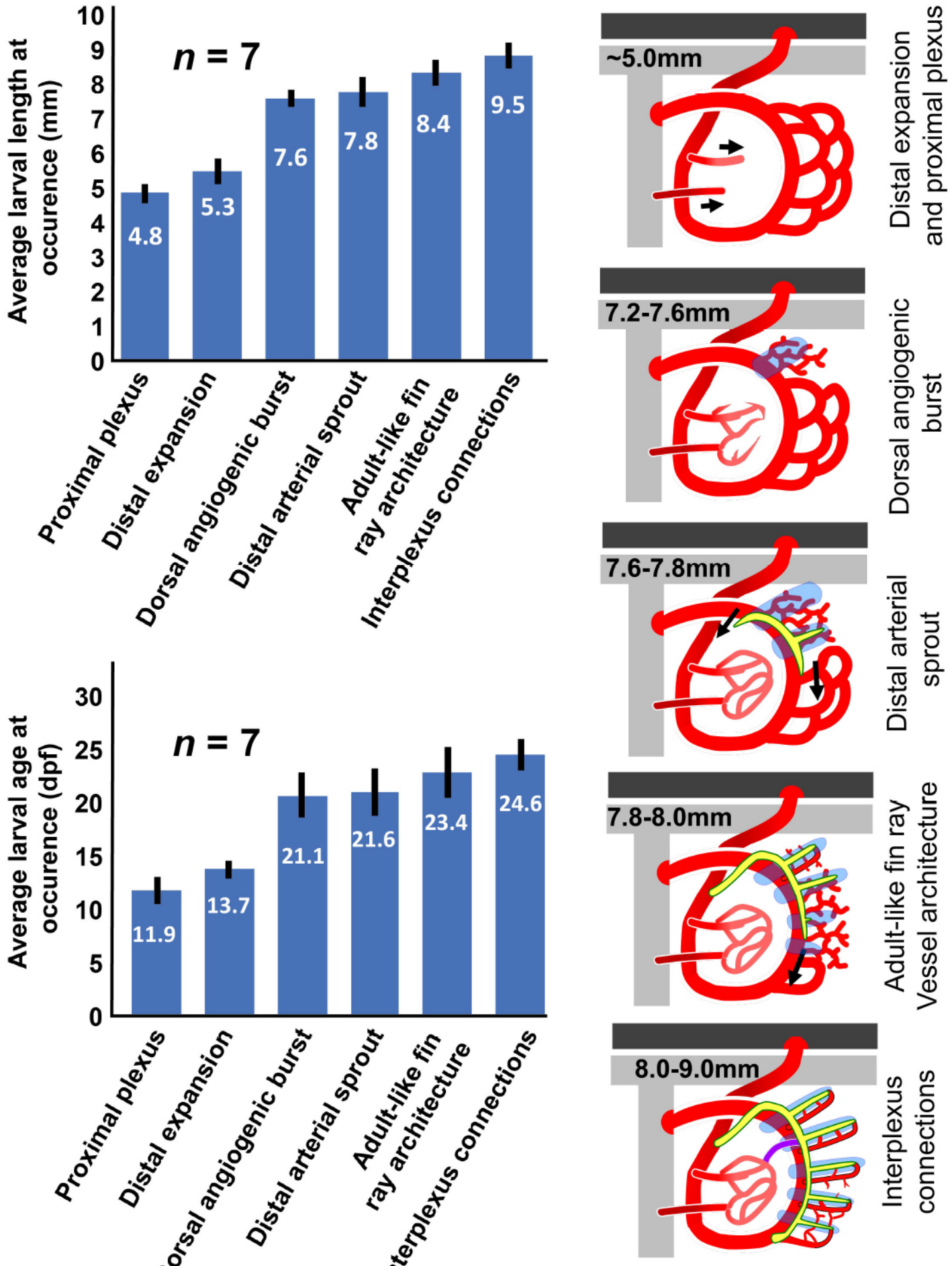

Fig. S7. Quantitation of the timing of developmental milestones in the pectoral fin vasculature.
The two graphs on the left show the same data for timing of six specific developmental milestones imaged in *Tg(kdrl:mcherry)*^{y206}, *Tg(mrc1a:egfp)*^{y251} double transgenic zebrafish larva, plotted versus either average larval length (top) or average chronological age (bottom) that the fish achieved the indicated developmental milestones. Measured fish include those imaged in **Fig. S6** and **Fig. 5**. All error bars indicate the standard deviation of the mean. *n* = 7 larva. The panels on the right show schematic representations of the events quantified in the graphs.

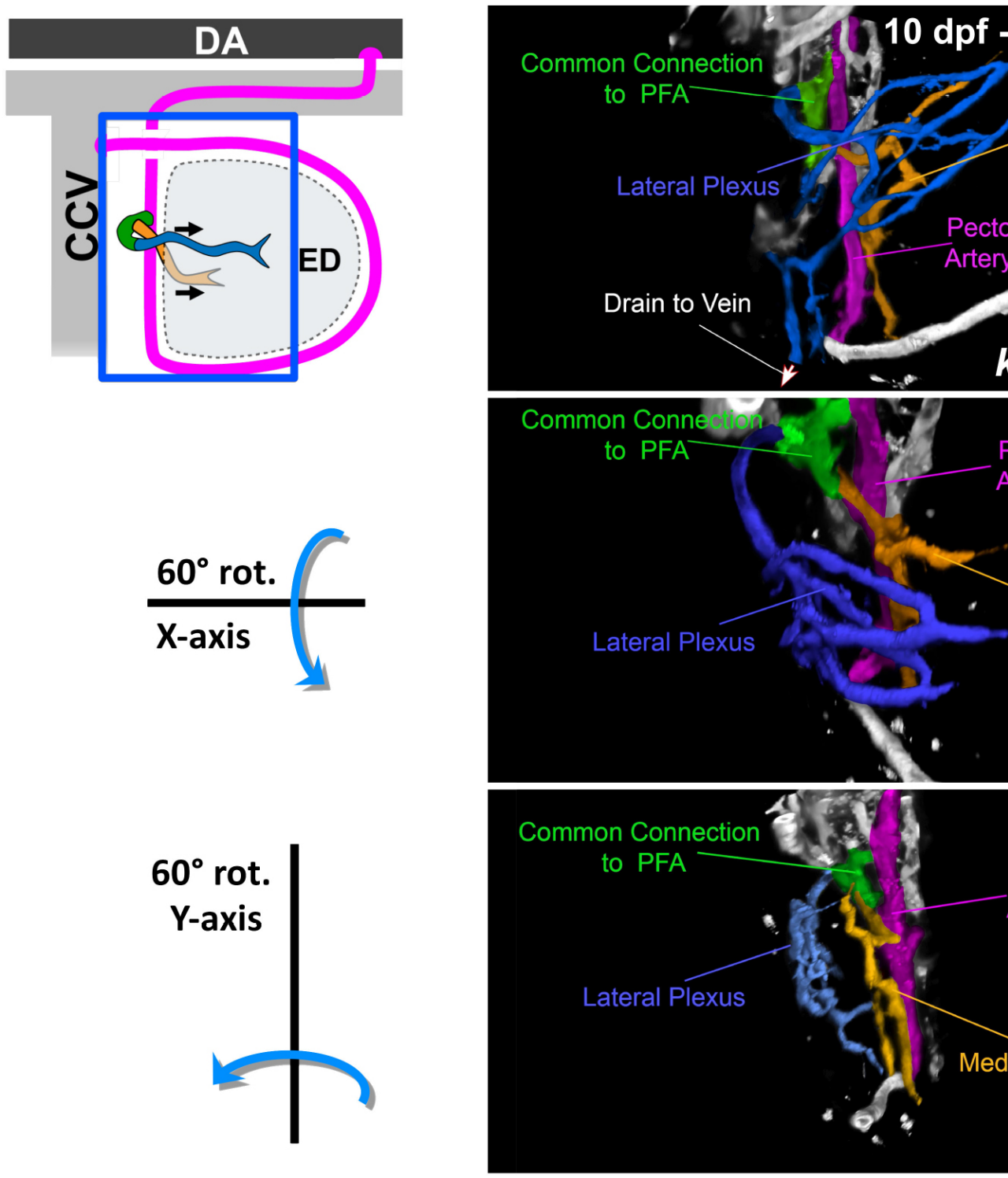

Fig.S8. Proximal plexus sprouts from the pectoral fin artery

Illustrative schematic diagram (top left) and confocal image reconstructions (right) of the fin vasculature of a 10 dpf/5.5 mm *Tg(kdrl:mcherry)*^{y206} animal with false coloring of the pectoral fin artery (magenta), the lateral proximal plexus (blue), medial proximal plexus (orange), and the common root sprouting from the pectoral fin artery that feeds both medial and lateral proximal plexuses (green). Images show a lateral view of the pectoral fin (top), a 60° x-axis rotation of the top image (middle), and a 60° y-axis rotation of the top image (bottom). See Movie 9 for animated 3-D reconstructions of the same confocal image stack, including the same views shown in these panels. Representative images from one of six embryos observed.

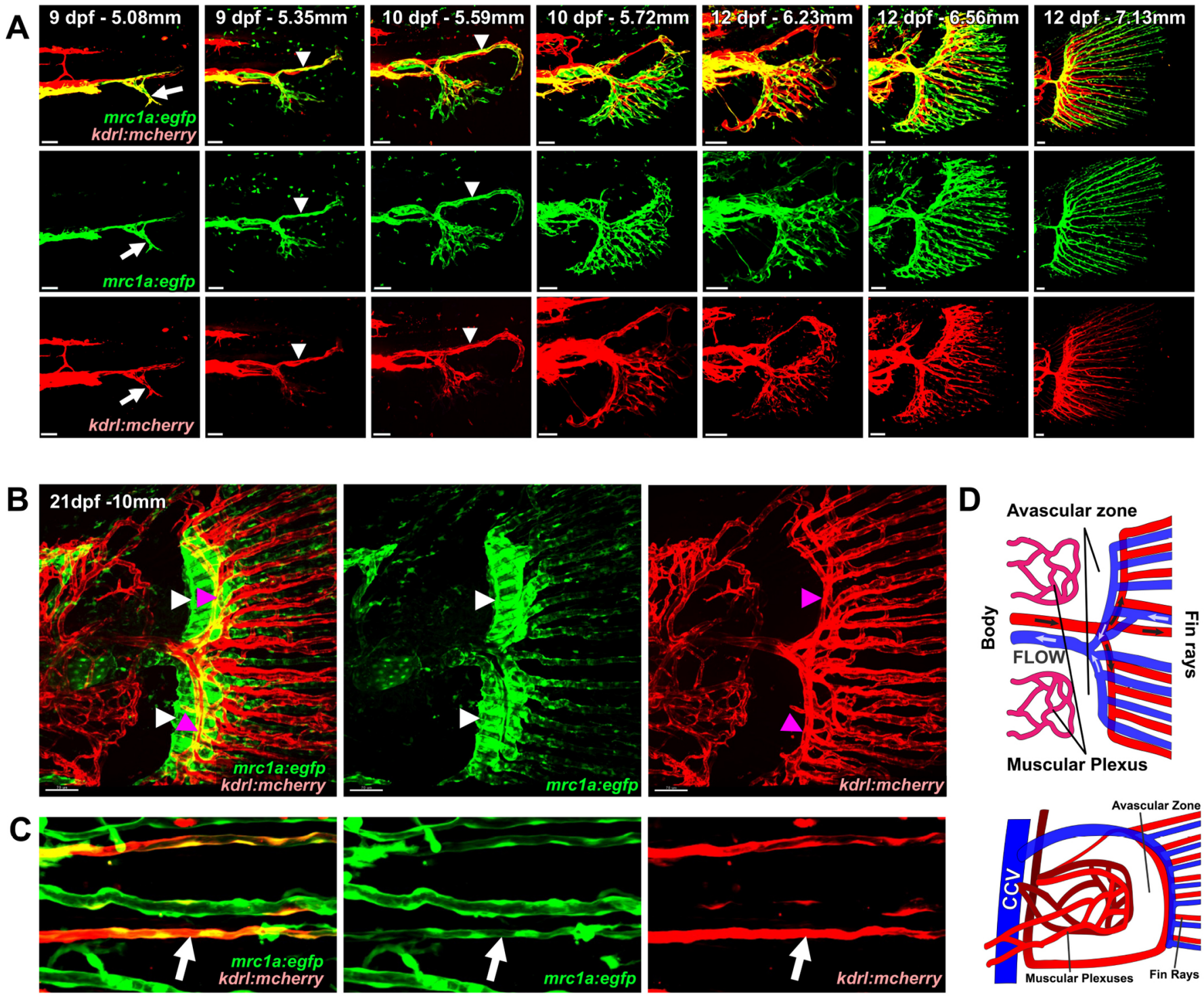

Fig. S9. The development of the caudal fin vasculature

Confocal images of the caudal fin vasculature in Tg(kdrl:mcherry)y206, Tg(mrc1a:egfp)y251 double transgenic zebrafish. **(A)** A series of representative *Tg(kdrl:mcherry)*^{y206}, *Tg(mrc1a:egfp)*^{y251} (top row), *Tg(mrc1a:egfp)*^{y251} (middle row), and *Tg(kdrl:mcherry)*^{y206} (bottom row) confocal images or the same fields, collected from six different animals, documenting stages from invasion of the caudal fin fold by endothelial cells at 5.08 mm to the largely adult-like architecture at 7.13mm. **(B)** Confocal images of a 10 mm larva with the parallel arterial and venous manifolds indicated with white and magenta arrowheads, respectively. **(C)** A representative higher-magnification image of the fin ray vasculature in the caudal fin of a 10 mm larva, showing a *Tg(kdrl:mcherry)*^{y206}-positive artery (arrow). **(D)** Illustrative schematic diagrams of caudal (top) and pectoral (bottom) fin vasculature, showing similarities in their broad structure. Representative images from one of six embryos observed per time point.

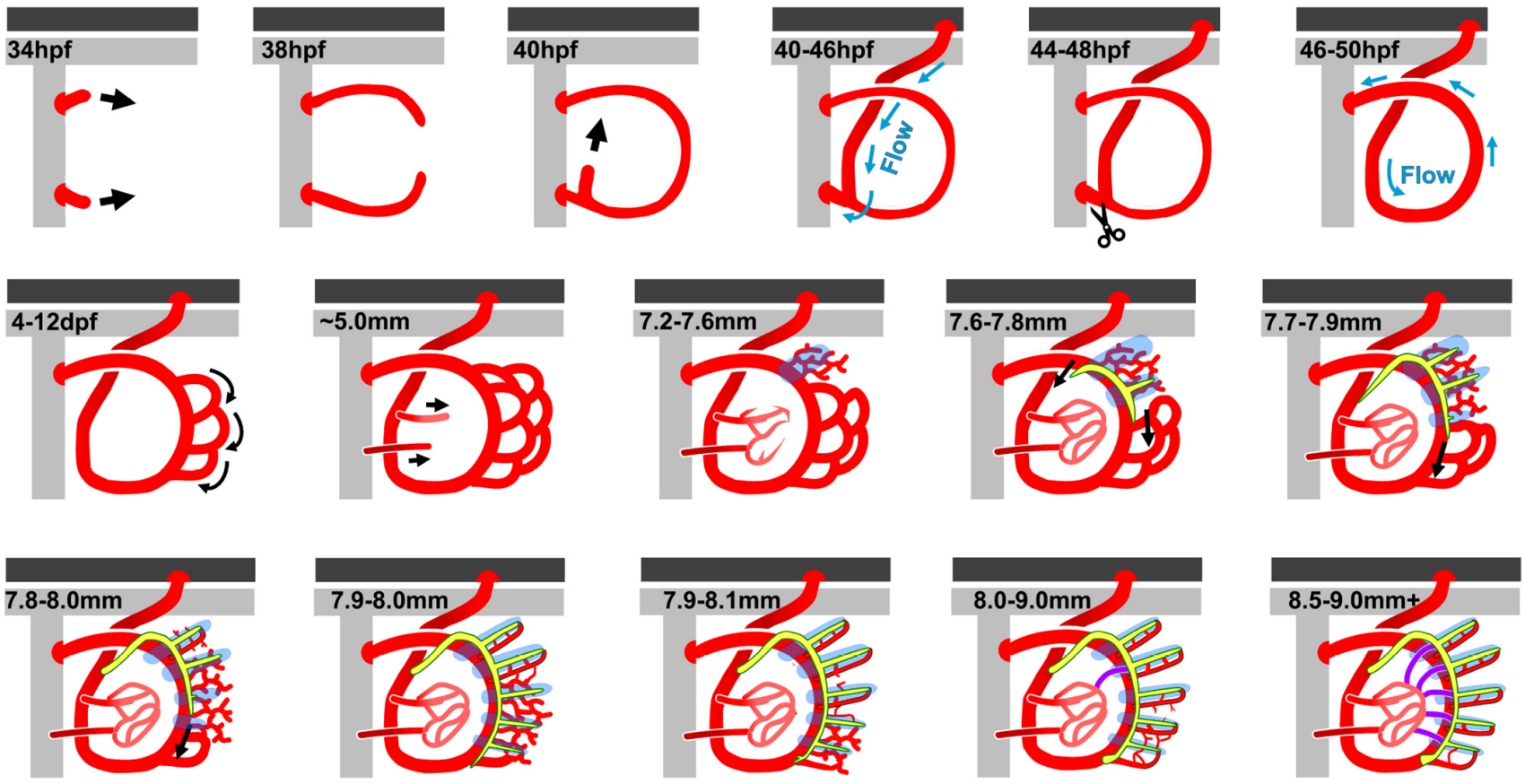

Fig. S10. Schematic Diagram of Pectoral Fin Vascular Development

Schematic diagrams illustrating stages of pectoral fin vascular development from emergence of the first pectoral vessel sprouts from the CCV to formation of a complex vascular network that includes the major vascular pathways found in the adult pectoral fin. After the first week of development larval length is used instead of age to stage animals, as this more accurately correlates with developmental events (see **Fig. S4**).

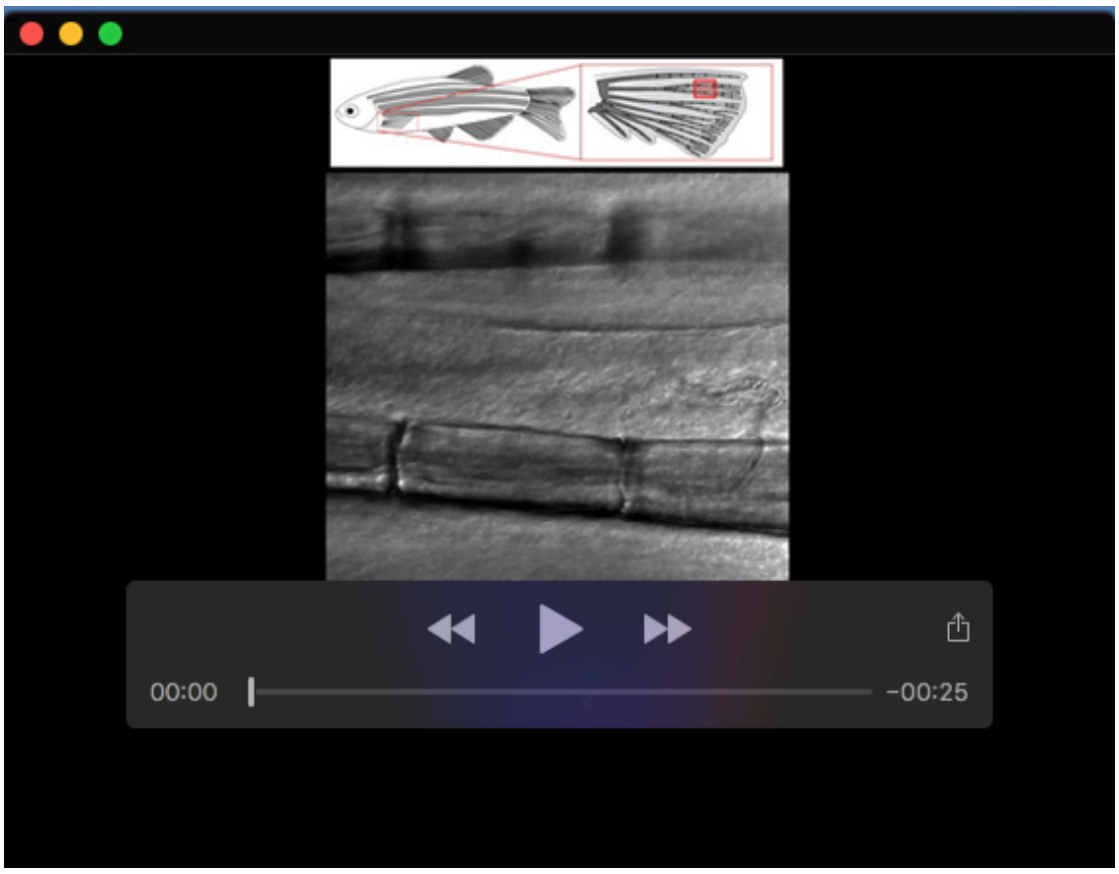

Movie 1. Circulation in the adult zebrafish fin

High magnification transmitted light imaging of circulation through fin ray arteries and veins and inter-ray interlinking vessels of an adult zebrafish fin. Transmitted light, real time video.

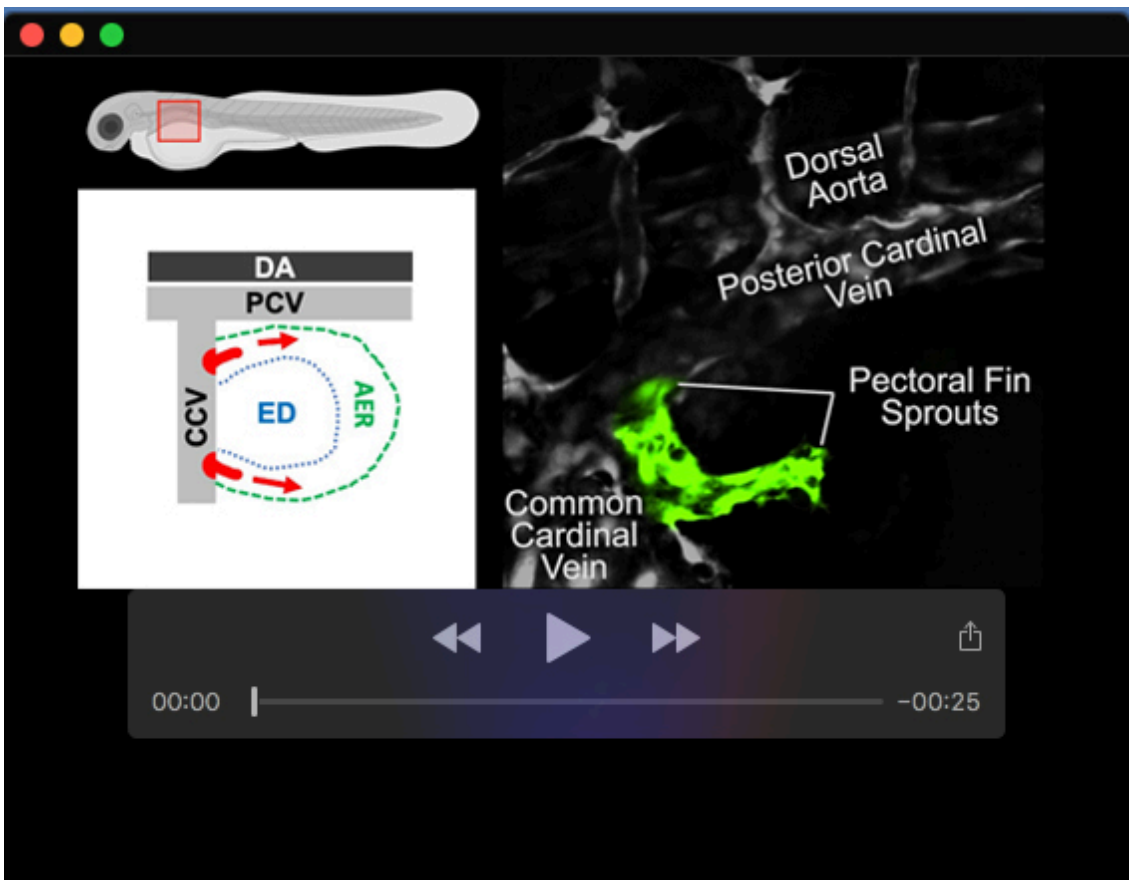

Movie 2. Formation and arterial connection of the primitive pectoral artery.

Time-lapse confocal imaging of a *Tg(kdrl:egfp)*^{s843} transgenic zebrafish from 34-50 hpf, showing formation of the primary arc of the primitive pectoral artery and its connection to the dorsal aorta. The movie shows the complete sequence for the images shown in **Fig. 3D-F** and **Fig. 4D-F**.

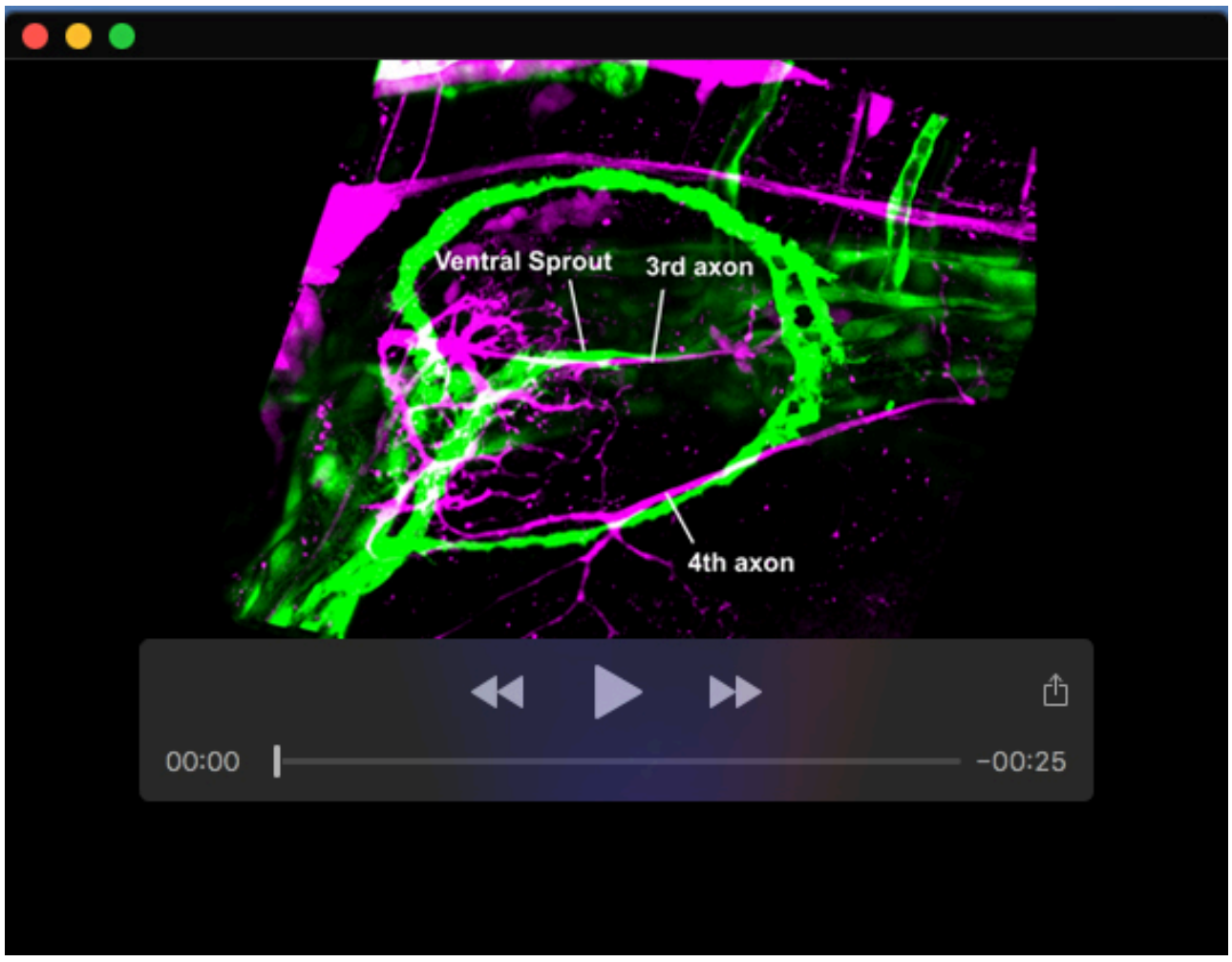

Movie 3. The path of the ventral arterial sprout follows a differing path from the pectoral fin enervating axons.

A 3d-reconstruction of a confocal z-stack of a representative *Tg(kdrl:egfp)*^{s843}, *Tg(elavl3:mCherry)*^{nia02tg} double transgenic zebrafish at 46 hpf, showing the differing paths of the 3rd and 4th axons of the pectoral fin with the ventral arterial sprout shown in **Fig. S3**.

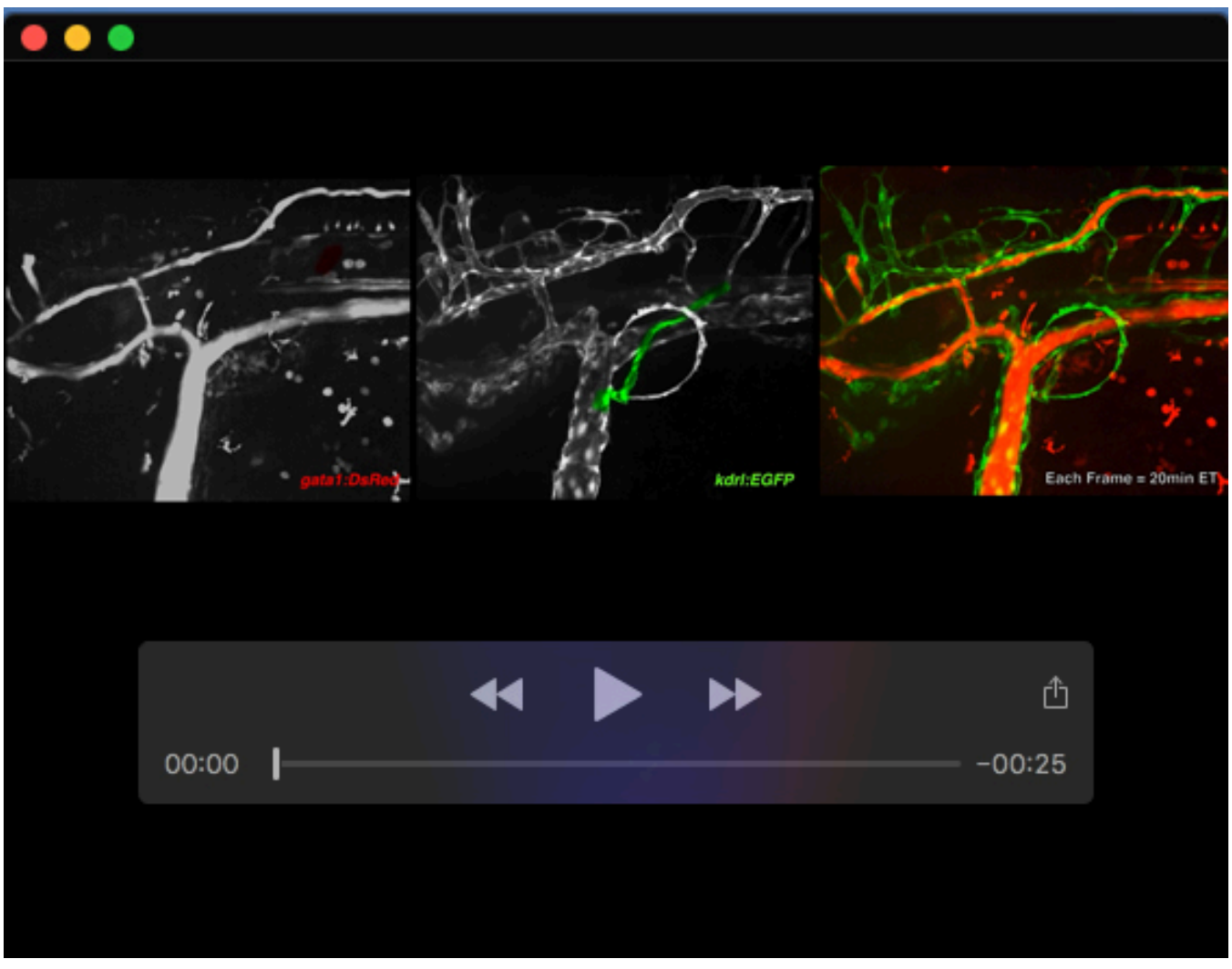

Movie 4. Perfusion of the primitive pectoral artery.

Time-lapse confocal imaging of a *Tg(kdrl:egfp)*^{s843}, *Tg(gata1:dsred)*^{sd2Tg} double transgenic zebrafish from 44-50 hpf, showing gata1:dsred marking active blood flow (left panel; pec fin flow colored red), *Tg(kdrl:egfp)*^{s843} showing both lumenized and unlumenized vessels (center panel; ventral connection to the DA colored green), and a merged *Tg(gata1:dsred)*^{sd2Tg} (red)/ *Tg(kdrl:egfp)*^{s843} (green) image (right panel). Flow initially shunts from the DA directly to the CCV, but then becomes re-routed through the full arc of the primitive pectoral artery. Each frame of the movie represents 20 minutes elapsed time. The movie shows the complete sequence for the images shown in **Fig. 4J-U**.

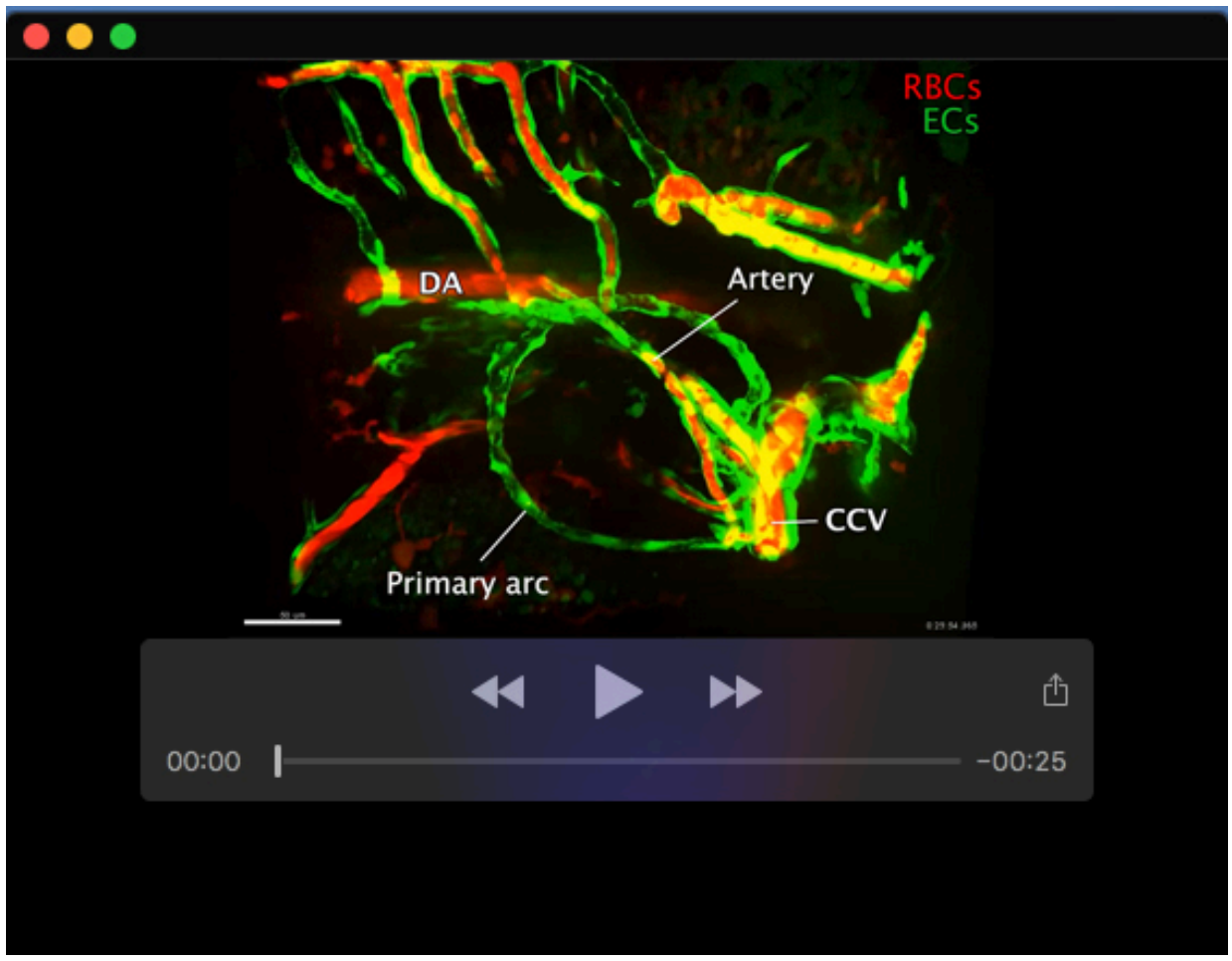

Movie 5. In**itial shunting flow of blood flow from the DA to the CCV.**

3-D reconstructions of a confocal image stack of the fin region of a 2 day-old *Tg(kdrl:egfp)*^{s843}, *Tg(gata1:dsred)*^{sd2Tg} double transgenic zebrafish, showing flow initially shunting from the DA directly to the CCV with no perfusion of the main circumferential loop of the primitive pectoral artery. The movie shows the same fish as in **Movie 6** but at a slightly earlier time point.

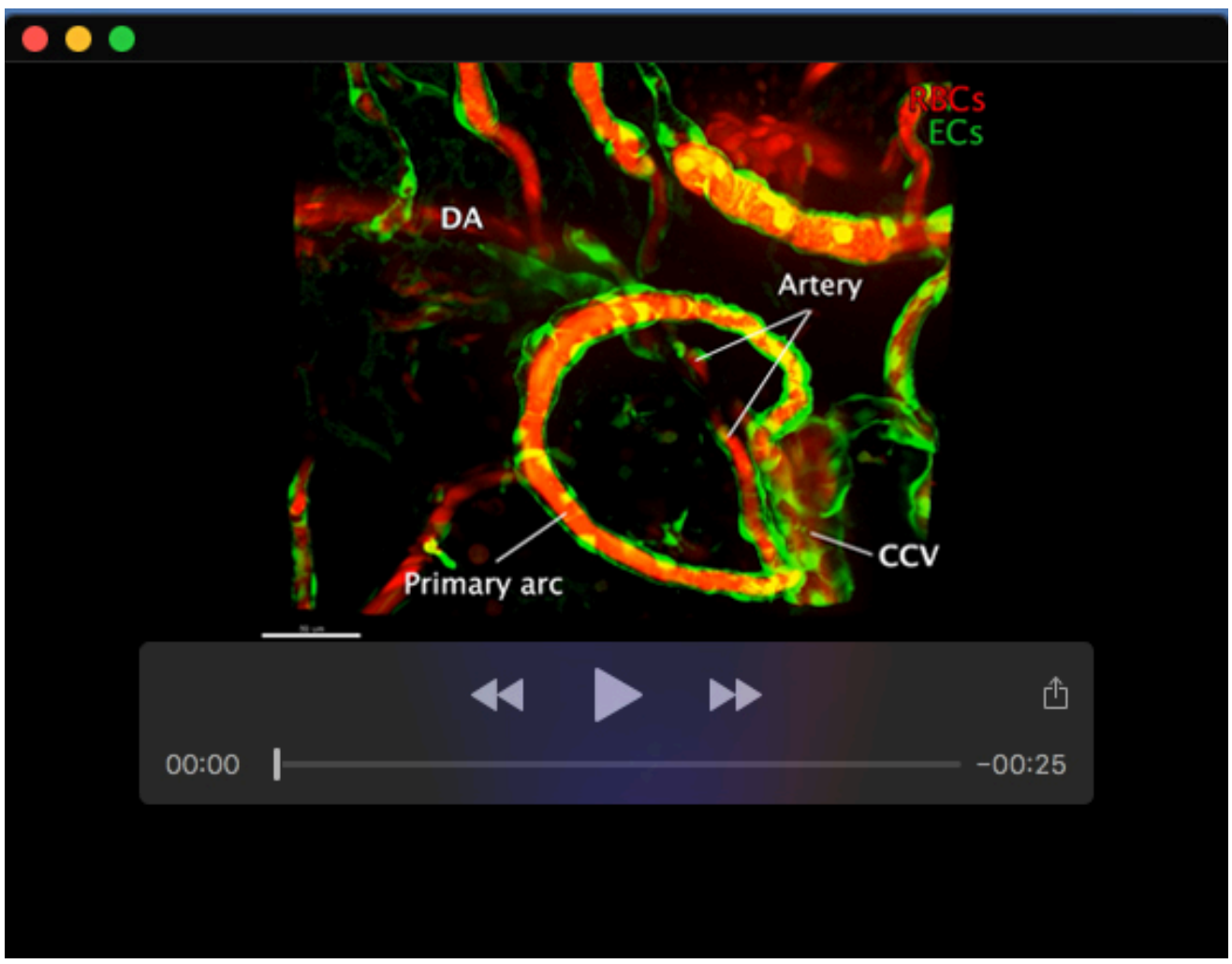

Movie 6. Subsequent re-routing of blood flow through the primitive pectoral artery.

3-D reconstructions of a confocal image stack of the fin region of the same 2 day-old *Tg(kdrl:egfp)*^{s843}, *Tg(gata1:dsred)*^{Sd2Tg} double transgenic zebrafish as in **Movie 5**, showing that the shunt has severed and that flow from the DA has now been re-routed through the main circumferential loop of the primitive pectoral artery.

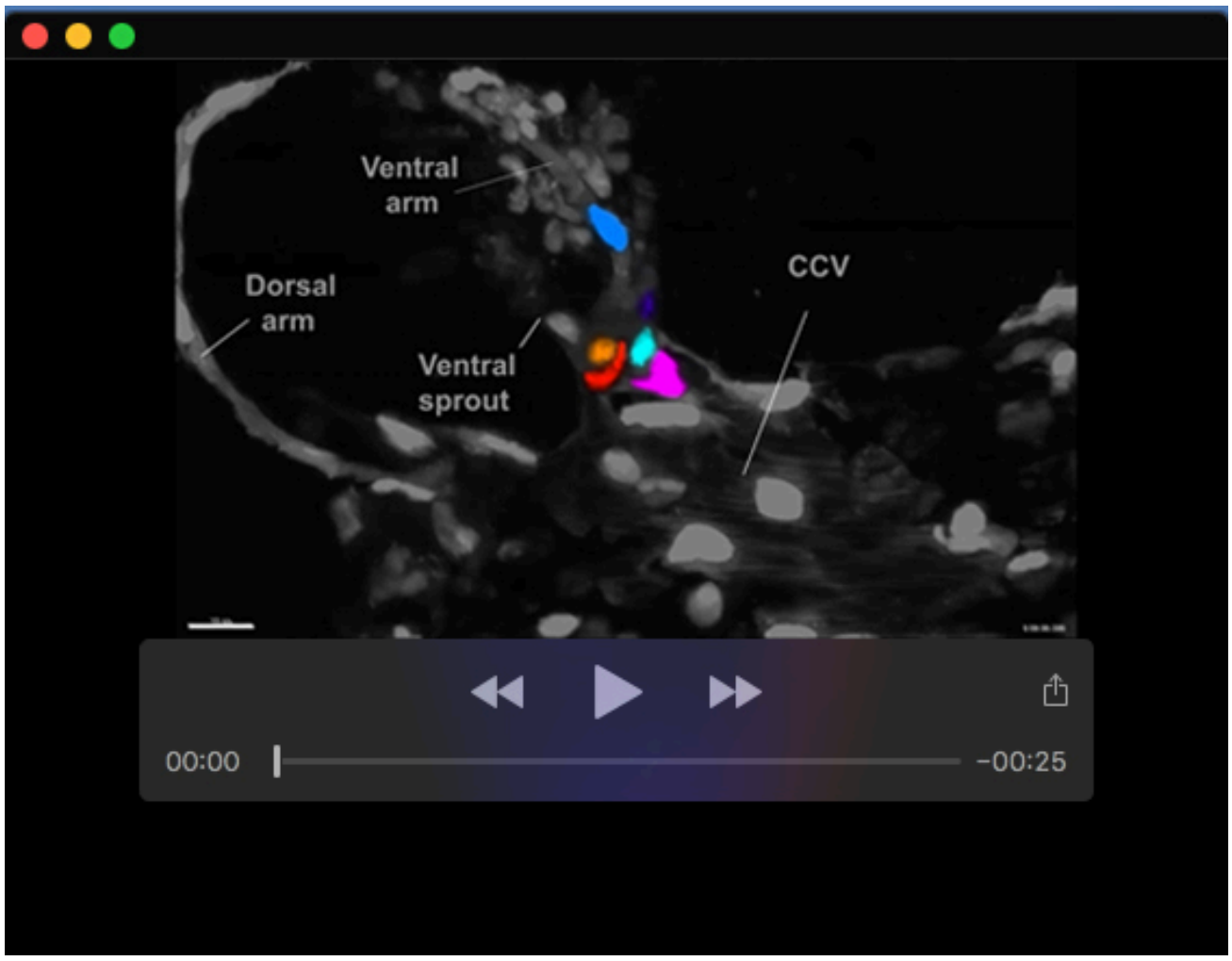

Movie 7. Resolution of the 3-way connection with residual vestigial sprout

Time-lapse confocal imaging of a *Tg(kdrl:egfp)*^{s843}, *Tg(kdrl:nlsmcherry)*^{y173} double transgenic zebrafish during the onset of flow with individual nuclei within the region of the junction false colored to follow their movement, shown in **Fig. S4**. This shows the presence of a residual vestigial sprout after resolution to proper flow.

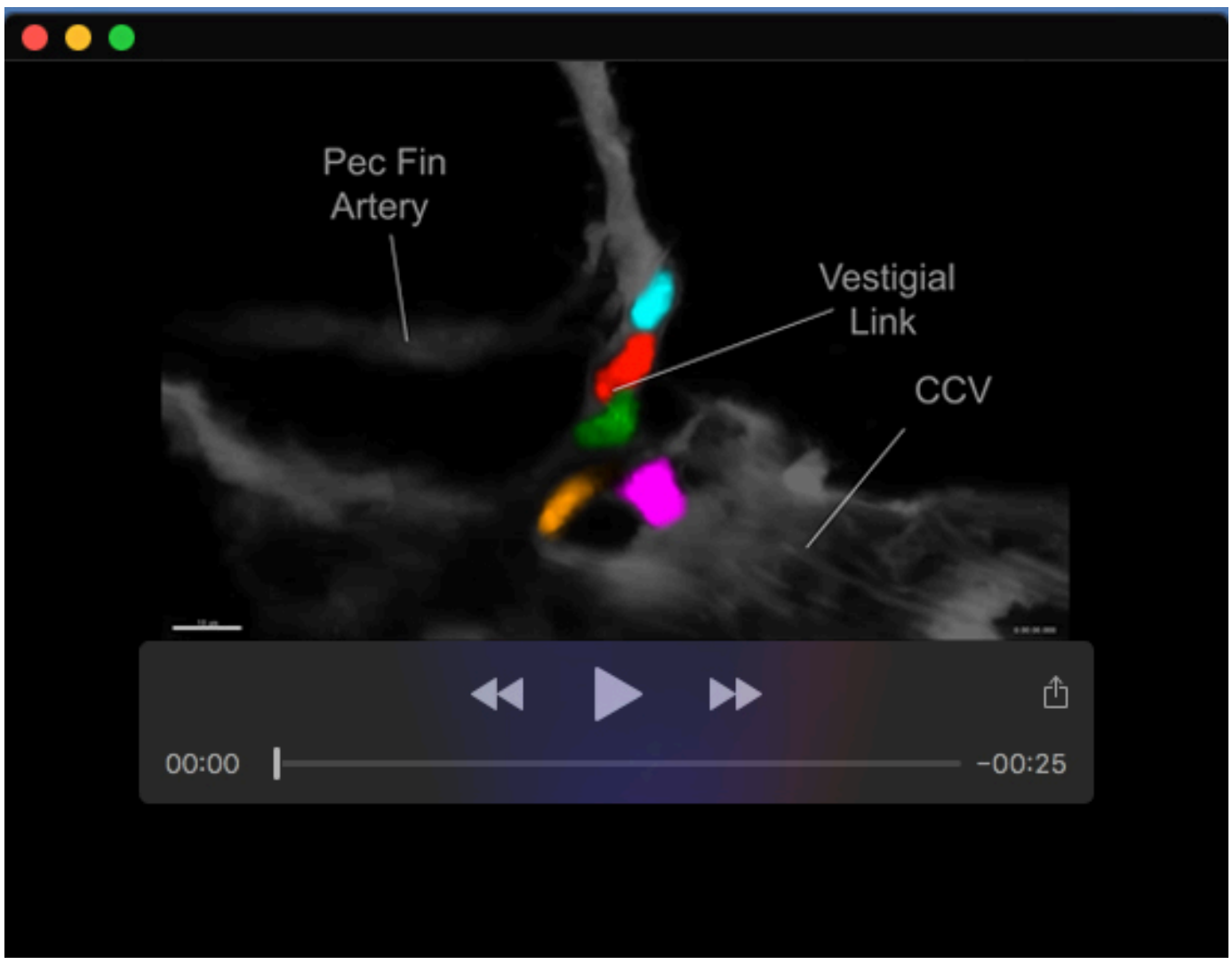

Movie 8. Resolution of the 3-way connection without residual vestigial sprout

Time-lapse confocal imaging of a *Tg(kdrl:egfp)*^{s843}, *Tg(kdrl:nlsmcherry)*^{y173} double transgenic zebrafish during the onset of flow with individual nuclei within the region of the junction false colored to follow their movement. This shows the lack of a residual vestigial sprout after resolution to proper flow.

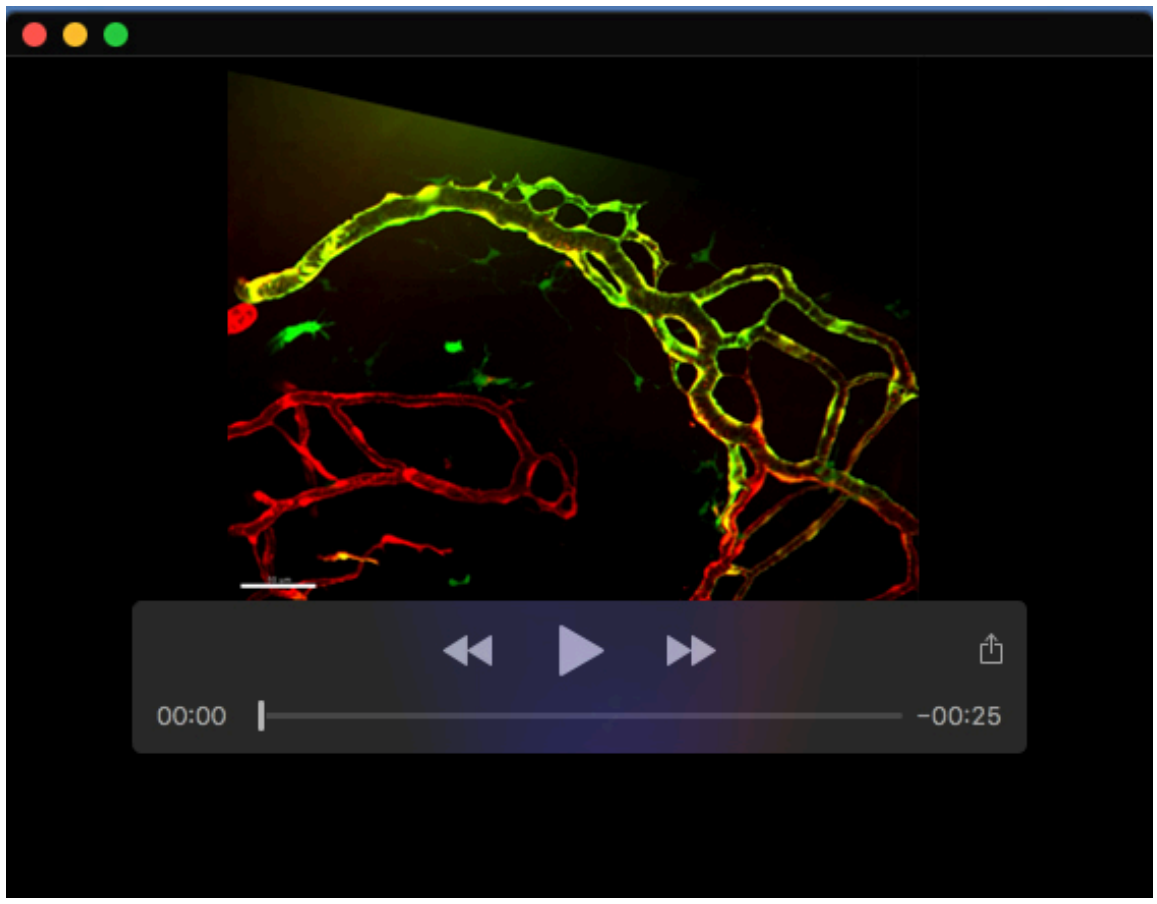

Movie 9. Distal vascular plexus of a 17 dpf larva

3-D reconstructions of the same confocal image stack of the fin of a 17 day old (7.0 mm length) *Tg(kdrl:egfp)*^{s843}, *Tg(gata1:dsred)*^{sd2Tg} double transgenic zebrafish shown in **Fig. 5L**, with close-ups of the dorsal hypersprouting area of the distal vascular plexus.

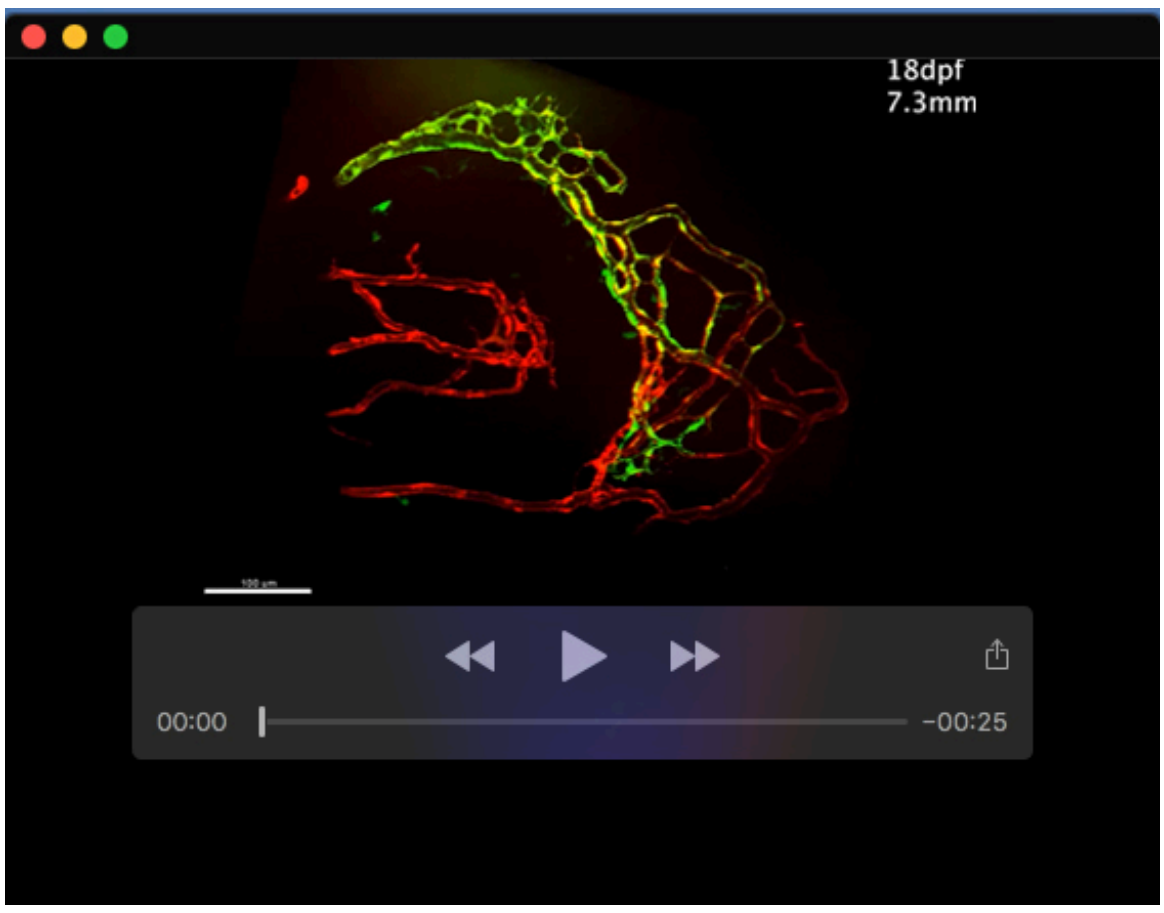

Movie 10. Distal vascular plexus changes in an 18-22 dpf larva

3-D reconstructions of the same confocal image stacks of the fin of an 18-22 day old (7.3-9.0 mm length *Tg(kdrl:egfp)*^{s843}, *Tg(gata1:dsred)*^{sd2Tg} double transgenic zebrafish as shown in **Fig. 5N-Q**, with close-ups of the dorsal hypersprouting area of the distal vascular plexus, including an addition 24 day old image of the same fish.

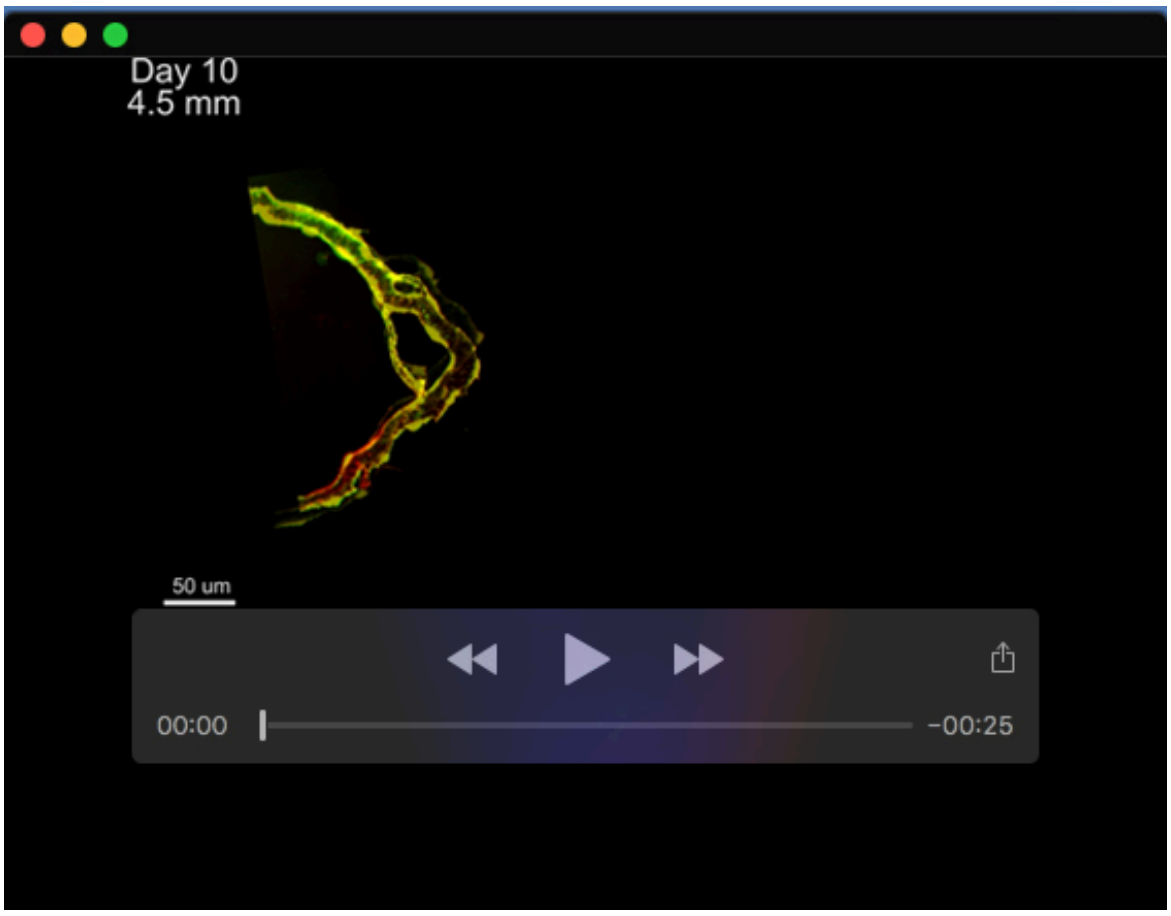

Movie 11. Development of the distal pectoral fin vasculature.

Confocal time-series of the distal vascular plexus in the same *Tg(kdrl:mcherry)*^{y206}*, Tg(mrc1a:egfp)*^{y251} double transgenic larva from day 9 through day 26 (4.3 mm to10.5 mm length). The movie shows the same images shown in **Fig. 5H-Q**.

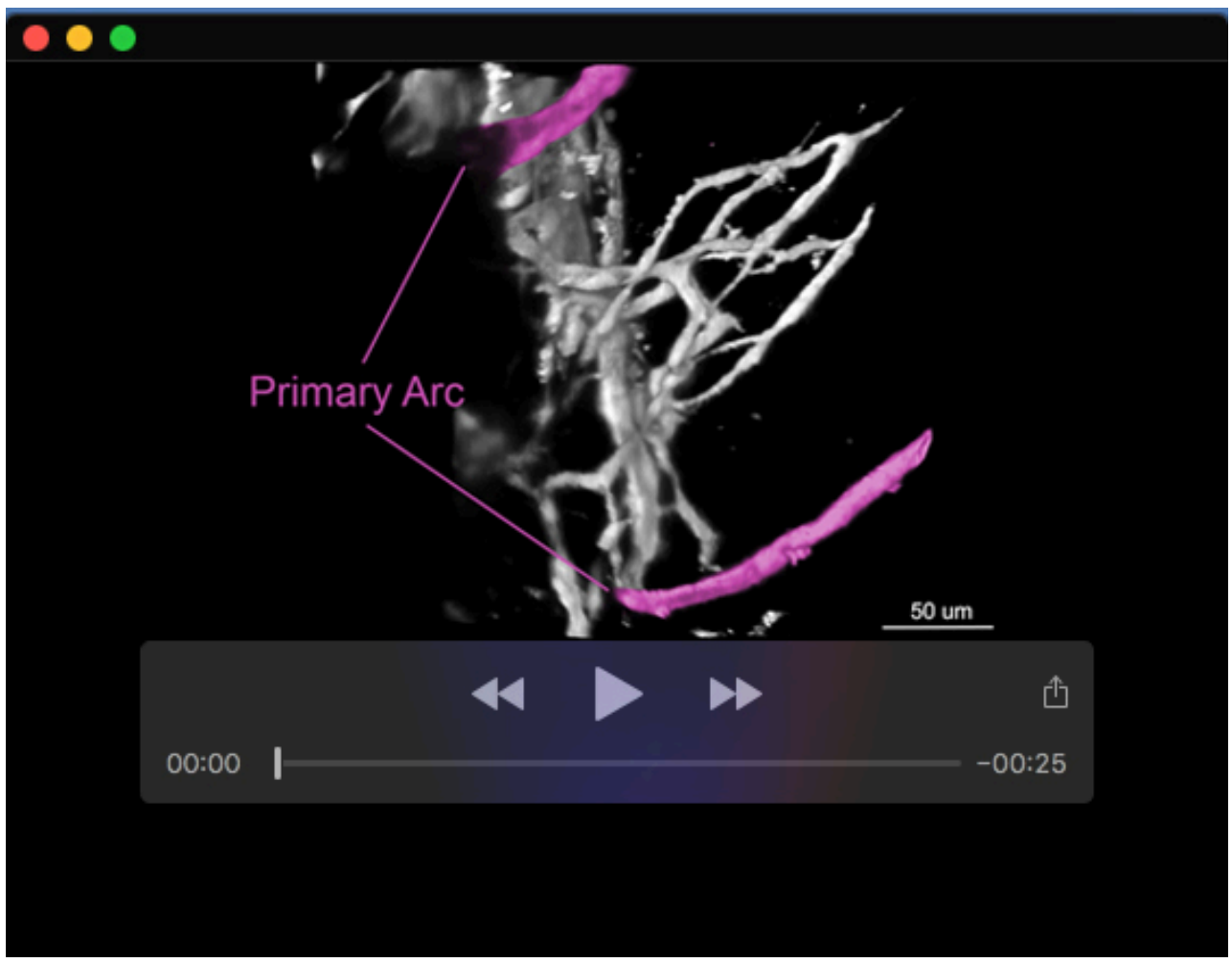

Movie 12. Lateral and medial proximal plexuses of an 18 dpf zebrafish

3D reconstruction of a confocal image stack of the proximal region of the pectoral fin of a representative 10dpf- 5.53mm, *Tg(kdrl:mcherry)*^{y206}*, Tg(mrc1a:egfp)*^{y251} double transgenic larva. False coloring and labels denote the medial and proximal plexuses as well as the common feed sprouting from the pectoral fin artery. The movie shows images of **Fig. S8**.

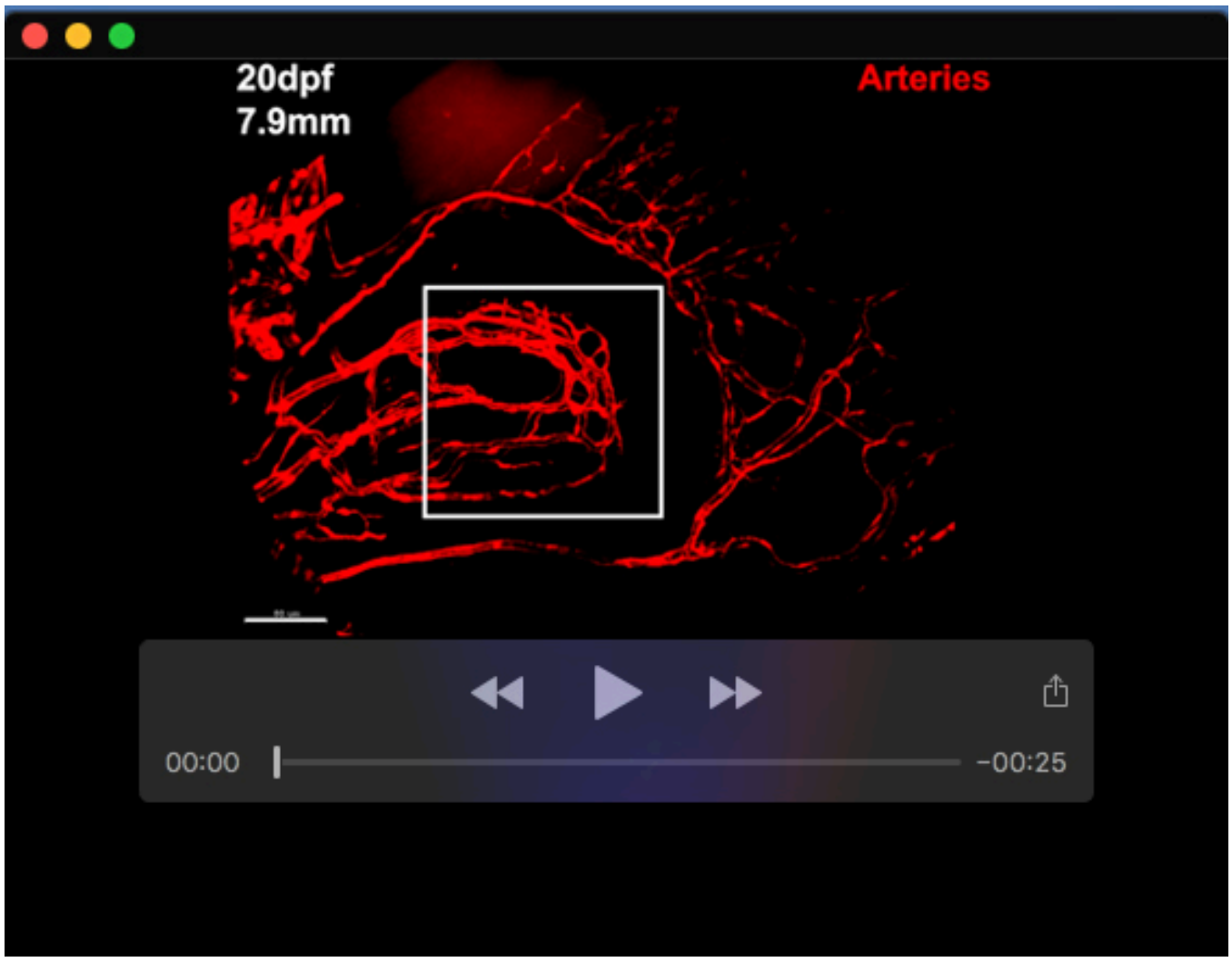

Movie 13. Lateral and medial proximal plexuses of an 18 dpf zebrafish

3D reconstructions of a confocal image stack of the fin of an 18 dpf (7.9 mm) , *Tg(kdrl:mcherry)*^{y206}, *Tg(mrc1a:egfp)*^{y251} double transgenic larva. The entire fin is initially shown, then only *Tg(kdrl:mcherry)*^{y206}-positive arteries (red), then only the proximal plexus region. 90-degree rotations of the proximal plexus show that it consists of two parallel plexuses, a lateral plexus (red) and a medial plexus (false-colored blue).